SCUOLA DI DOTTORATO
Università degli Studi di Milano - Bicocca

Dipartimento di Fisica "Giuseppe Occhialini"
Dottorato di ricerca in Fisica e Astronomia - XXXVII Ciclo
Curriculum in Fisica Teorica

Merging NLO QED corrections at hadron colliders: Z and $Z+\gamma$ production using the MiNLO′ method

Tutor:
Prof. Carlo Oleari

Supervisor:
Prof. Emanuele Re

Coordinator:
Prof. Stefano Ragazzi

Candidate:
Filippo Belloni

Registration Number:
789623

Anno Accademico 2023/2024

Abstract

In order to match the increasing precision of modern particle colliders, it is essential to have accurate theoretical predictions for the cross sections of physical processes and their associated distributions. These predictions are often obtained via Monte Carlo event generators which combine the fixed-order calculation, computed as a perturbative expansion in the coupling constants, with a parton shower and further hadronization. Due to the presence of soft and collinear emissions, in fact, there are some regions of the phase space in which the fixed-order computation is unreliable. In such regions, the presence of two or more widely separated scales leads to the dependence of those observables on large logarithms of the ratios between these scales that completely spoils the accuracy of the fixed-order computation. Using the Multi-Scale Improved NLO (MiNLO′) prescription, it is possible to resum to all orders the logarithms arising from kinematic configurations that involve different scales in such a way that the resulting distribution is NLO accurate both for fully inclusive and 1-jet predictions. The MiNLO′ method was introduced specifically for QCD radiation and it has already provided remarkable results. The extension to QED radiation, and its subsequent extension to full electroweak corrections, is still missing in the literature.

In this work we discuss the abelianization of the MiNLO′ method and its implementation in the context of QED radiation for the production of a lepton pair plus a photon, via a neutral vector boson. We discuss the behaviour of the Sudakov form factor when we switch from QCD to QED and the challenges that such Sudakov form factor poses in its actual computation. In order to circumvent some of the problems that would arise in the direct calculation of the Sudakov form factor, we propose a different solution and we discuss its implementation. Finally, we present a few distributions of physical interest and we study them both in a modified QED theory, with a "large" coupling constant, so that all the effects of MiNLO′ are clearly displayed, and with the physical value of the electromagnetic coupling constant.

Declaration

The content of this work is the result of my own efforts. It is based on my Ph.D. research project which is yet to be submitted for publication.
I hereby declare that except where specific reference is made to the work of others, the contents of this dissertation are original and have not been submitted in whole or in part for any other degree or qualification in this, or any other university.

28/10/2024 Filippo Belloni

Contents

Chapter 1

Introduction

Our knowledge of the fundamental elementary particles and their interactions can be described within a single theoretical framework, known as the Standard Model (SM) of Particle Physics, whose success has been established and confirmed in a number of experiments spanning over half a century.

Despite being a mathematically complete theory accommodating almost all known experimental data available to date, there is strong evidence that the SM is not the ultimate theory but a mere effective theory, valid only at the present accessible energies. Indeed, it fails to explain a number of experimental observations such as, among the others, the neutrino masses, the matter-antimatter asymmetry and the astrophysical evidence of dark matter and dark energy. Within the SM alone, even the presence of an elementary scalar particle, the Higgs boson, is unpleasant because when computing the radiative corrections to its mass, one encounters quadratically divergent contributions coming from self-energy corrections. This means that in order to accommodate for the relatively small value of the Higgs mass that was experimentally observed, an extreme fine tuning of the parameters is required. Moreover, the SM describes only three of the four fundamental forces of the universe, the gravitational interaction being left out.

Central to validating the predictions of the SM are hadron colliders, powerful machines that accelerate protons beams to near-light speed and collide them allowing experimental measurements at unprecedented high energies. At such energies the strong force responsible for the confinement of partons inside hadrons becomes less relevant and the accelerated protons start behaving as superpositions of free partons. When two partons from different beams interact in what is referred to as hard scattering, a large amount of particles is produced. Studying the mass distributions of the subsets of particles produced in the collisions offers a direct way to discover new massive particles by looking for peaks in differential distributions. Currently, the world's most high-energetic collider is the Large Hadron Collider (LHC), located at the CERN laboratory in Geneva, Switzerland. The crowning achievement of the

LHC is the discovery of the Higgs boson [1, 2], whose existence was crucial to confirming the mechanism that gives mass to other particles. The discovery, in 2012, marked a milestone in our quest to unravel the fundamental structure of the universe and started the precision era of hadron colliders.

The fact that, so far, experiments at the LHC have not yet found any sign of new physics beyond the SM, has exposed the clear necessity to consider complementary exploration strategies to the direct searches at the energy frontier. The High Luminosity phase of the Large Hadron Collider (HL-LHC) is due to start operations in the late 2020s. With this upgrade, the ATLAS and CMS experiments are expected to collect ten times more data than they will have recorded during the first three LHC runs. This dataset will unveil a new landscape for particle physicists to explore and offer unparalleled opportunities for understanding the forces of nature at their most basic level. This represents the beginning of a new rich experimental program set up to pursue the precise measurement of many fundamental SM parameters with an incredible percent or sub-percent target accuracy.

In order to make the most out of the data that will be collected, present and future LHC experiments demand theoretical simulations with increasingly better accuracy as many experimental analyses are (or will be) limited by theoretical uncertainties. In fact, high-precision predictions play a fundamental role in the quest for new physics when searching for small deviations from the SM. These predictions are formulated within the theoretical framework offered by Perturbation Theory in which the cross section is expressed in terms of a power series of the coupling constant truncated at some fixed order. Most low multiplicity processes at LHC are known up to next-to-next-to-leading order (NNLO) QCD corrections and in some cases even beyond that. For some processes also next-to-leading order (NLO) EW corrections need to be taken into account, as the QCD coupling constant squared is of the same order of magnitude as the electroweak one[1]. Moreover the matching of these fixed-order computations with increasingly accurate parton showers is crucial to fully exploit the vast amount of data coming from the experiments. In fact, not only it allows for a direct comparison between the theoretical computation and the measurements, but also it provides physical predictions in the regions of the phase space in which the fixed-order computation would be unreliable for observables sensitive to soft/collinear radiation. In such regions, the presence of two or more widely separated scales leads to the dependence of those observables on large logarithms of the ratios between these scales that completely spoils the accuracy of a fixed-order computation. By including soft/collinear emissions to all orders via a parton shower, one effectively resums the large logarithmic corrections at leading-logarithmic accuracy for generic observables, thus obtaining physical results.

Tools to achieve this goal for generic observables are Monte Carlo event gener-

[1]See Ref. [3] for a recent comprehensive review.

ators, which incorporates the effects described above. Their purpose is to simulate events, namely the production of sets of particles and their kinematical distribution. Event generators have evolved significantly over the decades, incorporating more sophisticated algorithms throughout the years. The first generators ever to be implemented provided an accurate description of QCD emission only in the collinear and/or soft limit via parton showers. Later on, these predictions were improved by matching the shower to the leading-order (LO) matrix element of the scattering process. In this way one obtains an accurate description of the scattering also far from the soft and collinear regions of the phase space. This is achieved by matching the LO matrix elements to general purpose Monte Carlo event generators like Pythia [4, 5], Herwig [6] or Sherpa [7–9]. A direct improvement to this approach relies on the matching of the shower to a NLO prediction (NLO+PS). This is done, for example, through the POWHEG [10–12] and MC@NLO [13, 14] methods, which are able to produce both NLO accurate distributions for radiation-inclusive observables and LO accurate ones for observables sensitive to the real radiation. A further extension of these methods can be obtained by merging two NLO computations with different multiplicity, namely one with one more resolved parton than the other, and matching them with parton showers. This is done by many different methods, such as MiNLO/MiNLO′ [15, 16], MEPS@NLO [17], UNLOPS [18, 19] and FxFx [20]. In recent years, a significant leap in this direction has been made by extending partonic event generators to NNLO in QCD matched to a parton shower (NNLO+PS), such as in GENEVA [21–23] and MiNNLO$_{\text{PS}}$ [24, 25][2]. Alongside these efforts, the extension of the NLO matching algorithms to the inclusion of EW effects is also an important goal, as it allows for a fully consistent simulation of higher order QED and EW corrections.

The topic of this thesis is the implementation of the Multi-Scale Improved NLO (MiNLO′) method in QED through an abelianization procedure. In this context we study the production of a lepton pair via neutral current Drell-Yan, i.e. the production of a Z boson [32], at the LHC. This process plays a central role in the precision physics program at the LHC both for calibration purposes as well as, in general, to measure SM parameters at very high accuracy [33–37]. It is also important for the extraction of PDFs (see e.g. Ref. [38]) and it is one of the main irreducible backgrounds to the searches for new physics [39, 40].

The outline of the work is the following. The first part consists of the review of the fundamental theoretical tools needed to describe the process under consideration and the methods employed. More specifically, in Chapter 2 the MiNLO′ method is introduced, together with the POWHEG framework and a brief description of the main ingredients needed for a fixed-order computation. In Chapter 3 we introduce

[2]Other less developed approaches exist, such as UNNLOPS [26–28] or the one presented in Ref. [29]. Matching to N3LO QCD corrections have also been discussed in Ref. [30] and [31].

the electroweak theory and the subtleties related to the different renormalization schemes. In Chapter 4 we discuss inclusion of final-state massive emitters within the framework of resummation and the modifications needed to implement them in the MiNLO′ method. Then, in Chapter 5, we introduce the abelianization prescription for the transition of the formalism from QCD to QED. Here we discuss the differences between the QCD and QED case and in particular the numerical issues that are exposed by said differences. In Chapter 6, we describe a way to overcome the numerical issues introduced in the previous chapter and we discuss the validity region of this formulation of the abelianized MiNLO′ method. Finally, in Chapter 7 we describe the implementation of the method in QED and we present our phenomenological results.

Chapter 2

Theoretical framework

2.1 Fixed-order computation

The starting point for the description of any hard scattering process in hadron collisions is given by the collinear factorization theorem [41]. Within this framework, colliding protons can be viewed as a collection of free massless particles, that are referred to as partons, each carrying a fraction of the total hadron energy. The probability of finding a parton i with some energy fraction x_i is given by a function $f_i(x_i)$, called the parton distribution function (PDF). These objects are universal, i.e. they do not depend on the process under investigation, which means that they can be determined in some processes and used to describe many others. We can write

$$\sigma = \sum_{i_1,i_2} \int dx_1 dx_2 \; f_{i_1}(x_1)\, f_{i_2}(x_2)\; \hat{\sigma}(x_1, x_2, \alpha_s) + \mathcal{O}\left(\frac{\Lambda_{\mathrm{QCD}}}{Q}\right). \tag{2.1.1}$$

The last term represents non-perturbative effects that are suppressed by powers of Λ_{QCD}/Q where $\Lambda_{\mathrm{QCD}} \approx 300$ MeV is the hadronization scale and Q is the hard scale of the process.

The partonic cross section $d\hat{\sigma}$ can be perturbatively expanded in powers of the strong coupling constant as

$$\hat{\sigma}(x_1, x_2, \alpha_s) = \sum_n \left(\frac{\alpha_s}{2\pi}\right)^n \hat{\sigma}^{(n)}(x_1, x_2), \tag{2.1.2}$$

At the lowest order (the Born order), the differential cross section can be written as

$$d\hat{\sigma}(x_1, x_2) = \mathcal{B}(p_1, p_2, k_1, ..., k_n)\; d\Phi_n(k_1, ..., k_n), \tag{2.1.3}$$

where the dependence on the energy fraction of the incoming partons is implicit in their momenta p_1 and p_2. We denoted with $\mathcal{B}$ the matrix elements squared at tree (Born) level, including the appropriate sums and averages over spin and colour as

well as the flux factor[1]. The usual n-body phase space $d\Phi_n$ is given by

$$d\Phi_n(k_1, ..., k_n) = \left[\prod_{i=1}^{n} \frac{d^3 k_i}{(2\pi)^3 k_i^0} \right] (2\pi)^4 \, \delta^4 \left(q - \sum_{i=1}^{n} k_i \right). \tag{2.1.4}$$

Schematically we can write the LO cross section as

$$\sigma_{\text{LO}} = \int d\Phi_N B(\Phi_N) \tag{2.1.5}$$

where $B = \sum_{i_1,i_2} f_{i_1} f_{i_2} \mathcal{B}$ is now the sum over all the relevant partonic contributions multiplied by the parton luminosity, namely the corresponding PDFs. As for the phase space we introduced the notation $d\Phi_N = dx_1 dx_2 \, d\Phi_n$.

In order to obtain meaningful predictions to be compared with experimental data, the computation must be performed at higher accuracy and higher-order contributions must be taken into account. The calculation of the NLO cross section requires the inclusion of new diagrams with extra vertices and it takes contributions from

- the interference between the one-loop virtual amplitudes and the LO ones, called virtual contributions;
- real emission amplitudes with a phase space including one extra parton with respect to the basic process, which are effectively the tree-level squared amplitudes for the process with $n + 1$ final state particles.

It is assumed that the amplitudes have already been renormalized so that there are no more divergences of ultraviolet origin. That being said, singular contributions can still arise in the regions in which the extra particle is either soft or collinear to one of the other particles. Thus eq. (2.1.5) becomes

$$\sigma_{\text{NLO}} = \int d\Phi_N \left[B(\Phi_N) + V_b(\Phi_N) \right] + \int d\Phi_{N+1} \, R(\Phi_{N+1}), \tag{2.1.6}$$

where the subscript in V_b means that there are infrared divergences explicit in the amplitude. The computation of the virtual contributions is typically performed using dimensional regularisation in $d = 4 - 2\epsilon$ dimensions: in this way the singularities are expressed analytically yielding $1/\epsilon$ and $1/\epsilon^2$ poles. Upon the full integration these divergences are exactly cancelled by the one arising in the evaluation of the real emission matrix element[2] in the soft/collinear regions, namely the regions of the

[1] To fix the idea and the notation, we limit the discussion to QCD corrections only, and, for simplicity, we do not specify that $\hat{\sigma}$ and $\mathcal{B}$ depend on i_1 and i_2, i.e. the flavours of the incoming partons. A more precise notation will be introduced in Section 2.2.

[2] In hadronic collisions, the complete cancellation of the initial-state collinear singularities requires also the inclusion of two additional counterterms known as the collinear remnants. To keep the discussion as simple as possible, we will not review them and we refer to [11] for the details on the topic.

$n+1$ phase space in which the real kinematics becomes indistinguishable from the Born one. This result is known as the Kinoshita-Lee-Nauenberg theorem [42, 43].

The explicit cancellation of the infrared poles between virtual and real contributions is often not a trivial task to achieve in an analytical computation due to the two terms belonging to different phase spaces and to the constraints on the phase-space integration present when computing a differential quantity. Moreover, because the divergences of the real emissions arise only upon the integration over $d\Phi_{N+1}$, such integration cannot be perfomed numerically. To address these issues, one can subtract the singularities at the integrand level via the so-called subtraction methods [44]. The two most widespread NLO subtraction methods are the dipole subtraction, introduced by Catani and Seymour [45], and the Frixione-Kunszt-Signer method [46, 47]. Both those methods rely on the introduction of counterterms, that we can collectively denote as C, in such a way that they reproduce the singular behaviour of the real term R in the soft and collinear regions and, once integrated over the extra radiation phase space, they yield the exact single and double poles of the virtual amplitude with opposite sign. Formally we have

$$\sigma_{\text{NLO}} = \int d\Phi_N \left[B(\Phi_N) + V(\Phi_N) \right] + \int d\Phi_{N+1} \left[R(\Phi_{N+1}) - C(\Phi_{N+1}) \right], \tag{2.1.7}$$

where V is the infrared subtracted virtual amplitude given by

$$V(\Phi_N) = \left[V_b(\Phi_N) + \int \frac{d\Phi_{N+1}}{d\Phi_N} \, C(\Phi_{N+1}) \right]_{d=4-2\epsilon}. \tag{2.1.8}$$

For the subtraction to take place, it must be possible to define a mapping between the real emission phase space Φ_{N+1} and its underlying n-body configuration, that we denote by $\bar{\Phi}_N$. This mapping is tailored specifically for each singular region in such a way that:

- for soft configurations, $\bar{\Phi}_N$ is obtained by removing the soft parton;
- for final-state collinear configurations, $\bar{\Phi}_N$ is obtained by replacing the momenta of the two collinear partons by a single momentum given by their sum;
- for initial-state collinear configurations, $\bar{\Phi}_N$ is obtained by removing the radiated collinear parton and by replacing the momentum fraction of the initial-state radiating parton with its momentum fraction after radiation.

For this reason, it is convenient to define a list of singular regions each identified uniquely by the superscript α_r. In this way for each singular region we have a mapping $M^{(\alpha_r)}$ that defines a one-to-one correspondence between Φ_{N+1} and its underlying n-body phase space configuration $\bar{\Phi}_N^{(\alpha_r)}$ plus three more variables that describe the radiation process. We have

$$M^{(\alpha_r)} : \Phi_{N+1} \to \{\bar{\Phi}_N^{(\alpha_r)}, \Phi_{\text{rad}}^{(\alpha_r)}\}, \tag{2.1.9}$$

such that the corresponding phase space element is given by

$$d\Phi_{N+1} = d\bar{\Phi}_N^{(\alpha_r)}\, d\Phi_{\text{rad}}^{(\alpha_r)}. \tag{2.1.10}$$

The term C, representing the subtraction counterterms in eq. (2.1.7), can then be written as the sum over all the singular regions of distinct counterterms $C^{(\alpha_r)}$, namely

$$C(\Phi_{N+1}) = \sum_{\alpha_r} C^{(\alpha_r)}(\bar{\Phi}_N^{(\alpha_r)}, \Phi_{\text{rad}}^{(\alpha_r)}). \tag{2.1.11}$$

To avoid unnecessary complications, in the following section we will adopt the short notation

$$[\dots]_{\alpha_r} \tag{2.1.12}$$

meaning that all the quantities appearing inside the square bracket that are affected by the superscript of the singular region must be evaluated in the region α_r.

2.2 The POWHEG method

The POWHEG method is a technique to perform the matching of the NLO fixed-order computations to parton shower generators. The procedure was first introduced in Ref. [10], discussed in detail in Ref. [11] and then implemented in the POWHEG-BOX framework, described in Ref. [12]. The core idea in POWHEG is the generation of the hardest radiation using the exact NLO matrix element before the event is passed to the shower generator, which in turn will provide any subsequent softer radiation. The main issue is avoiding double counting, as the emission generated by POWHEG is, in principle, already accounted for in an approximate way by the shower. For shower algorithms that are ordered in transverse momentum the solution is simple, since each radiation is generated with smaller p_{T} than the previous one, meaning the hardest emission is always the first. In this case POWHEG replaces the hardest emission with its own NLO accurate one. Angular ordered shower generators may instead generate soft radiation before generating the emission with the largest p_{T}. This requires the implementation of the so-called *vetoed-truncated shower*, described in details in Ref. [10], which consists in a shower algorithm that is fully equivalent to the angular ordered shower, but in which the hardest emission is generated first.

Before discussing the implementation of the method, we need to define some quantities related to the separations of the singular regions and the different flavour structure of the tree level process. We can introduce a label f_b to keep track of the flavours of the n-body process, ignoring any permutation of the final state particles. For any given flavour structure we then have a born and a virtual contribution, B^{f_b} and V^{f_b} respectively. As for the real emission terms, we can use the superscript α_r, introduced in the previous section, to isolate the contribution to the real cross section

that is singular in only one singular region of integration and has a specific flavour structure:

$$R = \sum_{\alpha_r} R^{(\alpha_r)}. \tag{2.2.1}$$

Now for each flavour structure we can define

$$\begin{aligned}\bar{B}^{f_b}(\Phi_N) = B^{f_b}(\Phi_N) \,+\, V^{f_b}(\Phi_N) \\ + \sum_{\alpha_r \in \{\alpha_r | f_b\}} \int \Big[d\Phi_{\rm rad} \left\{ R(\Phi_{N+1}) - C(\Phi_{N+1}) \right\} \Big]_{\alpha_r}^{\bar{\Phi}_N^{(\alpha_r)} = \Phi_N},\end{aligned} \tag{2.2.2}$$

where the sum is performed over all the singular regions that are mapped to an underlying n-body configuration characterized by the flavour structure f_b. In short, B^{f_b} and $\bar{B}^{f_b}$ are the LO and NLO differential cross sections for the process identified by the flavour structure f_b. The notation $\bar{\Phi}_N^{(\alpha_r)} = \Phi_N$ in the last term means that the arguments between the brackets, which depend on the kinematics obtained via the mapping in eq. (2.1.9), are evaluated for values of the barred phase-space variables $\bar{\Phi}_N$ equal to Φ_N. This identification only makes sense if the flavour structure of the underlying n-body process for the region corresponding to α_r is equal to f_b, which is guaranteed by the criterion specified via the sum.

Then we can introduce the following Sudakov form factor

$$\Delta_{\rm pwg}^{f_b}(\Phi_N, p_{\rm T}) = \exp\left\{ - \sum_{\alpha_r \in \{\alpha_r | f_b\}} \left[\int d\Phi_{\rm rad} \, \frac{R(\Phi_{N+1})}{B^{f_b}(\Phi_N)} \, \theta(k_{\rm T}(\Phi_{N+1}) - p_{\rm T}) \right]_{\alpha_r}^{\bar{\Phi}_N = \Phi_N} \right\}. \tag{2.2.3}$$

Here $k_{\rm T}^{(\alpha_r)}$ is a quantity used to measure the hardness of the emission. It is a function of the kinematics of the region α_r and becomes equal to the transverse momentum of the radiated parton as it approaches the singular limit. More specifically:

- for initial-state collinear singularities, in the collinear limit $k_{\rm T}$ is proportional to the transverse momentum of the emitted parton with respect to the beam axis;
- for final-state collinear singularities involving two momenta k_i and k_j becoming collinear, $k_{\rm T}$ is taken as the spatial component of one of the two momenta orthogonal to their sum.

With these ingredients, the POWHEG cross section for the generation of the hardest emission is defined as

$$\begin{aligned}d\sigma = \sum_{f_b} \bar{B}^{f_b}(\Phi_N) \, d\Phi_N \Bigg\{ \Delta_{\rm pwg}^{f_b}(\Phi_N, p_{\rm T}^{\rm min}) \\ + \sum_{\alpha_r \in \{\alpha_r | f_b\}} \left[\Delta_{\rm pwg}^{f_b}(\Phi_N, k_{\rm T}) \, \theta(k_{\rm T} - p_{\rm T}^{\rm min}) \, \frac{R(\Phi_{N+1})}{B^{f_b}(\Phi_N)} \, d\Phi_{\rm rad} \right]_{\alpha_r}^{\bar{\Phi}_N = \Phi_N} \Bigg\}.\end{aligned} \tag{2.2.4}$$

This result has the following properties:

- it is NLO accurate for inclusive observables;
- it correctly reproduces the NLO cross section for large values of k_{T}[3];
- the structure of the shower is left untouched, as only the first emission, which is the hardest, is replaced by the NLO accurate one.

2.3 The MiNLO′ method

In the previous section we discussed how POWHEG performs the matching of the NLO fixed-order computation to the parton shower without spoiling the leading logarithmic structure of the shower itself. This means that, if we consider for example the process in which a colour singlet F is produced, using POWHEG we obtain NLO accuracy for distributions inclusive in F, LO accuracy for observables that rely on the presence of one jet and leading-logarithmic (LL) accuracy (LL is the accuracy of standard parton showers[4]) from the second jet onwards. We can also construct a FJ generator, in which at lowest order the diagrams already contain one coloured final state parton. In this case we would have NLO accuracy for distributions inclusive in FJ, only LO accuracy for distributions with two jets and shower accuracy for subsequent emissions. This logic can be applied to processes with any number of jets at Born level. Moreover, all these processes achieve predictions that are complementary in accuracy and they overlap in some regions of the phase space. Thus it is desirable to merge them within a single framework in which for each jet multiplicity the highest accuracy is retained. For merging inclusive and 1-jet predictions[5] at NLO, this process can be realized via the MiNLO′ method [16], which provides a modification of the NLO cross-section formula for the production of a colour singlet plus one jet, such that it gives NLO accurate results also in the region in which the transverse momentum of the jet vanishes. More specifically we will briefly discuss the application of the method within a the POWHEG framework.

The merging problem was already addressed through multiple different solutions [17–20, 53–56], that typically share the same fundamental issue: they require the introduction of an arbitrary, therefore unphysical, scale. This scale is used for partitioning the phase space according to the jet multiplicity: in this way each generator contributes only to the jet bin for which it is NLO accurate. The results are

[3]There is an argument to be made for the accuracy of non-inclusive observable being spoiled by the ratio $\bar{B}/B$ encoded in the Sudakov form factor in eq. (2.2.4). To remedy, this one can introduce a damping procedure via the splitting of the real contribution into a singular part and a finite part. Additional details on the topic can be found in Refs. [12, 48]

[4]Much progress has been made in recent years as far as the accuracy of parton showers is concerned, see for example Refs [49–51].

[5]An extension of the method which includes higher jet multiplicities can be found in Ref. [52]

then assembled together to obtain inclusive predictions. The choice of the value of the arbitrary scale is very delicate, as it can spoil the reliability of the computation, leading for example to the hard jets being described with low accuracy. Moreover, within reasonable limits, the choice of the scale must not affect the final result as the latter cannot depend on the value of unphysical parameters.

The MiNLO′ approach was proposed to perform the merging of different generators without the need for the introduction of any additional scale. It was developed from the MiNLO method [15], which stands for Multi-scale Improved NLO, that was introduced to define an a priori criterion for the selection of central scales in NLO computation. It can be seen as the NLO extension of the reweighting method used in tree-level matrix element and parton shower (ME+PS) merging algorithms, such as the CKKW approach [57].

Consider the POWHEG implementation of the FJ process mentioned above, namely the production of a generic color singlet F plus one jet at tree-level. The NLO inclusive cross section for the computation of the underlying Born kinematics, denoted by $\bar{B}$ in the POWHEG formalism, is given by the sum over all the flavour structure f_b of eq. (2.2.2). In the original MiNLO method, a modification of the POWHEG $\bar{B}$ function is introduced via the inclusion of a Sudakov form factor and with the use of appropriate scales for the couplings, according to the formula

$$\bar{B} = \alpha_s(p_{\mathrm{T}})\,\Delta^2(Q, p_{\mathrm{T}}) \left[B\left(1 - 2\Delta^{(1)}(Q, p_{\mathrm{T}})\right) + V + \int d\Phi_{\mathrm{rad}}\, R \right]. \tag{2.3.1}$$

Here Q is the hard scale of the process, that can be identified with the virtuality of the color singlet F, while the transverse momentum of F is represented by p_{T}. Note that in eq. (2.3.1), one power of the coupling constant was stripped away from the Born, virtual and real contribution, and it was factorized in front with its explicit scale dependence. The Sudakov form factor Δ is given by

$$\Delta(Q, p_{\mathrm{T}}) = \exp\left\{ -\int_{p_{\mathrm{T}}^2}^{Q^2} \frac{dq^2}{q^2} \left[A(\alpha_s(q^2)) \log\frac{Q^2}{q^2} + B(\alpha_s(q^2)) \right] \right\} \tag{2.3.2}$$

and by expanding it in powers of α_s we get

$$\Delta(Q, p_{\mathrm{T}}) = 1 + \Delta^{(1)}(Q, p_{\mathrm{T}}) + \mathcal{O}(\alpha_s^2). \tag{2.3.3}$$

The functions A and B admit a perturbative expansion in the strong coupling constant

$$A(\alpha_s) = \sum_{n=1}^{\infty} \left(\frac{\alpha_s}{2\pi}\right)^n A^{(n)}, \qquad B(\alpha_s) = \sum_{n=1}^{\infty} \left(\frac{\alpha_s}{2\pi}\right)^n B^{(n)}, \tag{2.3.4}$$

so that at order α_s the expansion of the Sudakov form factor in eq. (2.3.3) can be written as

$$\Delta^{(1)}(Q, p_{\mathrm{T}}) = -\frac{\alpha_s}{2\pi} \left[\frac{1}{2} A^{(1)} \log^2\frac{Q^2}{p_{\mathrm{T}}^2} + B^{(1)} \log\frac{Q^2}{p_{\mathrm{T}}^2} \right]. \tag{2.3.5}$$

The inclusion of a Sudakov form factor in the calculation described by eq. (2.3.1) introduces NLO corrections to the FJ cross section, leading to double counting and spoiling the overall accuracy of the computation. The subtraction of the $\Delta^{(1)}$ term is a crucial ingredient of the method, as it compensates for the double counting thus restoring the NLO accuracy.

In the original MiNLO approach only $A^{(1)}$, $A^{(2)}$ and $B^{(1)}$ are taken into account and they are known in the literature (see Ref. [58] and references therein, in particular Refs. [59] and [60]). The A coefficients read

$$\begin{aligned} A_c^{(1)} &= C_c, \\ A_c^{(2)} &= C_c \left[C_{\text{A}} \left(\frac{67}{18} - \frac{\pi^2}{6} \right) - \frac{10}{9} T_{\text{R}} n_f \right], \end{aligned} \tag{2.3.6}$$

where $T_{\text{R}} = 1/2$ and n_f is the number of active flavours. Note that previously we dropped the flavour index for ease of notation. Now we reintroduced the subscript $c = q, \bar{q}, g$ to distinguish between quark and gluon lines respectively, with $C_q = C_{\bar{q}} = C_{\text{F}}$ and $C_g = C_{\text{A}}$. As for $B^{(1)}$ we have

$$B_{q,\bar{q}}^{(1)} = -\frac{3}{2} C_{\text{F}}, \qquad\qquad B_g^{(1)} = -2\pi\beta_0, \tag{2.3.7}$$

where β_0 is the customary first order QCD beta function, given by

$$\beta_0 = \frac{11 C_{\text{A}} - 2\, n_f}{12\pi}. \tag{2.3.8}$$

The improved MiNLO method, presented in Ref. [15] is based on the fact that the singular part of the NLO cross section for the FJ generator must yield the same result of the $\mathcal{O}(\alpha_s^2)$ expansion of the NNLL resummation formula for the transverse momentum of the color singlet. This can be achieved by introducing two upgrades to the original formalism:

- together with the coefficients $A^{(1)}$, $A^{(2)}$ and $B^{(1)}$, one must also include $B^{(2)}$ in the computation;
- the additional power of α_s entering the NLO contributions, namely V, R and the expansion of the Sudakov form factor $\Delta^{(1)}$, is evaluated at the transverse momentum of the color singlet F. The same scale choice is applied also to the factorization scale entering the PDFs.

Unlike the results described in eqs. (2.3.6) and (2.3.7), which are universal, the explicit expression for $B^{(2)}$ is process dependent. In the case of Drell-Yan production it was computed in Ref. [61] and it reads

$$\begin{aligned} B_{q,\,(\text{DY})}^{(2)} = &\left[\left(\frac{\pi^2}{2} - \frac{3}{8} - 6\zeta_3 \right) C_{\text{F}}^2 + \left(-\frac{11}{18}\pi^2 - \frac{17}{24} + 3\zeta_3 \right) C_{\text{A}} C_{\text{F}} + \left(\frac{1}{12} + \frac{\pi^2}{9} \right) C_{\text{F}} n_f \right] \\ &+ \pi\beta_0\, \zeta_2\, C_{\text{F}} + \pi\beta_0\, H_{(\text{DY})}^{(1)}, \end{aligned} \tag{2.3.9}$$

where

$$H^{(1)}_{(\mathrm{DY})} = C_{\mathrm{F}} \left[\frac{7}{6}\pi^2 - 8 \right] \tag{2.3.10}$$

is the hard virtual coefficient. By putting all terms together, along with the explicit expression for the one-loop beta function in eq. (2.3.8), we get

$$B^{(2)}_{q,(DY)} = \left[\left(\frac{\pi^2}{2} - \frac{3}{8} - 6\zeta_3 \right) C_{\mathrm{F}}^2 + \left(\frac{11}{18}\pi^2 - \frac{193}{24} + 3\zeta_3 \right) C_{\mathrm{A}} C_{\mathrm{F}} + \left(\frac{17}{12} - \frac{1}{9}\pi^2 \right) C_{\mathrm{F}} n_f \right]. \tag{2.3.11}$$

Note that these results come from the framework of resummation, which is often performed in b-space, where b is the impact parameter that is Fourier conjugate to the vector boson transverse momentum[6]. As shown by Ellis and Veseli [63], exact agreement at order α_s^2 can be achieved between the two formalisms by means of the following additional replacement

$$B_c^{(2)} \to B_c^{(2)} + 2\,\zeta_3\,(A_c^{(1)})^2. \tag{2.3.12}$$

In fact, at each order n in perturbation theory, one gets different logarithmic contributions of the type $\alpha_s^n L^m$ with $0 \leq m \leq 2n-1$, where $L = \log(Q^2/p_{\mathrm{T}}^2)$. At order α_s^2 we have perfect correspondence between the coefficients in b-space and the ones in p_{T}-space only if we drop NNNL contributions. That is, if we consider terms only up to NNL accuracy, meaning up to $\mathcal{O}(\alpha_s^2 L)$. By including the term in eq. (2.3.12), we absorb the first term in the NNNL tower of logarithms thus restoring the agreement between p_{T}-space and b-space formalisms (see also Appendix A of the MiNLO′ paper [16]).

Finally we stress that, because of the non perturbative behaviour of the strong coupling constant in the low energy regime, a minimum cut on the color singlet transverse momentum, say $p_{\mathrm{T}}^{\mathrm{min}} = 1$ GeV, must be necessarily introduced in eq. (2.3.1). Other than the physical motivation, a cutoff is also needed for practical reasons, mainly as a consequence of the numerical instabilities introduced by the computation of the matrix elements. However, due to the vanishing behaviour of the Sudakov form factor in the limit $p_{\mathrm{T}} \to 0$, the prediction is independent of the specific choice of the cutoff for sufficiently small $p_{\mathrm{T}}^{\mathrm{min}}$ values.

[6] In this context, b-space is the more natural space to use as it allows an exact all-orders factorization of the constraint $\delta^{(2)}(\vec{p}_{\mathrm{T}} - \sum_i \vec{k}_{\mathrm{T}i})$, where $\vec{p}_{\mathrm{T}}$ is the transverse momentum of the vector boson and $\vec{k}_{\mathrm{T}i}$ are the transverse momenta of the emitted gluons [62].

Chapter 3

Electroweak radiative corrections

Because of its large cross section and clean experimental signature, the production of a lepton pair via a Z boson, known as neutral current Drell-Yan (NC DY) process, plays a central role in the precision physics program at the LHC and therefore requires a very high theoretical accuracy. Given the high-precision measurement of the Z mass at LEP, in fact, the investigation of the Z resonance is of great importance for detector calibration at LHC and it represents a standard candle that can be used to constrain the PDFs. It also allows performing precise tests of the SM and it plays a fundamental role in the measurements of EW parameters, such as in the calibration of p_{T}^{W} from p_{T}^{Z} used in popular strategies for the determination of the mass of the W boson in hadronic collisions. Moreover, in the high tail of the transverse momentum and invariant mass distributions of the produced lepton pair, the NC DY represents one of the main irreducible backgrounds to the searches for new physics at the LHC.

Thus, on the theoretical side, all these tasks require precise predictions with an inclusion of both strong and electroweak radiative corrections and, simultaneously, careful control over the remaining theoretical uncertainties. The largest contributions to the differential cross section come from the strong interaction and were computed at NLO [64] and at NNLO [65–69] in perturbative QCD. Alongside the NNLO QCD corrections, the NLO EW corrections have been calculated long ago for NC DY in Refs. [70–76]. As far as N3LO QCD corrections are concerned, studies on the threshold effects have appeared in Refs. [77, 78] and, more recently, inclusive N3LO corrections have been calculated for the production of a lepton pair via photon exchange [79] and for the fully inclusive NC DY [80, 81], while N3LO correction to single-differential distributions can be found in Ref. [82]. The resummation of large logarithms arising from soft gluon emission at small transverse momentum has been studied in Ref. [83–94] and the combined effect of both QED and QCD transverse momentum resummation has been discussed in Ref. [95, 96]. The mixed NNLO contributions at order $\mathcal{O}(\alpha_s\alpha)$ have been addressed both in the pole approximation [97–99] and in the narrow width approximation for QCD×QED [100], QCD×EW in

inclusive Z production [101–103] and fully exclusive Z production [104–106]. Moreover, the complete mixed $\mathcal{O}(\alpha_s\alpha)$ NNLO corrections to the NC DY process have been reported for the first time in Refs. [107–110]. In the context of fully exclusive event generators, the state of the art for DY calculations is represented by matched computations which include a combination of factorisable effects of both QCD and EW origin in a unique simulation framework [111–115]. Very recently, the resummation of EW and mixed QCD-EW effects up to next-to-leading logarithmic accuracy has been presented in Ref. [116] for both charged and neutral current DY.

In order to perform higher-order computations in the electroweak sector of the Standard Model, one has to specify the choice of a set of input parameters and their numerical values. These parameters must be independent to guarantee gauge independence, well-defined and precisely measured. The electromagnetic coupling and many of the masses satisfy these conditions and are often considered the optimal choice. Such input parameters are well-suited for on-shell (OS) renormalization scheme. However, to make contact with QCD, sometimes $\overline{\text{MS}}$ renormalization schemes are preferred. The input parameter schemes described in the following section are formally equivalent, at a given perturbative order. Nonetheless the numerical results they provide can be different due to the truncation of the expansion. Although in principle the choice of the input-parameter scheme should be arbitrary, there can be phenomenological motivation to prefer one scheme with respect to the others, depending on the process or the observable under consideration.

3.1 Input parameter schemes

The most intuitive choice for the input parameters consists of the electromagnetic coupling $\alpha = e^2/(4\pi)$, the weak boson masses M_Z and M_Z, together with the Higgs boson mass M_H, the fermion masses m_f and, in general, the Cabibbo-Kobayashi-Maskawa matrix.

In the EW sector, the masses of the particles are defined as pole masses, which means that the value of the mass of a particle is determined by the position of the pole in its propagator. This is perfectly fine for massive bosons and leptons but not for light quarks, because, as soon as QCD corrections are involved, the non-perturbative behaviour of the strong interaction at the scale of the quark masses poses problems in the definition of the pole masses. By all means, properly defined observables are expected to be insensitive to the perturbatively problematic light quark masses, as will be discussed later.

The discussions on the Higgs sector falls outside the scope of this work. However it is worth mentioning that the Yukawa couplings between the Higgs and the fermions are not independent parameters and they are indeed fixed by the choice of the fermion masses and other parameters. As a consequence, tampering with the relation between

the masses and the Yukawa couplings introduces a violation of gauge invariance and can lead to inconsistencies in the results. In the same way we will not address the CKM matrix, as it can only become relevant in charged-current processes that involve the mixing between quark flavours.

For the boson masses, M_Z, M_W and M_H, the simplest choice is to use the real on-shell masses. This approach fails, however, when the instability of the bosons is taken into account via the inclusion of their finite decay widths. We can write the propagator function of a massive boson V with momentum q as

$$F_V(q^2) = \frac{q^2}{q^2 - \mu_V^2} \tag{3.1.1}$$

where the complex quantity $\mu_V^2 = M_V^2 - iM_V\Gamma_V$ specifies the location of the pole of the propagator in the complex plane. The width of the boson Γ_V enters the denominator of the propagator only after performing the Dyson summation of all the self-energies insertions, which leads to a mixing of the perturbative orders. Thus the proper introduction of finite-width effects is non trivial and, if done carelessly, can easily compromise gauge invariance. We briefly discuss two of the most popular solutions to this problem[1]:

- The pole scheme [118] is based on the observation that both the location of the pole of the propagator μ_V^2 and its residue in the amplitudes are gauge independent [119]. So one can first isolate the residue of the resonance under consideration and then introduce a finite decay width only in the gauge-independent resonant part. If higher-order corrections are taken into account, due to the difficulties posed by full off-shell calculations, a *pole approximation* is employed. The idea is to use the resonant amplitude defined in the pole scheme upon neglecting non-resonant parts. This procedure provides a gauge-invariant answer, but restricts the validity of the result to the resonance region only and is not reliable in the threshold regions.

- In the complex-mass scheme (CMS) [120, 121], the masses of each unstable particle V is consistently identified with μ_V^2, i.e. with the location of the poles of the propagator in the complex plane. This scheme fully respects all relations that follow from gauge invariance as long as the complex masses are introduced everywhere, meaning that also the couplings can become complex. This is the case, for example, for the couplings involving the weak mixing angle which, in CMS, is defined via the ratio of the complex mass squared of the gauge bosons, namely $\cos^2\theta_W = \mu_W^2/\mu_Z^2$. Additional details can be found in Ref. [122].

[1] A more detailed analysis on the topic can be found in Ref. [117].

Note that our choice[2] of the input-parameter scheme employs the coupling constant α and the two vector-boson masses M_Z and M_W, on top of M_H and m_f. This means that, in this context, the weak mixing angle, θ_W, is not an independent input parameter. Indeed, taking it as an independent parameter in addition to M_Z and M_W, like setting $\sin\theta_W$ to the sine of the effective weak mixing angle at the Z pole, can, in general, break gauge invariance, leading to wrong results even at LO.

For the electromagnetic coupling $\alpha = e^2/(4\pi)$, the standard definition is $\alpha = \alpha(0)$ which means that it employs an on-shell renormalization condition in the Thompson limit[3], i.e. photon momentum transfer $Q^\mu = 0$. When the typical EW scales are involved, such as the masses of the gauge bosons, this choice leads to large logarithms of the ratios between the fermion masses and the gauge-boson masses. These logarithms are related to the running of the coupling itself from $Q^2 = 0$ to the high scale $Q^2 \approx M_Z^2$. Therefore they can be reabsorbed by choosing a suitable scheme for α.

We report here the definition of three different input schemes. The various choices differ by 2-6% and the most appropriate scheme depends on the nature of the process. The possibilities are:

- $\alpha(0)$ scheme: the fine-structure constant is defined by the Thompson value, $\alpha \approx 1/137$. As mentioned above, in this scheme, the higher-order corrections depend on the light-quark masses via a factor of $\alpha \log m_q$ that enters the charge renormalization.

- $\alpha(M_Z)$ scheme: the value of the coupling constant is given by the effective electromagnetic coupling $\alpha(M_Z) \approx 1/129$, where $\alpha(0)$ is evolved via renormalization-group equations from the Thompson limit $Q^2 = 0$ to the Z pole. In this scheme the terms $\alpha \log m_q$ are cancelled by a quantity that is typically denoted by $\Delta\alpha(M_Z)$, which accounts for the running of the coupling from 0 to M_Z.

- G_μ scheme: an effective value derived from the Fermi constant G_μ is used, namely $\alpha_{G_\mu} = \sqrt{2} G_\mu M_W^2 (1 - M_W^2/M_Z^2)/\pi$. At higher orders it receives contributions from Δr, which describes the radiative corrections to muon decay. Again, the light-quark mass effects are cancelled, due to a compensation between Δr and $\Delta\alpha(M_Z)$.

Note that this does not imply that there is only one value of α, but it is crucial that a common coupling factor is used in complete subsets of diagrams that are gauge-invariant in order not to spoil consistency relations. Corrections to LO contributions

[2]There are other possible choices for the input-parameter scheme, such as for example the $(\alpha, \sin^2\theta_W, M_Z)$ scheme or the (α, G_μ, M_Z) scheme, that are described in details in Ref. [115].

[3]Note that, in literature, the Thompson limit can also be denoted as $\alpha(m_e)$, due to the electron being the lightest charged object whose quantum loops can contribute to the running

scaling with different numbers of powers of the coupling can be treated independently as they belong to disjoint gauge-invariant sets.

3.2 Renormalization in the OS scheme

Canonically, the discussion on renormalization requires the distinction between bare quantities, denoted here with the subscript 0, renormalized ones and counterterms. This procedure must be repeated for all the parameters, such as masses and coupling constants, as well as the fields that correspond to physical particle states and those that contribute to the unphysical sector, such as the ghost fields or the would-be Goldstone fields. In this section we are mainly interested in the charge renormalization, usually written as

$$e_0 = (1 + \delta Z_e)\, e_R, \tag{3.2.1}$$

and the changes that need to be introduced with the different definitions of α.

3.2.1 The $\alpha(0)$ scheme

We can proceed by steps, starting from a simplified case by considering a process without any external photon in the initial or final state. In QED each vertex gives a contribution $\delta Z_e + \frac{1}{2}\delta Z_A$, where δZ_A is the counterterm introduced for the photon field renormalization. For each internal photon propagator we get a contribution proportional to δZ_A that cancels with the two corresponding vertices. This means that for each power of the coupling α, we get a relative correction $2\delta Z_e$ to the cross section. The charge renormalization factor in the $\alpha(0)$ scheme is given then by

$$\delta Z_e^{\mathrm{OS}}\Big|_{\alpha(0)} = \frac{1}{2}\,\Pi^{AA}(0) - \frac{s_W}{c_W}\frac{\Sigma_T^{AZ}(0)}{M_Z^2} \tag{3.2.2}$$

where we introduced the shorthand notation for the trigonometric functions of the weak mixing angle

$$s_W = \sin\theta_W, \qquad c_W = \cos\theta_W. \tag{3.2.3}$$

In eq. (3.2.2) we denoted the transverse part of the photon-Z two-point function as Σ_T^{AZ}, while the vacuum polarization is related to the photon self-energy via the relation

$$\Pi^{AA}(q^2) = \frac{\Sigma_T^{AA}(q^2)}{q^2}, \tag{3.2.4}$$

that, since $\lim_{q^2\to 0}\Sigma_T^{AA}(q^2) = 0$, at vanishing photon momentum transfer, can be written as

$$\Pi^{AA}(0) = \left.\frac{\partial\Sigma_T^{AA}(q^2)}{\partial q^2}\right|_{q^2=0}. \tag{3.2.5}$$

We can isolate the fermionic contributions from the terms related to the W boson in the two-point functions

$$\begin{aligned}\Sigma_T^{AA}(q^2) &= \sum_f \Sigma_{T,f}^{AA}(q^2) + \Sigma_{T,W}^{AA}(q^2),\\ \Sigma_T^{AZ}(q^2) &= \sum_f \Sigma_{T,f}^{AZ}(q^2) + \Sigma_{T,W}^{AZ}(q^2).\end{aligned} \tag{3.2.6}$$

For the photon self-energy we have

$$\Sigma_{T,f}^{AA}(q^2) = -\frac{\alpha}{4\pi}\left\{\frac{2}{3}N_c^f\, 2\, Q_f^2\left[-(q^2+2m_f^2)\, B_0(q^2,m_f,m_f) + 2m_f^2\, B_0(0,m_f,m_f) + \frac{q^2}{3}\right]\right\}, \tag{3.2.7}$$

$$\Sigma_{T,W}^{AA}(q^2) = -\frac{\alpha}{4\pi}\left\{(3q^2+4M_W^2)\, B_0(q^2,M_W,M_W) - 4M_W^2\, B_0(0,M_W,M_W)\right\}, \tag{3.2.8}$$

where B_0 is the scalar two-point function which is uniquely specified by the momentum q^2 and the masses of the legs. If we take the derivatives with respect to q^2 we get

$$\frac{\partial\Sigma_{T,f}^{AA}}{\partial q^2} = -\frac{\alpha}{4\pi}\left\{\frac{2}{3}\, N_c^f\, 2\, Q_f^2\left[-B_0(q^2,m_f,m_f) - (q^2+2m_f^2)\frac{\partial}{\partial q^2}B_0(q^2,m_f,m_f) + \frac{1}{3}\right]\right\}, \tag{3.2.9}$$

$$\frac{\partial\Sigma_{T,W}^{AA}}{\partial q^2} = -\frac{\alpha}{4\pi}\left\{3B_0(q^2,M_W,M_W) + (3q^2+4M_W^2)\frac{\partial}{\partial q^2}B_0(q^2,M_W,M_W)\right\}. \tag{3.2.10}$$

We can now evaluate the equations above in the limit $q^2=0$ using

$$\left.\frac{\partial}{\partial q^2}B_0(q^2,m,m)\right|_{q^2=0} = \frac{1}{6m^2}, \tag{3.2.11}$$

so that eq. (3.2.5) becomes

$$\begin{aligned}\Pi^{AA}(0) &= -\frac{\alpha}{4\pi}\left\{\frac{2}{3}\sum_f N_c^f\, 2Q_f^2[-B_0(0,m_f,m_f)] + \left[3B_0(0,M_W,M_W) + \frac{2}{3}\right]\right\}\\ &= -\frac{\alpha}{4\pi}\left\{\underbrace{\frac{2}{3}\sum_f N_c^f\, 2Q_f^2\left[-\Delta_{\rm UV} + \log\frac{m_f^2}{\mu_{\rm D}^2}\right]}_{\text{fermions}} + \underbrace{3\left[\Delta_{\rm UV} - \log\frac{M_W^2}{\mu_{\rm D}^2}\right] + \frac{2}{3}}_{W\text{boson}}\right\},\end{aligned} \tag{3.2.12}$$

where we introduced the following notation to match the literature

$$\Delta_{\rm UV} \equiv \frac{\Gamma(1+\epsilon)}{\epsilon}\,(4\pi)^{\epsilon}\,. \tag{3.2.13}$$

Note that, in the on-shell scheme, $\Delta_{\rm UV}$ and $\mu_{\rm D}$ always come in the combination

$$\Delta_{\rm UV} - \log\frac{X^2}{\mu_{\rm D}^2} \tag{3.2.14}$$

where X is a generic scale of the problem. This introduces a dependence of the vacuum polarization on the logarithm of the masses of all the particles running in the loop, including the masses of the light quarks which are perturbatively ill-defined[4]. The issue with hadronic vacuum polarization will be discussed in details later.

We can proceed in the same way for the photon-Z two-point function. The fermionic part is given by

$$\Sigma^{AZ}_{T,f}(q^2) = -\frac{\alpha}{4\pi}\left\{\frac{2}{3}\,N_c^f(-Q_f)(g_f^+ + g_f^-)\left[-(q^2+2m_f^2)\,B_0(q^2,m_f,m_f)\right.\right.$$
$$\left.\left. + 2m_f^2\,B_0(0,m_f,m_f) + \frac{q^2}{3}\right]\right\}, \tag{3.2.15}$$

while the contribution coming from the W boson is

$$\Sigma^{AZ}_{T,W}(q^2) = -\frac{\alpha}{4\pi}\left\{-\frac{1}{3s_W c_W}\left[\left(\left(9c_W^2+\frac{1}{2}\right)q^2 + (12c_W^2+4)M_W^2\right)B_0(q^2,M_W,M_W)\right.\right.$$
$$\left.\left. - (12c_W^2-2)M_W^2\,B_0(0,M_W,M_W) + \frac{q^2}{3}\right]\right\}. \tag{3.2.16}$$

We note that for $q^2=0$

$$-(q^2+2m_f^2)\,B_0(q^2,m_f,m_f) + 2m_f^2\,B_0(0,m_f,m_f) = 0 \tag{3.2.17}$$

which means that, in the vanishing transfer momentum limit, all contributions to Σ_T^{AZ} originate from the W-boson loop, namely

$$\Sigma_T^{AZ}(0) = \Sigma_{T,W}^{AZ}(0) = -\frac{\alpha}{4\pi}\left\{-\frac{1}{3s_W c_W}\,6M_W^2\left(\Delta_{\rm UV} - \log\frac{M_W^2}{\mu_{\rm D}^2}\right)\right\}. \tag{3.2.18}$$

Putting all terms back together, eq. (3.2.2) becomes

$$\delta Z_e^{\rm OS}\Big|_{\alpha(0)} = -\frac{\alpha}{4\pi}\left\{\frac{2}{3}\sum_f N_c^f Q_f^2\left[-\Delta_{\rm UV} + \log\frac{m_f^2}{\mu_{\rm D}^2}\right] + \frac{7}{2}\left[\Delta_{\rm UV} - \log\frac{M_W^2}{\mu_{\rm D}^2}\right] + \frac{1}{3}\right\}. \tag{3.2.19}$$

[4]Quark masses can be estimated from mesons masses. However, being $q\bar{q}$ bound states, the values that can be extracted include also effects coming from the bounding energy.

This result explicitly includes mass-singular terms of the form $\alpha \log m_f^2$ for each light fermion f which practically speaking are contained in a new term that quantify the evolution of α induced by vacuum-polarization effects, coming from light fermions. More specifically we define

$$\Delta\alpha(M_Z^2) = \Pi^{AA}_{f\neq t}(0) - \mathrm{Re}\,\Pi^{AA}_{f\neq t}(M_Z^2), \tag{3.2.20}$$

where, excluding the top quark, all other fermions f contribute.

In order to compute $\Delta\alpha(M_Z^2)$, we can separate the contribution from fermions with well-defined masses, i.e. the leptonic contribution, from the hadronic one

$$\Delta\alpha(M_Z^2) = \Delta\alpha_L(M_Z^2) + \Delta\alpha_H(M_Z^2). \tag{3.2.21}$$

In the case of leptons we already have an expression for $\Pi_f^{AA}(0)$ that can be taken from eq. (3.2.12), so we just need to compute the second term in eq. (3.2.20). From eq. (3.2.4) we have

$$\Pi_f^{AA}(M_Z^2) = \frac{\Sigma^{AA}_{T,f}(M_Z^2)}{M_Z^2} = -\frac{\alpha}{4\pi}\frac{1}{M_Z^2}\left\{\frac{2}{3}N_c^f\,2Q_f^2\left[-(M_Z^2 - m_f^2)B_0(M_Z^2, m_f, m_f)\right.\right.$$
$$\left.\left. + 2m_q^2 B_0(0, m_f m_f) + \frac{M_Z^2}{3}\right]\right\}. \tag{3.2.22}$$

Assuming $M_Z \gg m_f$ we can take the $m_f \to 0$ limit

$$B_0(M_Z^2, m_f, m_f) \overset{m_f\to 0}{\to} \Delta_{\mathrm{UV}} + 2 - i\pi - \log\frac{M_Z^2}{\mu_{\mathrm{D}}^2} \tag{3.2.23}$$

so that

$$\mathrm{Re}\,\Pi_f^{AA}(M_Z^2) = -\frac{\alpha}{4\pi}\left\{\frac{2}{3}N_c^f\,2Q_f^2\left[-\Delta_{\mathrm{UV}} - \frac{5}{3} + \log\frac{M_Z^2}{\mu_{\mathrm{D}}^2}\right]\right\}. \tag{3.2.24}$$

Thus for a generic fermion f we would have

$$\Delta\alpha_f(M_Z^2) = -\frac{\alpha}{4\pi}\left\{\frac{2}{3}N_c^f\,2Q_f^2\left[\frac{5}{3} - \log\frac{M_Z^2}{m_f^2}\right]\right\} + \mathcal{O}\left(\frac{m_f^2}{M_Z^2}\right). \tag{3.2.25}$$

Note that there are contributions coming from $\Pi_f^{AA}(M_Z^2)$ that introduce a non-logarithmic dependence on the fermion mass and are power suppressed. Moreover, the result presented in eq. (3.2.25) is perfectly defined for leptons, but it still poses severe problems for light quarks, as they do not exist as free particles and they hadronize.

3.2.2 Hadronic vacuum polarization

The simplest and most straightforward way to solve the issue of hadronic vacuum polarization is just to define the light quark masses as non-physical parameters and enforce the constraint given by

$$\frac{\alpha(0)}{1-\Delta\alpha(M_Z^2)} = \alpha^{\text{exp.}}(M_Z^2) \tag{3.2.26}$$

where $\alpha^{\text{exp.}}(M_Z^2)$ is the experimentally measured value of the coupling constant at the scale of the Z boson mass and $\Delta\alpha(M_Z^2)$ is computed as a function of m_q. In practice this means using the same formal expression for $\Delta\alpha_f(M_Z^2)$ given for $f \in \{\text{leptons}\}$ in eq. (3.2.25) also for light quarks, while adjusting the values of the quark masses such that the resulting value equals the one obtained from experimental data.

Another option is to exploit the hadronic e^+e^- annihilation data by using an approach [123, 124] based on a dispersion relation and the optical theorem. In order to do so, let us slightly change the notation to match the literature

$$\Delta\alpha_f(q^2) = \left[\left.\frac{\partial\Sigma_{T,f}^{AA}(q^2)}{\partial q^2}\right|_{q^2=0} - \frac{\text{Re}\left(\Sigma_{T,f}^{AA}(q^2)\right)}{q^2} \right] = \Pi_f(0) - \Pi_f(q^2) \tag{3.2.27}$$

and

$$\Delta\alpha_H(q^2) = \sum_{f\in H} \Delta\alpha_f(q^2) \equiv -\,\text{Re}\,\hat{\Pi}(q^2). \tag{3.2.28}$$

We will show that

$$\text{Re}\,\hat{\Pi}(q^2) = \frac{\alpha}{3\pi}\, q^2\, \text{Re}\left[\int_{4m_\pi^2}^{\infty} ds\, \frac{R_{\text{had}}(s)}{s\,(q^2 - s + i\epsilon)}\right] \tag{3.2.29}$$

where

$$R_{\text{had}} = \frac{\sigma(e^+e^- \to \gamma^* \to \text{hadrons})}{\sigma(e^+e^- \to \gamma^* \to \mu^+\mu^-)} \tag{3.2.30}$$

is the ratio between the hadronic experimental cross section and the muon pair production cross section in e^+e^- annihilation.

We can start by briefly recalling the optical theorem, starting from the unitarity property of the $\mathbf{S}$ matrix

$$\mathbf{S} = \mathbb{1} + i\mathbf{T}, \qquad \mathbf{S}^\dagger\mathbf{S} = \mathbb{1}, \qquad -i(\mathbf{T} - \mathbf{T}^\dagger) = \mathbf{T}^\dagger\mathbf{T}, \tag{3.2.31}$$

where $\mathbf{S}$ and $\mathbf{T}$ are the customary scattering matrix and transition matrix respectively. Now if we write the generic matrix element between two states as

$$\langle f|\,\mathbf{T}\,|i\rangle = (2\pi)^4\,\delta^{(4)}(p_f - p_i)\,\mathrm{T}_{fi}\,, \tag{3.2.32}$$

via the insertion of a complete set of states written as $\mathbb{1} = \sum_n |n\rangle \langle n|$, we get

$$(2\pi)^4 \, \delta^{(4)}(p_f - p_i) \, (\mathrm{T}_{fi} - \mathrm{T}^*_{if}) = i \sum_n \langle f | \, \mathbf{T}^\dagger \, | n \rangle \, \langle n | \, \mathbf{T} \, | i \rangle \, , \tag{3.2.33}$$

so that

$$(\mathrm{T}_{fi} - \mathrm{T}^*_{if}) = i \sum_n (2\pi)^4 \, \delta^{(4)}(p_i - p_n) \, \mathrm{T}^*_{nf} \mathrm{T}_{in} \, . \tag{3.2.34}$$

If we consider an elastic scattering, that is $|i\rangle = |f\rangle$, then the real part on the left hand side cancels, namely

$$2 \, \mathrm{Im}(\mathrm{T}_{ii}) = \sum_n (2\pi)^4 \, \delta^{(4)}(p_i - p_n) \, |\mathrm{T}_{ni}|^2 = \sum_n 2s \, \sigma(i \to n). \tag{3.2.35}$$

This means that we can relate the imaginary part of the amplitude associated with the process, where the initial state goes into itself, to the total cross section with the same initial state, times a flux factor. Graphically we have

$$2 \, \mathrm{Im} \left[\quad \right] = 2s \sum_n \sigma \left[\quad \right] . \tag{3.2.36}$$

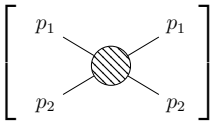

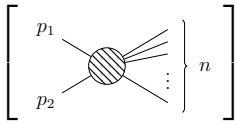

Going back to the fermionic contribution to the photon self energy we have that

$$\Pi^{AA}_f(q^2) \text{ is } \begin{cases} \text{real for } q^2 < 4m_*^2 \\ \text{complex for } q^2 > 4m_*^2 \end{cases}$$

where m_* corresponds to the lightest mass for producing a final-state pair of particles. In this context, it is given by the lightest hadron, i.e. the pion. It is possible to uniquely define an analytic continuation, $q^2 \to z \in \mathbb{C}$, such that

$$\Pi^{AA}_f(z) = \Pi^{AA^*}_f(z^*) \tag{3.2.37}$$

where

$$\begin{cases} \text{if } \mathrm{Re}(z) < 4m_\pi^2 \text{ then } \Pi^{AA}_f(z) \text{ is continuous,} \\ \text{if } \mathrm{Re}(z) > 4m_\pi^2 \text{ then we need a branch cut on the real axis.} \end{cases}$$

In order to compute $\Pi^{AA}_f(q^2)$ we can employ Cauchy's integral theorem that states that the value of a generic complex function f in a point z_0 in the complex plane can be obtained from the following integration

$$f(z_0) = \frac{1}{2\pi i} \oint_\Gamma dz' \frac{f(z')}{z' - z_0} \tag{3.2.38}$$

provided that z_0 is found within the region of the complex plane bounded by the contour Γ. We refer to Fig. 3.1 for the depiction of a convenient contour for this

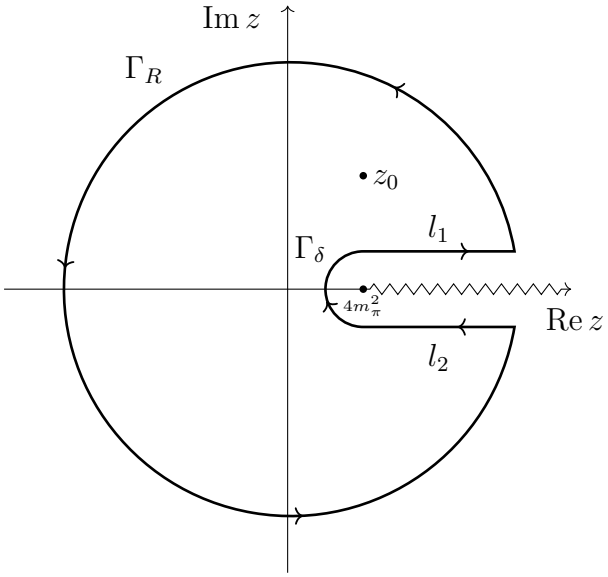

Figure 3.1: Integration contour for a function defined with a branch cut on the real axis, starting from $4m_\pi^2$.

integration. In the limit $R \to \infty$, the external circular contour denoted as Γ_R stretches to infinity in all directions on the complex plane. Assuming that $f(z) \to 0$ as $|z| \to \infty$ faster than $1/|z|^2$, the integral over Γ_R gives zero contribution. Similarly, in the limit $\delta \to 0$ the internal contour Γ_δ shrinks to a point and the integral over it vanishes. Thus if we take $z_0 = q^2 + i\epsilon$ with $\epsilon > \delta$, namely we move slightly away in the complex plane from the branch cut, we can compute the integral in eq. (3.2.38) as the sum of the two linear integrals over l_1 and l_2. We have

$$f(q^2 + i\epsilon) = \frac{1}{2\pi i} \int_{4m_\pi^2}^{\infty} dx \, \frac{f(x + i\delta) - f(x - i\delta)}{x - q^2 - i\epsilon}, \qquad x \in \mathbb{R}. \tag{3.2.39}$$

Using the property in eq. (3.2.37) and taking the $\delta \to 0$ limit, we get

$$\mathrm{Re}\,\Pi(q^2) = \mathrm{Re}\left[\frac{1}{\pi} \int_{4m_\pi^2}^{\infty} ds \frac{\mathrm{Im}\,\Pi(s)}{s - q^2 - i\epsilon}\right]. \tag{3.2.40}$$

Now if we consider the scattering process $e^+e^- \to e^+e^-$ in the forward limit we have

$$\begin{aligned} i\mathcal{M} = &\left[\quad\right] \\ &= (-ie)^2 \overline{u}(p_1)\gamma^\mu v(p_2) \left[-\frac{i}{q^2}(-\Pi(q^2))\right] \overline{v}(p_2)\gamma_\mu u(p_1) \end{aligned} \tag{3.2.41}$$

where $q = p_1 + p_2$ is the momentum of the virtual photon. Taking the trace

$$\mathrm{Tr}\,(\gamma^\mu v(p_2)\overline{v}(p_2)\gamma_\mu u(p_1)\overline{u}(p_1)) = -4q^2 \tag{3.2.42}$$

we end up with $\langle \mathcal{M} \rangle_{\text{spin}} = e^2 \Pi(q^2)$ where we use the notation $\langle \dots \rangle_{\text{spin}}$ to denote the appropriate sum and average over the spin of the external states. Thus, using the optical theorem given by eq. (3.2.35), we can write

$$\operatorname{Im} \Pi(q^2) = \frac{q^2}{e^2} \langle \sigma(q^2) \rangle_{\text{spin}}^{e^+e^- \to \text{hadrons}} \tag{3.2.43}$$

where q^2 is the flux factor for this process. Moreover, if we use the definition R_{had} in eq. (3.2.30) and the well known result for the $e^+e^- \to \mu^+\mu^-$ cross section

$$\langle \sigma(q^2) \rangle_{\text{spin}}^{e^+e^- \to \mu^+\mu^-} = \frac{4\pi\alpha^2}{3q^2}, \tag{3.2.44}$$

we end up with

$$\operatorname{Im} \Pi(q^2) = \frac{q^2}{e^2} R_{\text{had}}(q^2) \langle \sigma(q^2) \rangle_{\text{spin}}^{e^+e^- \to \mu^+\mu^-} = \frac{\alpha}{3} R_{\text{had}}(q^2) \tag{3.2.45}$$

which, together with eq. (3.2.40), gives us

$$\operatorname{Re} \Pi(q^2) = \frac{\alpha}{3\pi} \operatorname{Re} \left[\int_{4m_\pi^2}^{\infty} ds \frac{R_{\text{had}}(s)}{q^2 - s + i\epsilon} \right]. \tag{3.2.46}$$

In order to arrive to the final result in eq. (3.2.29) we need to discuss two remaining issues:

- In general the photon self-energy is not a finite quantity as it contains $1/\epsilon$ poles of ultraviolet origin. This means that $\Pi(q^2)$ does not meet the requirements for the use of Cauchy's integral formula, as its analytic continuation is not a holomorphic function.
- Unlike $\Pi(q^2)$, the quantity $\hat{\Pi}(q^2)$ does not comply with the condition $f(z) \to 0$ for $|z| \to \infty$ since, as can be seen from the definition in eq. (3.2.27), it contains $\Pi(0)$ which is constant in q^2.

To overcome these issues we can first take the non-divergent part of $\Pi(q^2)$ by removing the term containing the ultraviolet pole, namely

$$\Pi(q^2) - P_{\text{UV}}. \tag{3.2.47}$$

Since the poles are purely real, that is $\operatorname{Im} P_{\text{UV}} = 0$, we have that

$$\operatorname{Re} \Pi(q^2) - P_{\text{UV}} = \operatorname{Re} \left[\frac{1}{\pi} \int_{4m_\pi^2}^{\infty} ds \, \frac{\operatorname{Im} \Pi(s)}{s - q^2 - i\epsilon} \right] \tag{3.2.48}$$

and for $q^2 \to 0$ we get

$$\Pi(0) - P_{\text{UV}} = \left[\frac{1}{\pi} \int_{4m_\pi^2}^{\infty} ds \, \frac{\operatorname{Im} \Pi(s)}{s - i\epsilon} \right]. \tag{3.2.49}$$

Finally, putting all terms together, gives us

$$\begin{aligned}\mathrm{Re}\,\hat{\Pi}(q^2) &= \mathrm{Re}\,\Pi(q^2) - \Pi(0) \\ &= \mathrm{Re}\left[\frac{1}{\pi}\int_{4m_\pi^2}^{\infty} ds\,\left(\frac{\mathrm{Im}\,\Pi(s)}{s-q^2-i\epsilon} - \frac{\mathrm{Im}\,\Pi(s)}{s-i\epsilon}\right)\right] \\ &= \mathrm{Re}\left[\frac{1}{\pi}\,q^2\int_{4m_\pi^2}^{\infty} ds\,\frac{\mathrm{Im}\,\Pi(s)}{s(s-q^2-i\epsilon)}\right] \\ &= \frac{\alpha}{3\pi}\,q^2\,\mathrm{Re}\left[\int_{4m_\pi^2}^{\infty} ds \frac{R_{\mathrm{had}}(s)}{s\,(q^2-s+i\epsilon)}\right].\end{aligned} \tag{3.2.50}$$

3.2.3 The $\alpha(M_Z)$ scheme

In order to remove the problematic dependence on the light-quark masses, which is explicit in the result presented in eq. (3.2.19), it is convenient to move to a different scheme for the definition of the coupling constant. By including the evolution via renormalization group equation from $Q^2 = 0$ to $Q^2 = M_Z^2$ in the input value for α, in fact, one effectively resums the problematic contribution in the definition of the coupling. Therefore we have

$$\alpha(M_Z^2) = \frac{\alpha(0)}{1-\Delta\alpha(M_Z^2)} \tag{3.2.51}$$

where $\Delta\alpha(M_Z^2)$ is defined as in eq. (3.2.20). The introduction of this correction amounts to a difference of roughly 6% in the input value of the coupling. Moving to the $\alpha(M_Z)$ scheme, that is removing $\alpha(0)$ in favour of $\alpha(M_Z)$ at LO, means that at loop order the $\Delta\alpha(M_Z^2)$ terms are subtracted, resulting in the cancellation of light-fermion mass logarithms from the charge renormalization for the EW corrections. In practice, the implementation of the scheme, requires a replacement of δZ_e in eq.(3.2.2) with

$$\delta Z_e^{\mathrm{OS}}\Big|_{\alpha(M_Z)} = \frac{1}{2}\,\Pi^{AA}(0) - \frac{s_W}{c_W}\frac{\Sigma_T^{AZ}(0)}{M_Z^2} - \frac{1}{2}\Delta\alpha(M_Z^2). \tag{3.2.52}$$

This is the appropriate scheme choice for processes with only internal photons, as it guarantees the complete cancellations of the unpleasant fermion mass logarithms. If external photons are present, however, the EW corrections naturally include the photon wave-function renormalization constant, δZ_A, that already contains the terms needed to cancel the aforementioned logarithms. This is a consequence of the QED Ward identity which can be written as

$$\delta Z_e^{\mathrm{OS}} = -\frac{1}{2}\delta Z_A^{\mathrm{OS}}. \tag{3.2.53}$$

This relation is tied to the fact that external photons couple with the scale $Q^2 = 0$, which corresponds to the pure $\alpha(0)$ scheme[5]. As a consequence, if we consider a

[5] This is valid only if the photon acts as a proper external state and not, for example, in the case of photon-induced processes in hadronic collisions where the photon is considered as part of the content of the proton.

process with m external photons, the coupling factor α^n in the LO cross section should be parametrized as $\alpha(0)^m\alpha(M_Z^2)^{n-m}$. This defines a mixed scheme in which these large logarithms originating from light fermion masses can be avoided.

3.2.4 The G_μ scheme

In this scheme the input value α_{G_μ} for the electromagnetic coupling is defined from the Fermi constant G_μ, which is known with high precision from muon decay. Numerically we have

$$\alpha_{G_\mu} \equiv \frac{\sqrt{2}G_\mu M_W^2(M_Z^2 - M_W^2)}{\pi M_Z^2} \approx 1/132. \tag{3.2.54}$$

This scheme provides the opportunity to absorb some universal corrections related to the renormalization of the weak mixing angle in the LO contributions. More specifically we can define the following relation

$$\alpha_{G_\mu} = \alpha(0)\left(1 - \Delta r^{(1)}\right) + \mathcal{O}(\alpha^3), \tag{3.2.55}$$

where the factor $\Delta r^{(1)}$ represents the full one-loop electroweak corrections to the muon decay which, following the notation of Refs. [117, 125], can be written as

$$\Delta r^{(1)} = \Delta\alpha(M_Z^2) - \frac{c_W^2}{s_W^2}\Delta\rho^{(1)} + \Delta r_{\text{rem}}, \tag{3.2.56}$$

with $\Delta\rho^{(1)}$ being the universal correction to the ρ-parameter, which is defined as

$$\Delta\rho^{(1)} = \frac{\Sigma_T^{ZZ}(0)}{M_Z^2} - \frac{\Sigma_T^{W}(0)}{M_W^2}, \tag{3.2.57}$$

and a small remainder given by

$$\begin{aligned}\Delta r_{\text{rem}} = \text{Re}\,\frac{\Sigma_T^{AA}(M_Z^2)}{M_Z^2} - 2\frac{c_W}{s_W}\frac{\Sigma_T^{AZ}(0)}{M_Z^2} - \frac{c_W^2}{s_W^2}\frac{\Sigma_T^{ZZ}(M_Z^2) - \Sigma_T^{ZZ}(0)}{M_Z^2} \\ - \left(\frac{c_W^2}{s_W^2} - 1\right)\frac{\Sigma_T^{W}(M_W^2) - \Sigma_T^{W}(0)}{M_W^2} + \frac{\alpha(0)}{4\pi s_W^2}\left(6 + \frac{7 - 4s_W^2}{2s_W^2}\log c_W^2\right).\end{aligned} \tag{3.2.58}$$

As far as the running of the electromagnetic coupling is concerned, the G_μ scheme is similar to the $\alpha(M_Z)$ scheme, as in both schemes the input value of α is given at some electroweak scale. This makes both schemes preferable over the $\alpha(0)$ scheme as long as external photons are not involved. In particular, since the definition of $\Delta r^{(1)}$ contains $\Delta\alpha(M_Z^2)$, the G_μ scheme naturally reabsorbs the mass logarithmic terms that appear in the charge renormalization factor. Indeed we have

$$\delta Z_e^{\text{OS}}\Big|_{G_\mu} = \frac{1}{2}\Pi^{AA}(0) - \frac{s_W}{c_W}\frac{\Sigma_T^{AZ}(0)}{M_Z^2} - \frac{1}{2}\Delta r^{(1)}. \tag{3.2.59}$$

Moreover due to the presence of the factor $\Delta\rho^{(1)}$, which originates from the OS renormalization of the weak mixing angle, this scheme is the most appropriate choice when describing processes in which the W boson is involved, while it is actually not well suited for photonic couplings.

3.3 Renormalization in the $\overline{\text{MS}}$ scheme

Sometimes the $\overline{\text{MS}}$ scheme is preferred over the OS scheme for the renormalization of the EW gauge couplings. While one could, in principle, employ the $\overline{\text{MS}}$ scheme also in the renormalization of the masses, typically a hybrid scheme is chosen. Usually this translates in the masses being defined on shell and so is the external photon wave-function renormalization counterterm, while the electric charge and the weak mixing angle are renormalized in the $\overline{\text{MS}}$ scheme. The $\overline{\text{MS}}$ counterterms are obtained by taking their OS counterparts and by keeping only the Δ_{UV} term with the replacement

$$\Delta_{\text{UV}} \to \Delta_{\text{UV}} - \log \frac{\mu_{\text{R}}^2}{\mu_{\text{D}}^2}. \tag{3.3.1}$$

Although the choice of both scales in the previous equation is in principle arbitrary, we must stress an important difference between them. If the value of the renormalization scale μ_{R} does not affect the result of the computation once all terms in the perturbative expansion are taken into account, the truncation of the series introduces a dependence on μ_{R}, typically be estimated via a scale-variation procedure. The choice of the dimensional regularization scale μ_{D}, instead, has no effect at all on the result of the computation, provided that the same choice is applied in the computation of the amplitudes. Practically speaking, the logarithms resulting from the $\epsilon \to 0$ expansion of Δ_{UV} cancel the dependence of the amplitude on μ_{D}, trading it for a dependence on the renormalization scale.

For the charge renormalization factor we then would have

$$\begin{aligned}\delta Z_e^{\overline{\text{MS}}}(\mu_{\text{R}}^2) &= \left[\frac{1}{2}\,\Pi^{AA}(0) - \frac{s_W}{c_W}\frac{\Sigma_T^{AZ}(0)}{M_Z^2}\right]_{\text{UV}} \\ &= -\frac{\alpha(\mu_{\text{R}}^2)}{4\pi}\left\{\frac{2}{3}\sum_f N_c^f Q_f^2\left[-\Delta_{\text{UV}} + \log\frac{\mu_{\text{R}}^2}{\mu_{\text{D}}^2}\right] + \frac{7}{2}\left[\Delta_{\text{UV}} - \log\frac{\mu_{\text{R}}^2}{\mu_{\text{D}}^2}\right]\right\},\end{aligned} \tag{3.3.2}$$

where $\alpha(\mu_{\text{R}}^2) = e^2(\mu_{\text{R}}^2)/4\pi$ is the value of the renormalized fine structure constant in the $\overline{\text{MS}}$ scheme evaluated at the renormalization scale μ_{R}^2. Note that in eq. (3.3.2) all particles contributing to the self energy are considered light particles, i.e. with a mass $m < \mu_{\text{R}}$, thus the equation is only valid for the degrees of freedom that are lighter than μ_{R}^2. In order to avoid spurious logarithms, we then have to account for the decoupling of the heavier degrees of freedom by subtracting their contribution. In general this decoupling procedure can be defined for any particle, as the renormalization scale can, in principle, be taken small. For fermions the decoupling is given by the replacement

$$\delta Z_e^{\overline{\text{MS}}}(\mu_{\text{R}}^2) \to \delta Z_e^{\overline{\text{MS}}}(\mu_{\text{R}}^2) - \frac{\alpha(\mu_{\text{R}}^2)}{4\pi}\left[\frac{2}{3}\sum_f N_c^f Q_f^2\,\theta(m_f^2 - \mu_{\text{R}}^2)\log\frac{m_f^2}{\mu_{\text{R}}^2}\right], \tag{3.3.3}$$

while for the W boson the procedure is a bit more delicate as it depends on whether $\alpha(\mu_{\text{R}}^2)$ is defined with a threshold shift[6] at $\mu_{\text{R}}^2 = M_W^2$ or not. We have

$$\delta Z_e^{\overline{\text{MS}}}(\mu_{\text{R}}^2) \to \delta Z_e^{\overline{\text{MS}}}(\mu_{\text{R}}^2) - \frac{\alpha(\mu_{\text{R}}^2)}{4\pi}\left[-\frac{7}{2}\log\frac{M_W^2}{\mu_{\text{R}}^2} + \frac{1}{3}\right]\theta(M_W^2 - \mu_{\text{R}}^2). \tag{3.3.4}$$

It is important to note that the decoupling term contains exactly the contribution needed to go back to the OS scheme. For example, for every decoupled fermion ($m_f^2 > \mu_{\text{R}}^2$) we have

$$\delta Z_{e,f}^{\overline{\text{MS}}}(\mu_{\text{R}}^2) = -\frac{\alpha(\mu_{\text{R}}^2)}{4\pi}\left\{\frac{2}{3}N_c^2 Q_f^2\left[-\Delta_{\text{UV}} + \log\frac{\mu_{\text{R}}^2}{\mu_{\text{D}}^2} + \log\frac{m_f^2}{\mu_{\text{R}}^2}\right]\right\} = \delta Z_{e,f}^{\text{OS}} \tag{3.3.5}$$

and for the decoupling of the W boson

$$\delta Z_{e,W}^{\overline{\text{MS}}}(\mu_{\text{R}}^2) = -\frac{\alpha(\mu_{\text{R}}^2)}{4\pi}\left\{\frac{7}{2}\left[\Delta_{\text{UV}} - \log\frac{\mu_{\text{R}}^2}{\mu_{\text{D}}^2} - \log\frac{M_W^2}{\mu_{\text{R}}^2} + \frac{1}{3}\right]\right\} = \delta Z_{e,W}^{\text{OS}}. \tag{3.3.6}$$

For processes involving external photons it is customary to define a hybrid scheme, as mentioned before, where the wave-function renormalization factor for each external photon is computed in the on-shell scheme, that is

$$\delta Z_A^{\text{OS}} = 2\,\frac{\alpha}{4\pi}\sum_f \frac{2}{3}N_c^f Q_f^2\left[-\Delta_{\text{UV}} + \log\frac{m_f^2}{\mu_{\text{D}}^2}\right], \tag{3.3.7}$$

where, for simplicity, we are only considering the fermionic contributions. Note that for each external photon vertex we then have

$$\alpha(\mu_{\text{R}}^2)\left(1 + 2\delta Z_e^{\overline{\text{MS}}}(\mu_{\text{R}}^2) + \delta Z_A^{\text{OS}}\right) \tag{3.3.8}$$

and taking $\mu_{\text{R}}^2 = 0$, which is the prescription for external photons, we get

$$\alpha(\mu_{\text{R}}^2 = 0)\left(1 + 2\delta Z_e^{\overline{\text{MS}}}(\mu_{\text{R}}^2 = 0) + \delta Z_A^{\text{OS}}\right) = \alpha_0\left(1 + 2\delta Z_e^{\text{OS}} + \delta Z_A^{\text{OS}}\right) = \alpha_0. \tag{3.3.9}$$

For vertices with internal photons we can instead write the well-known relation between the bare parameters and renormalized ones both for the OS and $\overline{\text{MS}}$ couplings

$$e_0 = \left(1 + \delta Z_e^{\text{OS}}\right)e^{\text{OS}} = \left(1 + \delta Z_e^{\overline{\text{MS}}}(\mu_{\text{R}}^2)\right)e^{\overline{\text{MS}}}(\mu_{\text{R}}^2), \tag{3.3.10}$$

to introduce a prescription to go from the on-shell scheme to $\overline{\text{MS}}$. Note that the previous identity is well defined for all the OS-scheme choices related to the input value of the coupling constant presented in this section. If we take the $\alpha(0)$ scheme, for example, eq. (3.3.10) yields the following solution for the conversion of α^{OS} in $\overline{\text{MS}}$

$$\alpha(\mu_{\text{R}}^2) = \frac{\alpha(0)}{1 - \Delta\alpha^{\overline{\text{MS}}}(\mu_{\text{R}}^2)}, \tag{3.3.11}$$

[6] Additional details on this can be found in Ref. [126] and references therein.

with the definition

$$\Delta\alpha^{\overline{\text{MS}}}(\mu_{\text{R}}^2) = 2\left[\delta Z_e^{\text{OS}} - \delta Z_e^{\overline{\text{MS}}}(\mu_{\text{R}}^2)\right]. \tag{3.3.12}$$

The charge renormalization factors δZ_e^{OS} and $\delta Z_e^{\overline{\text{MS}}}(\mu_{\text{R}}^2)$ have, by construction, the same Δ_{UV} terms but paired with different logarithms, as can be seen in eqs. (3.2.14) and (3.3.1). This means that, in eq. (3.3.12), the two Δ_{UV} cancel each other leaving behind a term proportional to $\log(X^2/\mu_{\text{R}}^2)$, X being the generic scale in eq. (3.2.14). In addition we have the non-logarithmic finite contributions in δZ_e^{OS} and the terms related to the decoupling,

$$\begin{aligned}\Delta\alpha^{\overline{\text{MS}}}(\mu_{\text{R}}^2) = -2\,\frac{\alpha}{4\pi}\Bigg\{&\frac{2}{3}\sum_f N_c^2 Q_f^2 \log\frac{m_f^2}{\mu_{\text{R}}^2}\theta(\mu_{\text{R}}^2 - m_f^2) \\ &+\left[-\frac{7}{2}\log\frac{M_W^2}{\mu_{\text{R}}^2} + \frac{1}{3}\right]\theta(\mu_{\text{R}}^2 - M_W^2)\Bigg\},\end{aligned} \tag{3.3.13}$$

where we used

$$\log\frac{M^2}{\mu_{\text{R}}^2} - \log\frac{M^2}{\mu_{\text{R}}^2}\,\theta(M^2 - \mu_{\text{R}}^2) = \log\frac{M^2}{\mu_{\text{R}}^2}\,\theta(\mu_{\text{R}}^2 - M^2). \tag{3.3.14}$$

In this work, in order to avoid the complications introduced by the light quark masses, we first perform the computation in the OS scheme and then move to the $\overline{\text{MS}}$ scheme with the masses of all light quarks set to 0.

As a result, the decoupling described by eq. (3.3.3) needs to be implemented only for the top quark and the leptons, while the contribution coming from the light quarks is authomatically included in the input value of the coupling constant, as well as in its running.

Chapter 4

The MiNLO method for massive final state emitters

In this chapter we discuss the modifications of the MiNLO formalism needed to properly describe the production of massive final-state emitting particles. We start by presenting the resummation formalism for the case of heavy-quark pair production following the notation introduced in Ref. [127] and [128]. To this purpose we consider the production process of a heavy-quark pair

$$h_1(P_1) + h_2(P_2) \to Q(p_3) + \bar{Q}(p_4) + X \tag{4.0.1}$$

where X is to be intended as an arbitrary undetected final state. In the center-of-mass frame of the collision, the kinematics of the final state is fully specified by the invariant mass M of the heavy-quark pair, $M^2 = q^2$ with $q^\mu = p_3^\mu + p_4^\mu$, the transverse-momentum vector $\vec{q}_{\rm T}$[1] and the rapidity $y = \frac{1}{2}\log\frac{q\cdot P_1}{q\cdot P_2}$. Analogously, the individual momenta p_3^μ (p_4^μ) of the heavy quarks are specified by the heavy-quark mass m_Q, the rapidity y_3 (y_4) and the transverse-momentum vector $\vec{p}_{\rm T3}$ ($\vec{p}_{\rm T4}$).

The fully-differential cross section for this process is given by

$$\frac{d\sigma_{h_1h_2\to Q\bar{Q}+X}(s,\vec{q}_{\rm T},y,M,\Phi_{Q\bar{Q}})}{d^2\vec{q}_{\rm T}\,dM^2\,dy\,d\Phi_{Q\bar{Q}}} = \frac{1}{s}\sum_{a_1,a_2}\int_{x_1}^1\frac{dz_1}{z_1}\int_{x_2}^1\frac{dz_2}{z_2}$$
$$\times f_{a_1/h_1}\left(\frac{x_1}{z_1},\mu_{\rm F}^2\right) f_{a_2/h_2}\left(\frac{x_2}{z_2},\mu_{\rm F}^2\right)\frac{d\hat{\sigma}_{a_1a_2\to Q\bar{Q}+X}(\vec{q}_{\rm T},z_1,z_2,M,\Phi_{Q\bar{Q}},\alpha_s(\mu_{\rm R}^2),\mu_{\rm R}^2,\mu_{\rm F}^2)}{d^2\vec{q}_{\rm T}\,dz_1\,dz_2\,d\Phi_{Q\bar{Q}}}, \tag{4.0.2}$$

where $\Phi_{Q\bar{Q}}$ is just a place-holder for an independent set of kinematical variables needed to specify the distribution of the two final-state quarks with respect to the

[1] To make contact with the literature, in this chapter we will use $q_{\rm T}$ instead of $p_{\rm T}$ to denote the transverse momentum.

momentum q of the $Q\bar{Q}$ pair. The hadronic scaling variables x_1 and x_2 are defined as

$$x_1 = \frac{M}{\sqrt{s}} e^{y} \qquad x_2 = \frac{M}{\sqrt{s}} e^{-y} \tag{4.0.3}$$

so that $M^2 = x_1 x_2 s$ and $y = \frac{1}{2}\log(x_1/x_2)$. In the same way, the partonic scaling variables z_1 and z_2 are used to express the energy fractions carried by the parton entering the hard process

$$z_1 = \frac{M}{\sqrt{\hat{s}}} e^{\hat{y}} \qquad z_2 = \frac{M}{\sqrt{\hat{s}}} e^{-\hat{y}} \tag{4.0.4}$$

so that of course $M^2 = z_1 z_2 \hat{s}$ and $\hat{y} = \frac{1}{2}\log(z_1/z_2)$.

In the large transverse-momentum region, namely $q_{\mathrm{T}} \sim M$, the perturbative expansion of the cross section is controlled by the usual expansion parameter, namely the coupling constant α_s, and the fixed-order computation is well suited to describe the scattering process. In the small-q_{T} region, however, logarithmic contributions of the type $\log^n(M^2/q_{\mathrm{T}}^2)$ contained in the cross section become large and spoil the perturbative expansion. To separate the two regions, we can split the hadronic cross section into singular and finite components:

$$\frac{d\sigma_{h_1 h_2 \to Q\bar{Q}+X}}{d^2\vec{q}_{\mathrm{T}}\, dM^2\, dy\, d\Phi_{Q\bar{Q}}} = \frac{d\sigma^{(\mathrm{sing.})}_{h_1 h_2 \to Q\bar{Q}+X}}{d^2\vec{q}_{\mathrm{T}}\, dM^2\, dy\, d\Phi_{Q\bar{Q}}} + \frac{d\sigma^{(\mathrm{fin.})}_{h_1 h_2 \to Q\bar{Q}+X}}{d^2\vec{q}_{\mathrm{T}}\, dM^2\, dy\, d\Phi_{Q\bar{Q}}}. \tag{4.0.5}$$

This decomposition of the hadronic cross section implies a corresponding decomposition of the partonic cross section

$$\frac{d\hat{\sigma}_{a_1 a_2 \to Q\bar{Q}+X}}{d^2\vec{q}_{\mathrm{T}}\, dz_1\, dz_2\, d\Phi_{Q\bar{Q}}} = \frac{d\hat{\sigma}^{(\mathrm{sing.})}_{a_1 a_2 \to Q\bar{Q}+X}}{d^2\vec{q}_{\mathrm{T}}\, dz_1\, dz_2\, d\Phi_{Q\bar{Q}}} + \frac{d\hat{\sigma}^{(\mathrm{fin.})}_{a_1 a_2 \to Q\bar{Q}+X}}{d^2\vec{q}_{\mathrm{T}}\, dz_1\, dz_2\, d\Phi_{Q\bar{Q}}}. \tag{4.0.6}$$

The first term on the right-hand side $d\hat{\sigma}^{(\mathrm{sing.})}$ contains all the contributions that are singular in the small transverse-momentum limit. This includes both the usual logarithmically-enhanced terms and also the contributions proportional to $\delta(\vec{q}_{\mathrm{T}})$. The second term, instead, is finite in this limit and can be obtained by fixed-order truncation of the perturbative series. More precisely we define the finite component such that

$$\lim_{Q\to 0} \int_0^{Q^2} dq_{\mathrm{T}}^2 \left[\frac{d\hat{\sigma}^{(\mathrm{fin.})}(q_{\mathrm{T}}^2)}{dq_{\mathrm{T}}^2}\right]_{\mathrm{f.o.}} = 0 \tag{4.0.7}$$

order-by-order in perturbation theory. In the equation above the notation $[F]_{\mathrm{f.o.}}$ means that the quantity F is computed by truncating its perturbative expansion at a given fixed order in α_s.

4.1 Structure of the cross section at small $q_{\rm T}$

For the purpose of this section we shall focus on the singular part of the cross section which can be written as an inverse two-dimensional Fourier transformation with respect to the impact parameter $\vec{b}$

$$\frac{d\hat{\sigma}^{(\rm sing.)}_{a_1a_2\to Q\bar{Q}+X}}{d^2\vec{q}_{\rm T}\,dz_1\,dz_2\,d\Phi_{Q\bar{Q}}} = \frac{M^2}{\hat{s}}\int\frac{d^2\vec{b}}{(2\pi)^2}\,e^{i\vec{b}\cdot\vec{q}_{\rm T}}\,\mathcal{W}^{Q\bar{Q}}_{a_1a_2}(\hat{s},b,z_1,z_2,\Phi_{Q\bar{Q}};\alpha_s(\mu_{\rm R}^2),\mu_{\rm R}^2,\mu_{\rm F}^2). \tag{4.1.1}$$

This expression embodies the all-order resummation of the large logarithms $\log M^2b^2$ at large b [127]. For processes mediated by $q\bar{q}$ annihilation at tree level, the dependence of the partonic resummation factor $\mathcal{W}^{Q\bar{Q}}_{a_1a_2}$ on the impact parameter relies only on the modulus b and not on the azimuthal angle ϕ_b. Thus it is customary in literature to perform the angular integral

$$\begin{aligned}\int\frac{d^2\vec{b}}{4\pi}\,e^{i\vec{b}\cdot\vec{q}_{\rm T}}\,f(b^2) &= \frac{1}{2}\int_0^\infty b\,db\int_0^{2\pi}\frac{d\phi_b}{2\pi}\,e^{i\,b\,q_{\rm T}\cos\phi_b}\,f(b^2)\\ &= \frac{1}{2}\int_0^\infty db\,b\,J_0(bq_{\rm T})\,f(b^2)\end{aligned} \tag{4.1.2}$$

where the 0-th order Bessel function $J_0(z)$ is defined as

$$J_0(z) = \frac{1}{\pi}\int_0^\pi e^{iz\cos\theta}d\theta. \tag{4.1.3}$$

Therefore, the two-dimensional Fourier transform is often replaced by a one-dimensional Bessel transform, allowing eq. (4.1.1) to be written as

$$\frac{d\hat{\sigma}^{(\rm sing.)}_{a_1a_2\to Q\bar{Q}+X}}{dq_{\rm T}^2\,dz_1\,dz_2\,d\Phi_{Q\bar{Q}}} = \frac{M^2}{\hat{s}}\int_0^\infty db\,\frac{b}{2}\,J_0(bq_{\rm T})\,\mathcal{W}^{Q\bar{Q}}_{a_1a_2}(\hat{s},b,z_1,z_2,\Phi_{Q\bar{Q}};\alpha_s(\mu_{\rm R}^2),\mu_{\rm R}^2,\mu_{\rm F}^2) \tag{4.1.4}$$

where we used the fact that the integrand depends on $\vec{q}_{\rm T}$ only via its modulus to write

$$\frac{d\hat{\sigma}^{(\rm sing.)}_{a_1a_2\to Q\bar{Q}+X}}{d^2\vec{q}_{\rm T}\,dz_1\,dz_2\,d\Phi_{Q\bar{Q}}} = \frac{1}{\pi}\frac{d\hat{\sigma}^{(\rm sing.)}_{a_1a_2\to Q\bar{Q}+X}}{dq_{\rm T}^2\,dz_1\,dz_2\,d\Phi_{Q\bar{Q}}}. \tag{4.1.5}$$

This expression in eq. (4.1.4) contains, in the process-dependent term $\mathcal{W}^{Q\bar{Q}}_{a_1a_2}$, the all-order dependence on the large logarithms, which upon the Bessel integration correspond to the $q_{\rm T}$-space terms $\log(M^2/q_{\rm T}^2)$.

There is some arbitrariness in the factorization between constant and logarithmic terms [129, 130] which results in an intrinsic ambiguity in the choice of the logarithm taken to be resummed. Indeed, the argument of the b-space logarithms that appear in $\mathcal{W}^{Q\bar{Q}}_{a_1a_2}$ can be rescaled as $\log M^2b^2 = \log Q^2b^2 + \log M^2/Q^2$ as long as Q^2 does not depend on the impact parameter b and provided that $\log M^2/Q^2 = \mathcal{O}(1)$ if

$bM \gg 1$. Thus an auxiliary scale Q, such that $Q \sim M$, can be introduced to define the logarithmic expansion parameter L_b as

$$L_b \equiv \log \frac{Q^2 b^2}{b_0^2} \tag{4.1.6}$$

where $b_0 = 2e^{-\gamma_E}$ ($\gamma_E = 0.5772\ldots$ is the Euler-Mascheroni constant).

Note that the role played by the auxiliary scale Q is similar to the one attributed to the renormalization (factorization) scale $\mu_{\rm R}$ ($\mu_{\rm F}$) in the context of renormalization (factorization). The all-order resummed cross section is independent of Q and the explicit dependence only appears when it is truncated at some level of logarithmic accuracy. As it is the case for $\mu_{\rm R}$ and $\mu_{\rm F}$, one can estimate the uncertainties associated with the choice of the value of the scale Q by taking variations around its central value $Q = M$. These estimations are, however, beyond the purpose of this work.

The singular component of the hadronic cross section can be written as

$$\frac{d\sigma^{(\rm sing.)}_{h_1h_2\to Q\bar{Q}+X}}{d^2\vec{q}_{\rm T}\, dM^2\, dy\, d\Phi_{Q\bar{Q}}} = \frac{M^2}{s}\int \frac{d^2\vec{b}}{(2\pi)^2}\, e^{i\vec{b}\cdot\vec{q}_{\rm T}}\, W^{Q\bar{Q}}_{h_1h_2}(s, b, y, M, \Phi_{Q\bar{Q}}; \alpha_s(\mu_{\rm R}^2), \mu_{\rm R}^2, \mu_{\rm F}^2). \tag{4.1.7}$$

The factor $W^{Q\bar{Q}}_{h_1h_2}$ is given by

$$W^{Q\bar{Q}}_{h_1h_2} = \sum_{a_1,a_2}\int_{x_1}^1 \frac{dz_1}{z_1}\int_{x_2}^1 \frac{dz_2}{z_2}\, f_{a_1/h_1}\left(\frac{x_1}{z_1}, \frac{b_0^2}{b^2}\right)\, f_{a_2/h_2}\left(\frac{x_2}{z_2}, \frac{b_0^2}{b^2}\right) \times \sum_c \sigma^{(0)}_{c\bar{c},Q\bar{Q}}\, e^{-S_{c\bar{c}}(\frac{b_0}{b})}\, \left[H^{Q\bar{Q}} C_1 C_2\right]_{c\bar{c},a_1a_2}, \tag{4.1.8}$$

where $\sigma^{(0)}_{c\bar{c},Q\bar{Q}}$ is the lowest-order cross section for the $c+\bar{c}\to Q\bar{Q}$ partonic subprocess. The exponential term $e^{-S_{c\bar{c}}}$ is the b-space Sudakov form factor, analogous to the one given in eq. (2.3.2), namely

$$e^{-S_{c\bar{c}}} = \exp\left\{-\int_{\frac{b_0^2}{b^2}}^{M^2}\frac{dq^2}{q^2}\left[A_c(\alpha_s(q^2))\log\frac{M^2}{q^2} + B_c(\alpha_s(q^2))\right]\right\} \tag{4.1.9}$$

which encodes the resummation of the logarithms of the impact parameter originating from collinear and soft-collinear (meaning both single and double logarithms) radiation coming from the initial-state partons. We recall that the functions $A_c(\alpha_s)$ and $B_c(\alpha_s)$ can be written as power series in the coupling constant

$$A_c(\alpha_s) = \sum_{n=1}^{\infty}\left(\frac{\alpha_s}{2\pi}\right)^n A_c^{(n)} \tag{4.1.10}$$

$$B_c(\alpha_s) = \sum_{n=1}^{\infty}\left(\frac{\alpha_s}{2\pi}\right)^n B_c^{(n)}. \tag{4.1.11}$$

The term $\left[H^{Q\bar{Q}}C_1C_2\right]_{c\bar{c},a_1a_2}$, which includes the hard function and the convolution of the parton distribution functions with the coefficient functions, has a different form for the $q\bar{q}$ annihilation and the gluon fusion channels. Here we can restrict the discussion to $q\bar{q}$-initiated processes without the need to include the rich Lorentz structure that comes with the three gluon vertex, as once we go through the abelianization procedure, such terms will no longer contribute. We have

$$\left[H^{Q\bar{Q}}C_1C_2\right]_{c\bar{c},a_1a_2} = [(\mathbf{H\Delta})]^{Q\bar{Q}}_{c\bar{c},a_1a_2} = (\mathbf{H\Delta})^{Q\bar{Q}}_{c\bar{c}}\, C_{ca_1}(z_1,\alpha_s)\, C_{\bar{c}a_2}(z_2,\alpha_s) \tag{4.1.12}$$

where the operators in colour space are denoted in bold letters. The coefficient functions $C_{ab}(z,\alpha_s)$ are process-independent functions defined via the choice of the resummation scheme, as it is explained in Section 4.3. In eq. (4.1.12), the operator $\mathbf{\Delta}$, which is specific of heavy-quarks pair production, encodes the resummation of the single-logarithmic corrections due to the large-angle soft radiations from the $Q\bar{Q}$ pair and from interferences between the initial and final state. We can rewrite it in the following form

$$\mathbf{\Delta}(\vec{b}\,) = \mathbf{V}^\dagger(b)\,\mathbf{D}(\phi_b)\,\mathbf{V}(b), \tag{4.1.13}$$

where the operator $\mathbf{V}$ is the exponentiation of the soft anomalous dimension matrix for heavy-quark pair production $\mathbf{\Gamma}_t$, namely

$$\mathbf{V}(b) = P_q \exp\left\{-\int_{\frac{b_0^2}{b^2}}^{M^2}\frac{dq^2}{q^2}\mathbf{\Gamma}_t(\Phi_{QQ};\alpha_s(q^2))\right\}. \tag{4.1.14}$$

The symbol P_q means that the exponential matrix is path-ordered with respect to the integration variable q^2. A convenient choice for the parametrization of the final-state kinematic variables encoded in Φ_{QQ} is given by the rapidity difference $y_{34} = y_3 - y_4$ and one of the azimuthal angles $\phi_3 = \phi_4$. The explicit form of $\mathbf{\Gamma}_t$ is discussed in details in Ref. [127] and will be recalled later on in this chapter. The operator $\mathbf{D}$ encodes the azimuthal dependence of the heavy-quark pair system in the small transverse-momentum limit due to wide-angle soft radiations. It exhibits an important feature [127]: it is always possible to define it in such a way that $\langle\mathbf{D}\rangle_{\phi_b} = \mathbb{1}$, in other words its average over the azimuthal angle ϕ_b results in a trivial contribution at all orders.

It is important to note that for processes without final-state radiation, such as the production of a color singlet F in QCD, the factor $\mathbf{\Delta}$ assumes a trivial form and the color-space operator in eq. (4.1.12) becomes

$$(\mathbf{H\Delta})^F_{c\bar{c}} = H^F_{c\bar{c}}\,\mathbb{1} \tag{4.1.15}$$

where $H^F_{c\bar{c}}$ is the usual process-dependent hard-virtual coefficient.

We can write the color-space operator in eq. (4.1.12) in terms of the scattering amplitudes as

$$(\mathbf{H\Delta})^{Q\bar{Q}}_{c\bar{c}} = \frac{\langle\widetilde{\mathcal{M}}_{c\bar{c}\to Q\bar{Q}}|\,\mathbf{\Delta}\,|\widetilde{\mathcal{M}}_{c\bar{c}\to Q\bar{Q}}\rangle}{|\mathcal{M}^{(0)}_{c\bar{c}\to Q\bar{Q}}|^2}. \tag{4.1.16}$$

All the amplitudes here are considered to be renormalized. The dependence on the colour indices of the scattering amplitudes $\mathcal{M}$ for heavy-quark pair production is represented by a vector $|\mathcal{M}\rangle$ in colour space. The all-orders infrared-subtracted amplitudes $|\widetilde{\mathcal{M}}\rangle$ can be obtained from the un-subtracted ones $|\mathcal{M}\rangle$, which are infrared divergent, via the application of the appropriate subtraction operator

$$|\widetilde{\mathcal{M}}_{c\bar{c}\to Q\bar{Q}}\rangle = [\mathbb{1} - \mathbf{I}_{c\bar{c}\to Q\bar{Q}}(\epsilon)]\,|\mathcal{M}_{c\bar{c}\to Q\bar{Q}}\rangle\,. \tag{4.1.17}$$

The operator $\mathbf{I}_{c\bar{c}\to Q\bar{Q}}(\epsilon)$ contains both a divergent part, uniquely defined in order to cancel the infrared poles that appear at each order in the amplitude, and a finite part which is, in principle, arbitrary. The exact definition of the latter depends on the choice of the resummation scheme (see Section 4.3). Both the scattering amplitudes and the subtraction operator can be expanded perturbatively

$$\mathbf{I}_{c\bar{c}\to Q\bar{Q}}(\epsilon) = \sum_{i=1}^{\infty}\left(\frac{\alpha_s}{2\pi}\right)^i \mathbf{I}^{(i)}_{c\bar{c}\to Q\bar{Q}}(\epsilon) \tag{4.1.18}$$

$$|\mathcal{M}_{c\bar{c}\to Q\bar{Q}}\rangle = \sum_{i=0}^{\infty}\left(\frac{\alpha_s}{2\pi}\right)^i |\mathcal{M}^{(i)}_{c\bar{c}\to Q\bar{Q}}\rangle \tag{4.1.19}$$

where the additional powers of α_s already present at leading order are included in the definition of $|\mathcal{M}^{(i)}_{c\bar{c}\to Q\bar{Q}}\rangle$. Using eq. (4.1.17) we can obtain $\widetilde{\mathcal{M}}^{(n)}_{c\bar{c}\to Q\bar{Q}}$ at each order as a function of $\widetilde{\mathcal{M}}^{(k)}_{c\bar{c}\to Q\bar{Q}}$ and $\mathbf{I}^{(k)}_{c\bar{c}\to Q\bar{Q}}$ with $k \leq n$. For instance, up to NLO we have that

$$|\widetilde{\mathcal{M}}^{(0)}_{c\bar{c}\to Q\bar{Q}}\rangle = |\mathcal{M}^{(0)}_{c\bar{c}\to Q\bar{Q}}\rangle \tag{4.1.20}$$

$$|\widetilde{\mathcal{M}}^{(1)}_{c\bar{c}\to Q\bar{Q}}\rangle = |\mathcal{M}^{(1)}_{c\bar{c}\to Q\bar{Q}}\rangle - \mathbf{I}^{(1)}_{c\bar{c}\to Q\bar{Q}}(\epsilon)\,|\mathcal{M}^{(0)}_{c\bar{c}\to Q\bar{Q}}\rangle\,. \tag{4.1.21}$$

We can write the first-order contribution of the subtraction operator as the sum of two terms separating the final-state dependent part from the independent one

$$\mathbf{I}^{(1)}_{c\bar{c}\to Q\bar{Q}}(\epsilon) = I^{(1)}_{c\bar{c}}(\epsilon) + \mathbf{I}^{(1)}_{Q\bar{Q}}(\epsilon). \tag{4.1.22}$$

The first term contains the soft and collinear poles coming from the initial-state radiation in the following form

$$I^{(1)}_{c\bar{c}}(\epsilon) = -\frac{1}{2}\left(\frac{\mu_{\mathrm{R}}^2}{M^2}\right)^{\epsilon}\left[\left(\frac{1}{\epsilon^2} + \frac{i\pi}{\epsilon} - \frac{\pi^2}{12}\right)(\mathbf{T}_1^2 + \mathbf{T}_2^2) + \frac{2}{\epsilon}\gamma_c\right], \tag{4.1.23}$$

where $(\mathbf{T}_i)^a$ is the colour charge of the parton i. These colour charges are matrices in either the fundamental or the adjoint representation of $SU(N_c)$, and their square, defined via the product $\mathbf{T}_i \cdot \mathbf{T}_j \equiv (\mathbf{T}_i)^a(\mathbf{T}_j)^a$, is the corresponding Casimir factor (C_{F} or C_{A}). The coefficients γ_c ($c = q, g$) are given by

$$\gamma_q = \frac{3}{2}C_{\mathrm{F}}, \qquad \gamma_g = \frac{11C_{\mathrm{A}} - 2n_f}{6}. \tag{4.1.24}$$

Note that these coefficients match precisely, modulus a minus sign, the $B_c^{(1)}$ coefficients in eq. (2.3.7), as they both originate from hard-collinear radiation off the initial state. The second term in eq. (4.1.22) contains the poles that originate from soft radiation at large angles from the final-state heavy particles and from initial-final state interference and it is given by

$$\mathbf{I}_{Q\bar{Q}}^{(1)}(\epsilon) = -\frac{1}{2}\left(\frac{\mu_{\mathrm{R}}^2}{M^2}\right)^{\epsilon}\left[-\frac{4}{\epsilon}\,\mathbf{\Gamma}_t^{(1)}(y_{34}) + \mathbf{F}_t^{(1)}(y_{34})\right]. \tag{4.1.25}$$

In eq. (4.1.25), $\mathbf{\Gamma}_t^{(1)}$ is the first-order term of the expansion in powers of $(\alpha_s/2\pi)$ of the aforementioned soft anomalous dimension matrix. It can be written as

$$\mathbf{\Gamma}_t^{(1)} = -\frac{1}{4}\Bigg\{(\mathbf{T}_3^2+\mathbf{T}_4^2)(1-i\pi) + \sum_{\substack{j=1,2\\k=3,4}}\mathbf{T}_j\cdot\mathbf{T}_k\log\frac{(2\,p_j\cdot p_k)^2}{M^2m_Q^2} + 2\,\mathbf{T}_3\cdot\mathbf{T}_4\left[\frac{1}{2v}\log\frac{1+v}{1-v} - i\pi\left(\frac{1}{v}+1\right)\right]\Bigg\} \tag{4.1.26}$$

where v is the relative velocity of Q and $\bar{Q}$

$$v = \sqrt{1-\left(\frac{2m_Q^2}{M^2-2m_Q^2}\right)^2}. \tag{4.1.27}$$

The prefactor in eq. (4.1.26) might differ by a factor of 2 with respect to the one found in literature due to the choice of the expansion parameter, as explained in Appendix A. The dependence on the angular distribution of the heavy-quark pair can be expressed in terms of their rapidity difference y_{34}. Additionally we can introduce the transverse momentum of the heavy quarks $p_{\mathrm{T}3} = p_{\mathrm{T}4} \equiv p_{\mathrm{TQ}}$ and the transverse mass $m_{\mathrm{T}} = \sqrt{m_Q^2+p_{\mathrm{TQ}}^2}$. These kinematical quantities satisfy the relation $M = 2m_{\mathrm{T}}\cosh(y_{34}/2)$, where M is the invariant mass of the $Q\bar{Q}$ pair. Now we can write the IR finite part $\mathbf{F}_t^{(1)}$ as

$$\mathbf{F}_t^{(1)} = (\mathbf{T}_3^2+\mathbf{T}_4^2)\,\log\left(\frac{m_{\mathrm{T}}^2}{m_Q^2}\right) + (\mathbf{T}_3+\mathbf{T}_4)^2\,\mathrm{Li}_2\left(-\frac{p_{\mathrm{TQ}}^2}{m_Q^2}\right) + \mathbf{T}_3\cdot\mathbf{T}_4\,\frac{1}{v}\,L_{34}\,, \tag{4.1.28}$$

where the function L_{34} is

$$L_{34} = \log\left(\frac{1+v}{1-v}\right)\log\left(\frac{m_{\mathrm{T}}^2}{m_Q^2}\right) - 2\,\mathrm{Li}_2\left(\frac{2v}{1+v}\right) - \frac{1}{4}\log^2\left(\frac{1+v}{1-v}\right) + 2\left[\mathrm{Li}_2\left(1-\sqrt{\frac{1-v}{1+v}}\,e^{y_{34}}\right) + \mathrm{Li}_2\left(1-\sqrt{\frac{1-v}{1+v}}\,e^{-y_{34}}\right) + \frac{1}{2}\,y_{34}^2\right], \tag{4.1.29}$$

with Li_2 representing the dilogarithm function defined by

$$\mathrm{Li}_2(z) = -\int_0^z \frac{dt}{t}\log(1-t). \tag{4.1.30}$$

These first-order coefficients, namely $\mathbf{\Gamma}_t^{(1)}$, $\mathbf{F}_t^{(1)}$ and $\mathbf{D}^{(1)}$, specify completely the process dependent contributions to eq. (4.1.8) at NLL. Moreover, at NNLL the second-order coefficients, $\mathbf{\Gamma}_t^{(2)}$, $\mathbf{D}^{(2)}$ and the equivalent of $\mathbf{F}_t^{(2)}$ that would be the IR finite contribution to the two-loop subtraction operator, are also needed. We report in Appendix B the explicit expression for $\mathbf{\Gamma}_t^{(2)}$, computed in Ref. [127].

4.2 MiNLO′ formalism for heavy-quark pair production

We can start by isolating the NLL contributions in eq. (4.1.14) by expanding the second-order term. We have

$$\mathbf{V}(b) = \mathbf{V}_{\mathrm{NLL}}\left[1 - \int_{\frac{b_0^2}{b^2}}^{M^2}\frac{dq^2}{q^2}\frac{\alpha_s^2(q)}{(2\pi)^2}\mathbf{\Gamma}_t^{(2)}\right] + \mathcal{O}(\alpha_s^3), \tag{4.2.1}$$

where

$$\mathbf{V}_{\mathrm{NLL}} = P_q \exp\left\{-\int_{\frac{b_0^2}{b^2}}^{M^2}\frac{dq^2}{q^2}\frac{\alpha_s(q)}{2\pi}\mathbf{\Gamma}_t^{(1)}\right\}. \tag{4.2.2}$$

This procedure gives rise to several different corrections to the MiNLO′ formalism that we presented in Section 2.3. Such corrections are described in details in Ref. [131] and we will briefly discuss them. First of all, since it is no longer in exponential form, the contribution to eq. (4.1.16) coming from the two-loop anomalous dimension can be written as

$$-\frac{\langle\mathcal{M}_{c\bar{c}}^{(0)}|\,\mathbf{\Gamma}_t^{(2)\dagger} + \mathbf{\Gamma}_t^{(2)}\,|\mathcal{M}_{c\bar{c}}^{(0)}\rangle}{|\mathcal{M}_{c\bar{c}}^{(0)}|^2}\int_{\frac{b_0^2}{b^2}}^{M^2}\frac{dq^2}{q^2}\frac{\alpha_s^2(q)}{(2\pi)^2} \tag{4.2.3}$$

where we shortened the subscript of the amplitudes for ease of notation. Such term has the same functional form of the contributions stemming from the $B_{c\bar{c}}^{(2)}$ coefficient upon expanding the exponential $e^{-S_{c\bar{c}}}$, so we can absorb it into a redefinition of the Sudakov form factor via the replacement

$$B_{c\bar{c}}^{(2)} \to B_{c\bar{c}}^{(2)} + \frac{\langle\mathcal{M}_{c\bar{c}}^{(0)}|\,\mathbf{\Gamma}_t^{(2)\dagger} + \mathbf{\Gamma}_t^{(2)}\,|\mathcal{M}_{c\bar{c}}^{(0)}\rangle}{|\mathcal{M}_{c\bar{c}}^{(0)}|^2}. \tag{4.2.4}$$

Then we consider the terms coming from $\mathbf{V}_{\mathrm{NLL}}$: by plugging it back in eq. (4.1.16) we obtain

$$(\mathbf{H\Delta})_{c\bar{c}}^{Q\bar{Q}} = \frac{\langle\widetilde{\mathcal{M}}_{c\bar{c}}|\,\mathbf{V}_{\mathrm{NLL}}^\dagger\mathbf{V}_{\mathrm{NLL}}\,|\widetilde{\mathcal{M}}_{c\bar{c}}\rangle}{|\mathcal{M}_{c\bar{c}}^{(0)}|^2}(\mathbf{HD})_{c\bar{c}}^{Q\bar{Q}} + \mathcal{O}(\alpha_s^3) \tag{4.2.5}$$

plus terms that vanish upon azimuthal integration and can therefore be safely neglected. The first term in eq. (4.2.5) produces contributions that are purely NLL,

when $\mathbf{V}_{\rm NLL}$ hits the LO amplitudes, and higher-order ones when the interference with NLO amplitudes is involved. We can obtain both contributions via the following replacement

$$\frac{\langle\widetilde{\mathcal{M}}_{c\bar{c}}|\,\mathbf{V}_{\rm NLL}^{\dagger}\mathbf{V}_{\rm NLL}\,|\widetilde{\mathcal{M}}_{c\bar{c}}\rangle}{|\mathcal{M}_{c\bar{c}}^{(0)}|^2}\to\frac{\langle\mathcal{M}_{c\bar{c}}^{(0)}|\,\mathbf{V}_{\rm NLL}^{\dagger}\mathbf{V}_{\rm NLL}\,|\mathcal{M}_{c\bar{c}}^{(0)}\rangle}{|\mathcal{M}_{c\bar{c}}^{(0)}|^2}\frac{\langle\widetilde{\mathcal{M}}_{c\bar{c}}|\widetilde{\mathcal{M}}_{c\bar{c}}\rangle}{|\mathcal{M}_{c\bar{c}}^{(0)}|^2} \tag{4.2.6}$$

which, in addition, requires the adjustment of the $B_{c\bar{c}}^{(2)}$ coefficient via the inclusion of two new terms needed to restore the MiNLO′ accuracy[2], namely

$$\begin{aligned}B_{c\bar{c}}^{(2)}\to B_{c\bar{c}}^{(2)}&-2\,\mathrm{Re}\left[\frac{\langle\widetilde{\mathcal{M}}_{c\bar{c}}^{(1)}|\widetilde{\mathcal{M}}_{c\bar{c}}^{(0)}\rangle}{|\mathcal{M}_{c\bar{c}}^{(0)}|^2}\right]\frac{\langle\mathcal{M}_{c\bar{c}}^{(0)}|\,\mathbf{\Gamma}_t^{(1)\dagger}+\mathbf{\Gamma}_t^{(1)}\,|\mathcal{M}_{c\bar{c}}^{(0)}\rangle}{|\mathcal{M}_{c\bar{c}}^{(0)}|^2}\\&+2\,\mathrm{Re}\left[\frac{\langle\widetilde{\mathcal{M}}_{c\bar{c}}^{(1)}|\,\mathbf{\Gamma}_t^{(1)\dagger}+\mathbf{\Gamma}_t^{(1)}\,|\widetilde{\mathcal{M}}_{c\bar{c}}^{(0)}\rangle}{|\mathcal{M}_{c\bar{c}}^{(0)}|^2}\right].\end{aligned} \tag{4.2.7}$$

As for the azimuthally-dependent term $(\mathbf{HD})_{c\bar{c}}^{Q\bar{Q}}$, it gives trivial contributions once the average over the azimuthal angle is taken. This is true at NLO, but it would be spoiled at higher orders in gluon-initiated channels, due to the interference between $\mathbf{D}^{(1)}$ and the coefficient functions. We can ignore this complication as it is needed only when going beyond MiNLO′ accuracy. We have

$$(\mathbf{HD})_{c\bar{c}}^{Q\bar{Q}}=\frac{|\widetilde{\mathcal{M}}_{c\bar{c}}|^2}{|\mathcal{M}_{c\bar{c}}^{(0)}|^2}\equiv\mathcal{H}_{c\bar{c}}^{Q\bar{Q}}(\alpha_s) \tag{4.2.8}$$

where the quantity $\mathcal{H}_{c\bar{c}}^{Q\bar{Q}}$, representing the infrared-subtracted hard-virtual contributions, can be perturbatively expanded as

$$\mathcal{H}_{c\bar{c}}^{Q\bar{Q}}(\alpha_s)=\sum_{n=0}^{\infty}\left(\frac{\alpha_s}{2\pi}\right)^n\mathcal{H}_{c\bar{c}}^{Q\bar{Q}\,(n)}. \tag{4.2.9}$$

To summarize, with all the modifications introduced above, eq. (4.1.8) becomes

$$\begin{aligned}W_{h_1h_2}^{Q\bar{Q}}=\sum_c\frac{1}{s}\,e^{-\hat{S}_{c\bar{c}}\left(\frac{b_0}{b}\right)}\,\langle\mathcal{M}_{c\bar{c}}^{(0)}|\,\mathbf{V}_{\rm NLL}^{\dagger}\mathbf{V}_{\rm NLL}\,|\mathcal{M}_{c\bar{c}}^{(0)}\rangle\\\times\sum_{a_1,a_2}\left[\mathcal{H}_{c\bar{c}}^{Q\bar{Q}}(\alpha_s)\left(C_{ca_1}\otimes f_{a_1/h_1}\right)\left(C_{\bar{c}a_2}\otimes f_{a_2/h_2}\right)\right],\end{aligned} \tag{4.2.10}$$

where the symbol $\otimes$ denotes the usual convolution

$$(f\otimes g)(x)=\int_x^1\frac{dz}{z}f\left(\frac{x}{z}\right)g(z). \tag{4.2.11}$$

[2]A detailed explanation of this procedure can be found in Ref. [131]

The effective Sudakov form factor is obtained from the one written in eq. (2.3.2) via the following replacement $B_{c\bar{c}}^{(2)} \to \hat{B}_{c\bar{c}}^{(2)}$ with

$$\begin{aligned}\hat{B}_{c\bar{c}}^{(2)} = B_{c\bar{c}}^{(2)} &+ \frac{\langle \mathcal{M}_{c\bar{c}}^{(0)} | \, \mathbf{\Gamma}_t^{(2)\dagger} + \mathbf{\Gamma}_t^{(2)} \, | \mathcal{M}_{c\bar{c}}^{(0)} \rangle}{|\mathcal{M}_{c\bar{c}}^{(0)}|^2} \\ &- 2\,\mathrm{Re}\left[\frac{\langle \widetilde{\mathcal{M}}_{c\bar{c}}^{(1)} | \widetilde{\mathcal{M}}_{c\bar{c}}^{(0)} \rangle}{|\mathcal{M}_{c\bar{c}}^{(0)}|^2}\right] \frac{\langle \mathcal{M}_{c\bar{c}}^{(0)} | \, \mathbf{\Gamma}_t^{(1)\dagger} + \mathbf{\Gamma}_t^{(1)} \, | \mathcal{M}_{c\bar{c}}^{(0)} \rangle}{|\mathcal{M}_{c\bar{c}}^{(0)}|^2} \\ &+ 2\,\mathrm{Re}\left[\frac{\langle \widetilde{\mathcal{M}}_{c\bar{c}}^{(1)} | \, \mathbf{\Gamma}_t^{(1)\dagger} + \mathbf{\Gamma}_t^{(1)} \, | \widetilde{\mathcal{M}}_{c\bar{c}}^{(0)} \rangle}{|\mathcal{M}_{c\bar{c}}^{(0)}|^2}\right].\end{aligned} \tag{4.2.12}$$

Finally, in order to evaluate explicitly the exponential factor encoded in the term $\langle \mathcal{M}_{c\bar{c}}^{(0)} | \, \mathbf{V}_{\mathrm{NLL}}^\dagger \mathbf{V}_{\mathrm{NLL}} \, | \mathcal{M}_{c\bar{c}}^{(0)} \rangle$, it is possible to perform a rotation in colour space such that the one-loop soft anomalous dimension is written in diagonal form. We have

$$e^{-\hat{S}_{c\bar{c}}} \langle \mathcal{M}_{c\bar{c}}^{(0)} | \, \mathbf{V}_{\mathrm{NLL}}^\dagger \mathbf{V}_{\mathrm{NLL}} \, | \mathcal{M}_{c\bar{c}}^{(0)} \rangle = |\mathcal{M}_{c\bar{c}}^{(0)}|^2 \sum_{i=1}^{n_c} e^{-\hat{S}_{c\bar{c}}^{[\gamma_i^{c\bar{c}}]}} C_{c\bar{c}}^{[\gamma_i^{c\bar{c}}]}(\Phi_{Q\bar{Q}}) \tag{4.2.13}$$

where n_c depends on the $SU(3)$ representation of the initial-state configuration, precisely $n_c = 4$ for quarks and $n_c = 9$ for gluons. In this way the contribution from $\mathbf{\Gamma}_t^{(1)}$ can be included in the $B_{c\bar{c}}^{(1)}$ coefficients of the Sudakov exponent as

$$B_{c\bar{c}}^{(1)} \to B_{c\bar{c}}^{(1)} + \gamma_i^{c\bar{c}}(\Phi_{Q\bar{Q}}) \tag{4.2.14}$$

where the functions $\gamma_i^{c\bar{c}}$ are obtained from the eigenvalues of $\mathbf{\Gamma}_t^{(1)}$ and the coefficients $C_{c\bar{c}}^{[\gamma_i^{c\bar{c}}]}$ of the linear combination, satisfy the normalization $\sum_{i=1}^{n_c} C_{c\bar{c}}^{[\gamma_i^{c\bar{c}}]}(\Phi_{Q\bar{Q}}) = 1$.

4.3 Resummation scheme dependence

As mentioned before, the definition of some terms discussed in this chapter depends on the choice of the so-called resummation scheme. It is the case, for example, for the hard-virtual function $H_{c\bar{c}}$ and the coefficient functions C_{ab} introduced in eq. (4.1.12) as well as the $B_{c\bar{c}}$ coefficients in the Sudakov exponent. More specifically, it can be shown [132] that the resummed component of the differential cross section for colour singlet production, usually written in the form of eq. (4.1.8), is invariant under the transformation

$$\begin{aligned} H_{c\bar{c}}(\alpha_s) &\to H_{c\bar{c}}(\alpha_s)\,[f(\alpha_s)]^{-1}\,, \\ B_{c\bar{c}} &\to B_{c\bar{c}} - \beta(\alpha_s)\frac{d\log f(\alpha_s)}{d\log\alpha_s}, \\ C_{ab}(z,\alpha_s) &\to C_{ab}(z,\alpha_s)\,[f(\alpha_s)]^{1/2}\,, \end{aligned} \tag{4.3.1}$$

where $f(\alpha_s) = 1 + \mathcal{O}(\alpha_s)$ is an arbitrary perturbative function. This ambiguity in the definition of the factors in the set of equations above is a consequence of

the fact that the transverse-momentum cross section is a divergent quantity. The arbitrariness involved in the regularization procedure is reflected in the way the coefficient functions are defined and it is then propagated to the Sudakov form factor and the hard-virtual function due to the collinear radiation. Therefore these factors must be computed via the choice of a resummation scheme, which amounts to the definition of $H_{c\bar{c}}$ or C_{ab} for both a $q\bar{q}$-initiated and a gg-initiated process. Based on the choice of the scheme, the process dependence of the factor $[HCC]_{c\bar{c}}$ in eq. (4.1.8) is distributed between $H_{c\bar{c}}$ and C_{ab}[3].

A simple choice for the resummation scheme for Drell-Yan processes consists of a trivial definition of the hard-virtual factor, namely $H_{c\bar{c}}^{\mathrm{DY}}(\alpha_s) = 1$, which corresponds to $f(\alpha_s) = H_{c\bar{c}}(\alpha_s)$. In this way, one fixes completely the process-independent form factor $e^{-S_{c\bar{c}}}$ and coefficients functions C_{ab} as those determined from the DY process. This prescription is widespread in literature due to its simplicity, because the Drell-Yan transverse-momentum distribution is very well known.

One of the most popular choices is given by the so-called hard scheme, that is the scheme in which order-by-order in perturbation theory the coefficients $C_{ab}^{(n)}(z)$ with $n \geq 1$ do not contain any $\delta(1-z)$ terms. This definition entails that the process dependence of the term $[HCC]_{c\bar{c}}$ is all contained in the hard-virtual coefficient $H_{c\bar{c}}$, while the collinear functions C_{ab} are completely process independent. The first-order perturbative coefficients of the collinear functions in this scheme are given by

$$\begin{aligned} C_{qq}^{(1)}(z) &= C_{\mathrm{F}}(1-z), \\ C_{gq}^{(1)}(z) &= C_{\mathrm{F}} z, \\ C_{qg}^{(1)}(z) &= z(1-z), \\ C_{gg}^{(1)}(z) &= C_{q\bar{q}}^{(1)}(z) = C_{qq'}^{(1)}(z) = C_{q\bar{q}'}^{(1)}(z) = 0, \end{aligned} \tag{4.3.2}$$

where q and q' denote quarks of different flavours.

In this work we employ the following definition for the first-order terms of the expansion of the collinear coefficient functions

$$C_{ab}^{(1)}(z) = -P_{ab}^{(0),\epsilon}(z) - C_{\mathrm{F}}\delta_{ab}\delta(1-z)\frac{\pi^2}{12}. \tag{4.3.3}$$

In this scheme, the first-order hard-virtual coefficient for the DY production of a Z boson is given by

$$H_{\mathrm{DY}}^{(1)} = C_{\mathrm{F}}\left(\frac{7}{6}\pi^2 - 8\right). \tag{4.3.4}$$

[3]Details on the discussion about the appropriate choice of the resummation scheme for the production process of a heavy-quark pair can be found in Ref. [127]

The functions $P_{ab}^{(0),\epsilon}$ are defined as the $\mathcal{O}(\epsilon)$ part of the leading-order regularized Altarelli-Parisi splitting functions $P_{ab}^{(0)}$ and they are given by

$$\begin{aligned} P_{qq}^{(0),\epsilon}(z) &= -C_{\mathrm{F}}(1-z), & P_{gq}^{(0),\epsilon}(z) &= -C_{\mathrm{F}}z, \\ P_{gg}^{(0),\epsilon}(z) &= 0, & P_{qg}^{(0),\epsilon}(z) &= -z(1-z). \end{aligned} \tag{4.3.5}$$

For completeness we report also the regularized splitting functions:

$$\begin{aligned} P_{qq}^{(0)}(z) &= C_{\mathrm{F}}\left[\frac{1+z^2}{(1-z)_+} + \frac{3}{2}\delta(1-z)\right], \\ P_{gq}^{(0)}(z) &= C_{\mathrm{F}}\frac{1}{z}\left[1+(1-z)^2\right], \\ P_{qg}^{(0)}(z) &= \frac{1}{2}\left[z^2+(1-z)^2\right], \\ P_{gg}^{(0)}(z) &= 2C_{\mathrm{A}}\left[\frac{z}{(1-z)_+} + \frac{1-z}{z} + z(1-z)\right] + 2\pi\beta_0\delta(1-z). \end{aligned} \tag{4.3.6}$$

Chapter 5

Abelianization of the MiNLO′ method

So far, the MiNLO′ method, described in Section 2.3, has only been used to describe QCD radiation, as the method is tailored for its application to the physics of hadron colliders, where the processes are dominated by the strong interactions. As already pointed out before, however, with the increase in the precision of the experimental data, the relevance of the EW corrections is becoming more and more clear for the precision physics program of the LHC and the future colliders. In general, handling EW corrections is known to be a much harder task than dealing with QCD ones, however, as long as we consider only IR divergences, EW processes are much simpler. That is because they are either associated to the propagation of a virtual photon or the emission of a real one, while the electroweak corrections, where massive boson are involved, do not suffer from the presence of IR divergences due to the mass of the boson acting as a natural regulator. As a consequence, the structure of the IR counterterms required for EW corrections is in one-to-one correspondence with the abelian subset of the QCD ones. As a result, for the purpose of this work we can focus on the description of NLO QED corrections without having to add to the diagrams any massive electroweak boson other than the one already present at the lowest order.

In this chapter we want to describe the abelianization process needed to translate QCD corrections to QED ones. We will give a general prescription for the abelianization procedure as well as the results for the description of the MiNLO′ method applied to the production of a massive lepton pair in neutral Drell-Yan production.

5.1 Abelianization prescription

We want to describe the abelianization procedure for the production process of a colour singlet plus one jet starting at Born level. Clearly the first step consists of removing any diagram where non-abelian vertices are involved, that is three-gluon

and four-gluon vertices. Note that in this context, photons are considered as partons, i.e. constituents of the protons, to which we must associate the corresponding parton density function, namely the photon PDF. This requires the use of a PDF set compatible with the determination of the photon content of the proton, as described in Ref. [133, 134]. Then the abelianized processes can be obtained by simply replacing the gluon with the photon. At NLO the strategy is the same, but keeping in mind that unlike gluons, photons can be also radiated off charged leptons. In this work we only consider QED corrections, so we will ignore the diagrams where the photon is emitted from the massive electroweak bosons.

We introduce the following prescription to translate the equations discussed in the previous chapters into QED formalism. For each particle we substitute the colour operator $\mathbf{T}_i$ with

$$\mathbf{T}_i \to Q_i \sigma_i \tag{5.1.1}$$

where Q_i is the charge of the i-th particle. We introduced the sign factor σ_i for the charge flow related to each fermion: specifically we have $\sigma_i = +1$ or $\sigma_i = -1$ when the particle is incoming or outgoing respectively. With this prescription the equation for charge conservation becomes

$$\sum_{i=\text{initial}} Q_i = \sum_{j=\text{final}} Q_j \qquad \longrightarrow \qquad \sum_k Q_k \sigma_k = 0 \tag{5.1.2}$$

where the last sum k runs over both initial and final-state fermions. Note that in this way the equation for charge conservation becomes very similar to the one used for colour conservation in Appendix A, namely

$$\sum_i \mathbf{T}_i = 0. \tag{5.1.3}$$

To complete the abelianization process we can then use the prescription we just presented to determine the QED equivalent of the resummation coefficients, $A_c^{(i)}$ and $B_c^{(i)}$, as well as the Altarelli-Parisi splitting functions $P_{ab}^{(i)}(z)$ and the collinear coefficient functions $C_{ab}^{(i)}(z)$. From the definition of the Casimir operators in QCD we easily obtain their corresponding factors in QED as

$$C_{\text{F}} \to Q_f^2, \qquad C_{\text{A}} \to 0. \tag{5.1.4}$$

Additionally we have the replacement

$$n_f \to N^{(2)} \tag{5.1.5}$$

where we defined

$$N^{(i)} \equiv N_C \sum_{q=1}^{n_q} e_q^i + \sum_{l=1}^{n_l} e_l^i \tag{5.1.6}$$

with n_q and n_l denoting the number of active quarks and leptons respectively. This is a subtlety related to the difference between the presence of quark loops in pure QCD results and charged-fermion loops in QED. In the former case, the coupling of the gluon is the same for all quark flavours, resulting in a factor n_f being produced. Once we replace gluons with photons, we have to allow for the presence of virtual charged leptons inside the loop and the coupling of each fermion is different as it is proportional to its electromagnetic charge.

With the rules written above we get the resummation coefficients in QED: from eqs. (2.3.6) and (2.3.7) we have the process-independent terms

$$\begin{aligned} A_f^{(1),\mathrm{QED}} &= Q_f^2\,, \\ A_f^{(2),\mathrm{QED}} &= -\frac{5}{9} Q_f^2 N^{(2)}\,, \\ B_f^{(1),\mathrm{QED}} &= -\frac{3}{2} Q_f^2\,, \end{aligned} \tag{5.1.7}$$

while the process-dependent coefficient in eq. (2.3.9) becomes

$$\begin{aligned} B_{f,\mathrm{DY}}^{(2),\mathrm{QED}} = &\left[\left(\frac{\pi^2}{2} - \frac{3}{8} - 6\zeta_3\right)(Q_f^2)^2 + \left(\frac{1}{12} + \frac{\pi^2}{9}\right) Q_f^2 N^{(2)}\right] \\ &+ \pi\beta_0^{\mathrm{QED}} \zeta_2 Q_f^2 + 2\zeta_3 (A_f^{(1),\mathrm{QED}})^2 + \pi\beta_0^{\mathrm{QED}} H_{(\mathrm{DY})}^{(1),\mathrm{QED}}\,, \end{aligned} \tag{5.1.8}$$

where the hard-virtual coefficient is

$$H_{(\mathrm{DY})}^{(1),\mathrm{QED}} = Q_f^2 \left[\frac{7}{6}\pi^2 - 8\right] \tag{5.1.9}$$

and

$$\beta_0^{\mathrm{QED}} = -\frac{N^{(2)}}{3\pi} \tag{5.1.10}$$

is the lowest-order QED beta function. Then we report the leading-order regularized splitting functions [135, 136]

$$\begin{aligned} P_{ff}^{(0),\mathrm{QED}}(z) &= Q_f^2 \left[\frac{1+z^2}{(1-z)_+} + \frac{3}{2}\delta(1-z)\right], \\ P_{\gamma f}^{(0),\mathrm{QED}}(z) &= Q_f^2 \frac{1}{z}\left[1 + (1-z)^2\right], \\ P_{f\gamma}^{(0),\mathrm{QED}}(z) &= Q_f^2 \left[z^2 + (1-z)^2\right], \end{aligned} \tag{5.1.11}$$

and the coefficient functions at the first non-trivial order

$$\begin{aligned} C_{ff}^{(1),\mathrm{QED}}(z) &= Q_f^2 \left[(1-z) - \frac{\pi^2}{12}\delta(1-z)\right], \\ C_{\gamma f}^{(1),\mathrm{QED}}(z) &= Q_f^2\, z, \\ C_{f\gamma}^{(1),\mathrm{QED}}(z) &= Q_f^2\, z(1-z). \end{aligned} \tag{5.1.12}$$

Note that the equations reported in this section match the results of Ref. [95].

5.2 Heavy-lepton pair production

Now we can apply these abelianization rules to the quantities introduced in the previous chapter. In doing so, the colour structure is completely trivialized as the QED equivalent of the colour matrices are just complex numbers. Starting with the colour operator $\mathbf{\Delta}$ in eq. (4.1.13) we can write it as

$$\Delta^{\text{QED}}(\vec{b}) = D(\phi_b)|V(b)|^2, \tag{5.2.1}$$

where

$$|V(b)|^2 = \exp\left\{-\int_{\frac{b_0^2}{b^2}}^{M^2} \frac{dq^2}{q^2}\, 2\,\text{Re}\,\Gamma_t^{\text{QED}}(y_{34}, \alpha(q^2))\right\}. \tag{5.2.2}$$

Note that the path ordering with respect to q^2 in the definition of the exponentiation of the soft anomalous dimension operator in eq. (4.1.14) is no longer required. By inserting Δ^{QED} in eq. (4.1.16) we get

$$(H\Delta)^{ll}_{c\bar{c}} = |V(b)|^2 D(\phi_b)\, \mathcal{H}^{ll}_{c\bar{c}}. \tag{5.2.3}$$

In this expression, the term $D(\phi_b)$ can be safely dropped once again, as the abelianization does not spoil the fact that, as soon as the average over the angle ϕ_b is taken, it gives a trivial contribution. In a similar way to what we already discussed for the QCD case, the exponential term in $|V(b)|^2$ can be absorbed in the Sudakov exponent. Indeed, from eq. (5.2.2) it is explicitly manifest that the contribution coming from the QED soft anomalous dimension has the same functional form of the B-type coefficients in the Sudakov form factor at all orders. We have the replacement

$$B_c^{\text{QED},(i)} \to \hat{B}_c^{\text{QED},(i)} = B_c^{\text{QED},(i)} + 2\,\text{Re}\,\Gamma_{t,c}^{\text{QED},(i)}. \tag{5.2.4}$$

Note that this is the exact same result that one would get by abelianizing directly the expression for $\hat{B}^{(2)}_{c\bar{c}}$ in eq. (4.2.12). That is because in QED the two contributions coming from the interplay of the one-loop soft anomalous dimension with the interference between the LO and NLO matrix elements, namely the second and third lines in eq. (4.2.12), cancel each other entirely.

Finally, the last term can be written as

$$\mathcal{H}^{ll}_{c\bar{c}} = \frac{\langle \widetilde{\mathcal{M}}_{c\bar{c}\to ll} \,|\, \widetilde{\mathcal{M}}_{c\bar{c}\to ll}\rangle}{|\mathcal{M}^{(0)}_{c\bar{c}\to ll}|^2} = \sum_{i=0}^{\infty} \left(\frac{\alpha_s}{2\pi}\right)^i \mathcal{H}^{ll\,(i)}_{c\bar{c}}. \tag{5.2.5}$$

and from eqs. (4.1.17), (4.1.20) and (4.1.21) we have

$$\mathcal{H}^{ll}_{c\bar{c}} = 1 + \frac{\alpha}{2\pi}\left(\frac{2\,\text{Re}\,\langle \mathcal{M}^{(0)}_{c\bar{c}\to ll} \,|\, \mathcal{M}^{(1)}_{c\bar{c}\to ll}\rangle}{|\mathcal{M}^{(0)}_{c\bar{c}\to ll}|^2} - 2I^{(1)}_{c\bar{c}\to ll}(\epsilon)\right) + \mathcal{O}(\alpha^2). \tag{5.2.6}$$

The first-order subtraction operator $I^{(1)}_{c\bar{c}\to ll}$ not only removes the double and single poles of both initial-state and final-state radiation origin, but also contains a finite part, $F_t^{\mathrm{QED},(1)}$, obtained via the abelianization of eq. (4.1.28). For a heavy-lepton pair in the final state $Q_3 = -Q_4$, so if we apply the abelianization rules we have

$$\mathbf{T}_3 \to \sigma_3 Q_3, \qquad \mathbf{T}_4 \to \sigma_4 Q_4 = -\sigma_3 Q_3 \tag{5.2.7}$$

thus

$$\begin{aligned} (\mathbf{T}_3^2 + \mathbf{T}_4^2) &\to 2Q_l^2, \\ (\mathbf{T}_3 + \mathbf{T}_4)^2 &\to 0, \\ (\mathbf{T}_3 \cdot \mathbf{T}_4) &\to Q_l^2. \end{aligned} \tag{5.2.8}$$

where Q_l^2 is the squared electromagnetic charge of the final-state lepton. The IR finite part of the abelianized subtraction operator then reads

$$F_t^{\mathrm{QED},(1)} = 2Q_l^2 \log\left(\frac{m_{\mathrm{T}}^2}{m_l^2}\right) - Q_l^2 \frac{1}{v} L_{34}, \tag{5.2.9}$$

with m_l being the mass of the final-state heavy leptons. We can then write the order α contribution to $\mathcal{H}^{ll}_{c\bar{c}}$ as the sum of the one-loop infrared subtracted hard-virtual coefficient for heavy-lepton pair production, $H^{ll\,(1)}_{c\bar{c}}$, and the finite part of the first-order subtraction operator, $F_t^{\mathrm{QED},(1)}$.

Now we can write the abelianized counterpart of eq. (4.1.8) as

$$\begin{aligned} W^{ll}_{h_1 h_2} = \sum_{a_1,a_2} \int_{x_1}^1 \frac{dz_1}{z_1} \int_{x_2}^1 \frac{dz_2}{z_2}\, f_{a_1/h_1}\left(\frac{x_1}{z_1}, \frac{b_0^2}{b^2}\right) f_{a_2/h_2}\left(\frac{x_2}{z_2}, \frac{b_0^2}{b^2}\right) \\ \times \sum_c e^{-\hat{S}_{c\bar{c}}\left(\frac{b_0}{b}\right)}\, \sigma^{(0)}_{c\bar{c},ll} \left[\, \mathcal{H}^{ll}_{c\bar{c}}\, C_{ca_1}(z_1,\alpha)\, C_{\bar{c}a_2}(z_2,\alpha) \,\right], \end{aligned} \tag{5.2.10}$$

where the hard-virtual factor is given by

$$\mathcal{H}^{ll}_{c\bar{c}} = 1 + \frac{\alpha}{2\pi}\left(H^{ll\,(1)}_{c\bar{c}} + F_t^{\mathrm{QED},(1)}\right) + \mathcal{O}(\alpha^2) \tag{5.2.11}$$

and the effective Sudakov radiator $\hat{S}_{c\bar{c}}$ is obtained from the usual colour-singlet case by replacing at all orders the coefficient $B_c^{\mathrm{QED}}(\alpha) \to \hat{B}_c^{\mathrm{QED}}(\alpha)$, with

$$B_c^{\mathrm{QED}}(\alpha) = \sum_{n=1}^{\infty} \left(\frac{\alpha}{2\pi}\right)^n B_c^{\mathrm{QED},(n)} \to \hat{B}_c^{\mathrm{QED}}(\alpha) = \sum_{n=1}^{\infty} \left(\frac{\alpha}{2\pi}\right)^n \left(B_c^{\mathrm{QED}(n)} + 2\,\mathrm{Re}\,\Gamma_{t,c}^{\mathrm{QED},(n)}\right). \tag{5.2.12}$$

The computation of the first and second-order anomalous dimensions and their relative abelianizations can be found in Appendices A and B. We summarize the results

here for completeness

$$\Gamma_{t,q}^{\mathrm{QED},(1)} = -\frac{1}{2}\left[1 - \frac{1}{2v}\log\frac{1+v}{1-v} + \frac{i\pi}{v} - Q_q \log\frac{(p_1\cdot p_3)(p_2\cdot p_4)}{(p_1\cdot p_4)(p_2\cdot p_3)}\right], \tag{5.2.13}$$

$$\begin{aligned}\Gamma_{t,q}^{\mathrm{QED},(2)} = & -\frac{5}{36}N^{(2)}\left[Q_q \log\frac{(p_1\cdot p_3)(p_2\cdot p_4)}{(p_1\cdot p_4)(p_2\cdot p_3)} - Q_q^2 + \frac{1}{2v}\log\left(\frac{1+v}{1-v}\right) - \frac{1}{4}\frac{i\pi}{v}\right] \\ & - \pi\,\beta_0\,F_t^{\mathrm{QED},(1)},\end{aligned} \tag{5.2.14}$$

where Q_q is the charge of the initial-state parton with momentum p_1 and β_0 is the first-order coefficient of the QED beta function. Note that depending on the choice of the resummation scheme, as discussed at the end of Chapter 4, the $B_c^{(2)}$ coefficient in the Sudakov form factor might contain the first-order coefficient of the perturbative expansion of the hard-virtual function. If this is the case, such as in eq. (5.1.8), one must include the finite part of the subtraction operator, that is $F_t^{\mathrm{QED},(1)}$, as well.

With the prescription discussed in the previous sections we managed to completely define the abelianization procedure needed to describe the constituents of the MiNLO′ formula in QED. Despite the trivialization of the colour structures introduced with the QED equivalent of the heavy-quark pair production terms, the similarities between the two descriptions, the non-abelian and the abelian ones, are evident.

Indeed the modifications of the resummation coefficients in the Sudakov form factor introduced via the exponentialization of the soft anomalous dimension matrix are almost equivalent in the two cases. More specifically, as one might expect, the one-loop soft anomalous dimension contributes at lowest order to the first term of the perturbative expansion of the B_c coefficient, then the two-loop soft anomalous dimension introduces at the lowest order a modification to the second term of the expansion and so on. The main differences between the two descriptions are embodied in the interference terms that express the contributions coming from the one-loop soft anomalous dimension to the two-loop coefficient $B_c^{(2)}$ and in the fact that in QCD a diagonalization in colour space is needed to extract the eigenvalues of $\mathbf{\Gamma}_t^{(1)}$. Where possible, the results presented in this section have been compared to the one discussed in Refs. [116, 137, 138].

5.3 Computational aspects

It is well known that QED and QCD are very different theories. Indeed, despite using the same underlying framework, namely the one provided by quantum field theory, the interactions that they describe arise from different symmetry groups, $U(1)$ and $SU(3)$ respectively. This is reflected in the non-abelian nature of the QCD operator, resulting in the rich colour structure that needs to be addressed when computing

the amplitudes. Moreover, since the vector of the strong interaction carries a colour charge itself, it is affected by self-interactions. As a consequence, amplitudes in QCD can contain pure bosonic vertices, such as the three-gluon and four-gluon vertices. This leads to the presence of bosonic loops in the virtual diagrams and it affects the flow of the renormalization group. In this section we want to focus on the numerical differences between the two theories and on the way in which such effects will affect our results. We stress that these differences should not be underestimated, as even small changes in the Sudakov exponent can strongly affect the suppression of the cross section in the small transverse-momentum limit spoiling, in principle, the method described in Section 2.3.

The first and most obvious difference is related to the coupling constant and its running. We can take as a starting point the value of both α_s and α at the Z boson resonance, namely

$$\alpha_s(M_Z) \approx 0.118, \qquad \alpha(M_Z) \approx \frac{1}{128.95} \approx 0.00775 \tag{5.3.1}$$

where, for the sake of simplicity, we can ignore the differences between the different schemes in the definition of the QED coupling constant discussed in Chapter 3. These values already suggest a clear picture, with the QCD coupling constant being more than ten times larger than the electroweak one, which is the reason why typically the NLO EW corrections are taken into consideration together with the NNLO QCD ones. The main difference, however, is not just in the value at the scale of the Z boson mass, but also in the beta function and consequently in the running of the two coupling constants. Indeed, due to the presence of the gluons running in the loops, the QCD beta function has opposite sign with respect to the QED one. This is true also at the lowest order, as it can be seen from the relative sign between eq. (2.3.8) and eq. (5.1.10). As a consequence, the value of $\alpha_s(\mu_{\text{R}}^2)$ decreases as the scale μ_{R} at which it is evaluated increases (asymptotic freedom), while at low energies it becomes very large, making perturbative computation completely unreliable. On the other hand, the value of $\alpha(\mu_{\text{R}}^2)$ increases logarithmically with the scale μ_{R} but it remains relatively small over a wide range of energies. This behaviour, despite being very useful for the perturbative approach, turned out to be an issue from the point of view of implementing the various terms arising from resummation. That is because the natural cutoff given by QCD ensures that the Sudakov form factor goes very fast to zero when it is evaluated at smaller and smaller transverse momenta, due to the rapid increase of the value of the coupling constant. This is definitely not the case in QED, where the value of α at low energies can be basically considered constant, meaning that the suppression provided by the Sudakov form factor is not enhanced in the $p_{\text{T}} \to 0$ limit, with p_{T} being the transverse momentum of the Z boson. Despite not being an issue per se, since everything is still well defined in that region, this peculiarity of QED represents a problem in the numerical sense.

We recall that our goal is to upgrade the $Z + \gamma$ QED computation with the MiNLO′ procedure. In order to understand why the small transverse-momentum region might be problematic in the context of pure QED, we shall briefly summarize what happens in our computation when we approach such region:

- The differential cross section $d\sigma/dp_{\mathrm{T}}$ for the production of a Z boson plus a jet (or a photon in QED) is divergent in the $p_{\mathrm{T}} \to 0$ region.

- The Sudakov form factor $\Delta(Q, p_{\mathrm{T}}^2)$ approaches zero in such region and it guarantees that the divergence of the cross section is suppressed. Because of this behaviour, eq. (2.3.1) yields a finite result for vanishing transverse momentum and more specifically the MiNLO′ differential cross section has a peak in the small transverse-momentum region. It is important to note that this remains true also in QED, despite the suppression of the differential cross section happens much more slowly.

- Since the MiNLO′ $\bar{B}$ function is finite in the $p_{\mathrm{T}} \to 0$ limit, the integration can in principle be performed over all the possible values of the transverse momentum, from 0 to the kinematical limit. However, as will be explained shortly, this is not the case and a cutoff, say $p_{\mathrm{T}}^{\mathrm{min}}$, must be introduced in the region close to 0.

The motivations behind the need for a transverse momentum cutoff are both of theoretical and practical nature. First of all, as it was already mentioned, in QCD we have a natural cutoff represented by the hadronization scale $\Lambda_{\mathrm{QCD}} \approx 300$ MeV. This is a pure theoretical limit and it marks the energy scale at which the perturbative approach is no longer valid. Obviously this restriction is no longer present if we are only considering QED, as the intrinsic limit of the theory is located at the Landau pole, namely at values of the energy many orders of magnitude higher that what is accessible at present colliders. Then we are left with the practical reasons for the introduction of a transverse momentum cutoff:

- As far as the amplitudes are concerned, the computation of the virtual corrections is typically one of the delicate parts and pushing the calculation deep into difficult regions can results in numerical instabilities.

- As it was discussed in Section 2.1, the contribution coming from the real emission amplitudes is made finite via the subtraction procedure. However both the real amplitude and the subtraction counterterms are computed separately and the cancellations happen point-by-point in the phase space. As a result, although the sum of the two contributions must yield finite results for each kinematical configuration, going too close to the $p_{\mathrm{T}} \to 0$ limit causes numerical instabilities in the cancellation between real matrix elements and counterterms.

In general, the minimum value of the cutoff depends on the process under consideration and the way the computation is carried out. For our computation we found out that the value of the cutoff should not be taken smaller than $p_{\mathrm{T}}^{\mathrm{min}} \approx 10^{-3}$ GeV, since below this threshold the integration grids, produced by the adaptive integration algorithm employed by POWHEG-RES framework that we are using, start showing signs of numerical instabilities. It is important to note that the value chosen for the cutoff has to be smaller than the value of the transverse momentum at which the MiNLO′ differential cross section has its maximum. In other words, $p_{\mathrm{T}}^{\mathrm{min}}$ should be in the region where the Sudakov form factor is small enough to strongly suppress the divergences of the fixed-order computation. In this way we ensure that the missing portion of the integral, i.e. the one between 0 and $p_{\mathrm{T}}^{\mathrm{min}}$, is small and can therefore be safely neglected.

The numerical issue at the core of this computation lies in the fact that the transverse-momentum distribution for the abelianized MiNLO′ cross section has a maximum at a value of p_{T} which is completely inaccessible with the numerical integration, many orders of magnitude smaller than the 10^{-3} GeV threshold that was mentioned above. If we look at QCD, in Ref. [16] for example, the peak of the transverse momentum differential cross-section for neutral Drell-Yan plus one jet is in the GeV region. In order to roughly estimate the position of the peak for the QED case we can use the following approximations:

- Due to the slow logarithmic scaling, the value of α can be taken fixed at the Thompson limit, namely

$$\alpha(q^2) = \alpha(0) \approx 1/137. \tag{5.3.2}$$

- We can restrict the computation at the lowest order, both for what concerns the amplitude and the resummation coefficients in the Sudakov form factor. Of course doing so will not yield an accurate result, however it will be sufficient to understand the numerical problem underlying the computation and to appreciate the difference between the standard QCD case and the abelianized one.

- Moreover we can just take into account a single partonic subprocess for the production of a Z boson plus the emission of a photon from initial state radiation, i.e. $u + \bar{u} \to Z + \gamma$ with $Z \to \nu\bar{\nu}$. Variations in the initial state partons, such as the process $d + \bar{d} \to Z + \gamma$, and the inclusion of massive final-state leptons, for example $Z \to \mu^+\mu^-$, will be briefly addressed later on.

In the small transverse-momentum limit, using the collinear approximation, we can schematically write the amplitude as

$$B_{Z\gamma} \sim B_Z \, dP_\gamma(z, p_{\mathrm{T}}), \tag{5.3.3}$$

where dP_γ is the probability for the emission of a collinear photon, namely

$$dP_\gamma(z, p_{\mathrm{T}}) = \frac{\alpha}{2\pi} \sum_q \frac{dp_{\mathrm{T}}}{p_{\mathrm{T}}} P_{q\to q\gamma}(z) dz \tag{5.3.4}$$

and $P_{q\to q\gamma}(z)$ is the splitting kernel. The Sudakov form factor can then be written in terms of the splitting function as

$$\Delta^2(Q, p_{\mathrm{T}}) = e^{-S(Q,p_{\mathrm{T}})} = \exp\left\{ -\sum_q \frac{\alpha}{2\pi} \int_{p_{\mathrm{T}}}^{Q} \frac{dq'_{\mathrm{T}}}{q'_{\mathrm{T}}} \int_{z_{\min}}^{z_{\max}} P_{q\to q\gamma}(z') dz' \right\}, \tag{5.3.5}$$

so that at the lowest order the MiNLO′ differential cross section in the transverse momentum and in the Born phase space Φ_B becomes

$$\frac{d\sigma^{\mathrm{MiNLO}}_{\mathrm{LO}}}{dp_{\mathrm{T}} d\Phi_B} \sim \frac{dB_{Z\gamma}}{d\Phi_B} e^{-S(Q,p_{\mathrm{T}})} \sim \frac{dB_Z}{d\Phi_B} \frac{d}{dp_{\mathrm{T}}} e^{-S(Q,p_{\mathrm{T}})}. \tag{5.3.6}$$

Note that this discussion is only schematic, a more rigorous derivation comprehensive also of the full NLO case can be found in Chapter 6 and references therein. For our purpose we want to focus on the fact that p_{T} dependence of the transverse-momentum distribution at leading order is completely driven by the MiNLO-improved derivative of the Sudakov form factor. This means that the value at which the differential cross section peaks can be found by computing the second derivative of the Sudakov form factor with respect to the transverse momentum and taking its root. In other words we want to find the value $p_{\mathrm{T}}^{\mathrm{peak}}$ such that

$$\frac{d^2}{dp_{\mathrm{T}}^2} e^{-S(Q,p_{\mathrm{T}})} \bigg|_{p_{\mathrm{T}}=p_{\mathrm{T}}^{\mathrm{peak}}} = 0. \tag{5.3.7}$$

The numerical evaluation of the above equation for the pure QED Sudakov form factor can be problematic even with the use of dedicated tools such as Wolfram Mathematica, so we opted for a graphical solution. With the approximations that we discussed above we can rewrite the Sudakov form factor as

$$e^{-S(Q,p_{\mathrm{T}})} = \exp\left\{ -\frac{\alpha}{2\pi} \left(A^{(1)} \log^2 \frac{Q^2}{p_{\mathrm{T}}^2} + 2B^{(1)} \log \frac{Q^2}{p_{\mathrm{T}}^2} \right) \right\}. \tag{5.3.8}$$

We consider two different cases:

- "Standard QED" which corresponds to the following value for the coupling constant

  $$\alpha = \alpha(0) \approx 1/137 \tag{5.3.9}$$

  and the Sudakov coefficients

  $$A_u^{(1),\mathrm{QED}} = Q_u^2 \approx 0.444, \qquad B_u^{(1),\mathrm{QED}} = -\frac{3}{2} Q_u^2 \approx -0.666. \tag{5.3.10}$$

- "Inflated QED", where we use the standard QED coefficients of the form factor but the QED coupling constant is inflated to a non-physical value, that is

$$\alpha = \widetilde{\alpha}(0) = 0.04, \tag{5.3.11}$$

  which is roughly 5 times larger than the standard value. This value represents an approximation of the maximum value that α can assume at the Thompson limit if we require that the QED Landau pole is not within the reach of the LHC, as explained in Appendix C.

By taking the derivative with respect to the transverse momentum of the Sudakov form factor as written in eq. (5.3.8), we get

$$D[e^{-S}](p_{\mathrm{T}}) = e^{-S(M_Z,p_{\mathrm{T}})}\frac{\alpha}{2\pi}\frac{1}{p_{\mathrm{T}}}\left(A^{(1)}\log\frac{M_Z^2}{p_{\mathrm{T}}^2} + B^{(1)}\right) \tag{5.3.12}$$

where we set $Q = M_Z$ as the hard scale of the process. In Fig. 5.1 we show the plot of $D[e^{-S}](p_{\mathrm{T}})$ for both cases on a logarithmic scale in p_{T}. The huge difference in the position of the peak between the two curves is only caused by the choice of the value of α which must be compensated by the logarithm. Note that these curves should not be considered as proper approximations of their relative differential cross sections and they are only used to estimate the position of the maximum of the distribution. Indeed the difference in the height between the two curves, enhanced by the $1/p_{\mathrm{T}}$ in eq. (5.3.12), is not of physical interest.

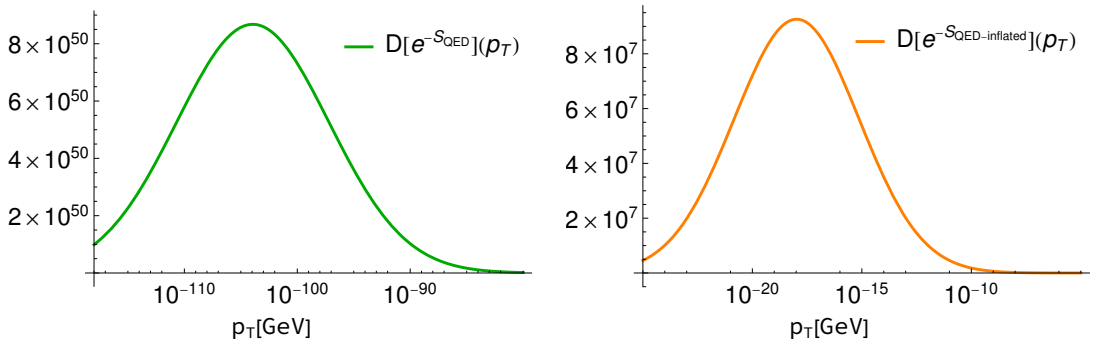

Figure 5.1: Derivative of the Sudakov form factor with respect to p_{T} for pure QED (left) and inflated QED (right).

Now if we were to consider the $d\bar{d}$-initiated process instead, the effect would just amount to a factor of 4 in both the first order resummation coefficients, namely

$$A_d^{(1),\mathrm{QED}} = \frac{1}{4}A_u^{(1),\mathrm{QED}}, \qquad B_d^{(1),\mathrm{QED}} = \frac{1}{4}B_u^{(1),\mathrm{QED}}. \tag{5.3.13}$$

In practical terms, this would only shift the plot further towards the problematic region similarly to what happens when we go from the inflated value of α to the

physical one. If instead we consider a different final state, where the Z boson decays into massive charged leptons, things get slightly more complicated. The coefficient $A^{(1)}$ is left completely untouched, while $B^{(1)}$ is modified according to eq. (5.2.12) in order to take into account the large-angle soft radiation from final-state heavy particles. It is important to note that the term coming from the first-order soft anomalous dimension, $2\,\mathrm{Re}\,\Gamma^{\mathrm{QED},(1)}_{t,u}$, is kinematic dependent. As a result, $B^{(1)}$ is not a constant anymore, which means that the approximations we used to write eq. (5.3.8) are no longer valid. However we can simplify the expression in eq. (5.2.13) to try to estimate its contribution for the $\mu^+\mu^-$ final state. First we note that the last term in the expression can be neglected as it is much smaller than the rest. Then we can write the parameter v as

$$v = \sqrt{1 - \frac{4m_\mu^4}{(M^2 - 2m_\mu^2)^2}} \approx 1 - \frac{2m_\mu^4}{M_Z^4} = 1 - r \tag{5.3.14}$$

where $r \approx 10^{-12}$ and we get $2\,\mathrm{Re}\,\Gamma^{\mathrm{QED},(1)}_{t,u} \approx 13.8$.

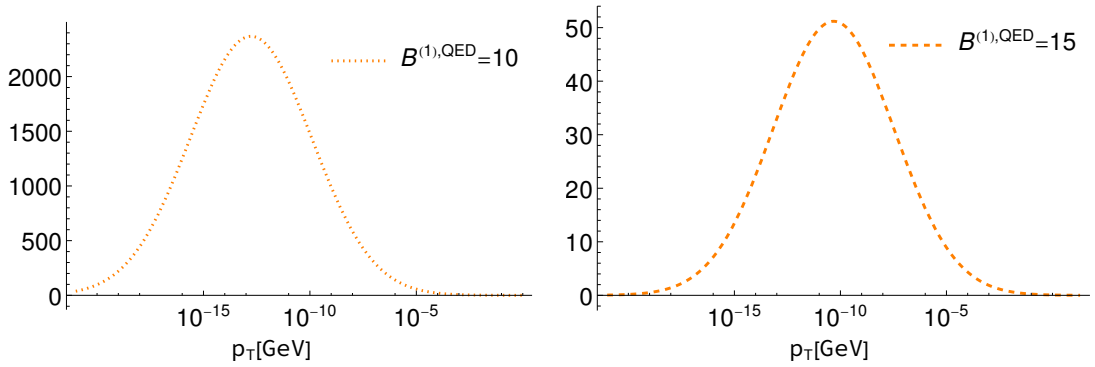

Figure 5.2: Comparison between $D[e^{-S^{\mathrm{QED}}_{\mathrm{inflated}}}](p_{\mathrm{T}})$ with two different values for $B^{(1)}$

In Fig. 5.2 we present the plot for the derivative of the Sudakov form factor with $\alpha = \widetilde{\alpha}(0)$ and two different values of the $B^{(1)}$ coefficient that mimic the effect of the $\mu^+\mu^-$ final state. Note that despite using the unphysical value for the coupling constant, the position of the peak is still deep in the region of phase space that cannot be probed by the integration.

Finally, as a reference, in Fig. 5.3, we compare the first two QED curves to the QCD case which corresponds to the following values for the Sudakov coefficients

$$A_q^{(1),\mathrm{QCD}} = C_{\mathrm{F}} \approx 1.333, \qquad B_q^{(1),\mathrm{QCD}} = -\frac{3}{2}C_{\mathrm{F}} = -2. \tag{5.3.15}$$

Despite only being a rough approximation, it is clear that the QCD Sudakov is perfectly compatible with the numerical restriction given by the introduction of a cutoff in transverse momentum, while the same is not true for QED even in the

unphysical inflated case. We shall keep in mind that the need for some sort of cutoff in the integration cannot be overlooked, thus in order to be able to implement the MiNLO′ method correctly in QED without accuracy loss we need to find a way to include, or at least estimate, the contribution given by the terms below the cutoff.

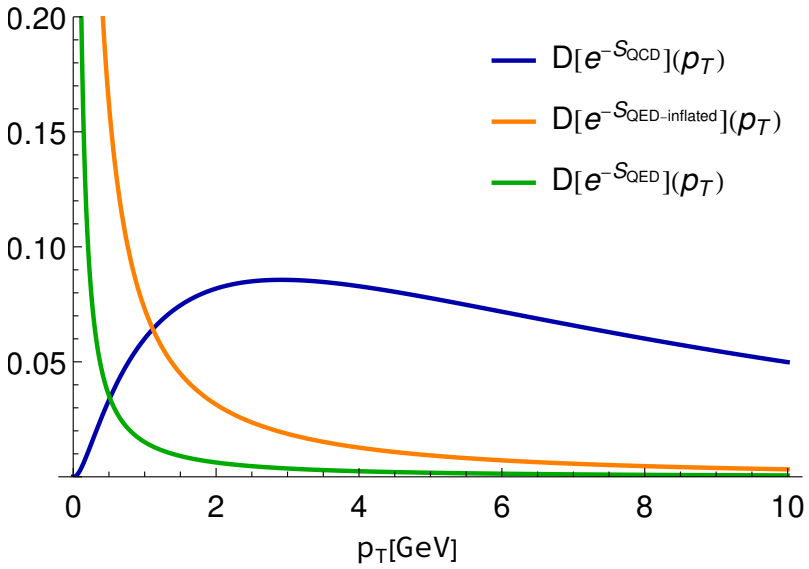

Figure 5.3: Comparison between the derivative of the Sudakov form factor with respect to p_T for three different cases. The orange and green curves are the same that appear in Fig. 5.1 while the blue one corresponds to an approximation of the QCD case. The latter was obtained by fixing $\alpha_s = 0.4$ which is roughly the value of the strong coupling constant in the GeV region. This of course is not a good approximation due to the low energy behaviour of α_s discussed previously in this section, however it is helpful to show the enormous difference between QCD and QED.

Chapter 6

The cross section below the transverse momentum cut

We can divide the full MiNLO′ cross section into two contributions, above and below some value of the transverse momentum p_{T}^{δ}, so that we can write

$$\sigma_{\mathrm{TOT}} = \int \frac{d\sigma}{dp_{\mathrm{T}}} dp_{\mathrm{T}} = \sigma_{<}(p_{\mathrm{T}}^{\delta}) + \sigma_{>}(p_{\mathrm{T}}^{\delta}), \tag{6.0.1}$$

where we have defined, depending on the value of p_{T}^{δ},

$$\sigma_{>}(p_{\mathrm{T}}^{\delta}) \equiv \int_{p_{\mathrm{T}}^{\delta}}^{p_{\mathrm{T}}^{\mathrm{max}}} \frac{d\sigma}{dp_{\mathrm{T}}} dp_{\mathrm{T}}, \qquad \sigma_{<}(p_{\mathrm{T}}^{\delta}) \equiv \int_{0}^{p_{\mathrm{T}}^{\delta}} \frac{d\sigma}{dp_{\mathrm{T}}} dp_{\mathrm{T}}, \tag{6.0.2}$$

and where $p_{\mathrm{T}}^{\mathrm{max}}$ is the kinematic boundary for p_{T}, i.e. $p_{\mathrm{T}}^{\mathrm{max}} \simeq \sqrt{s}/2$. In the expression for $\sigma_{>}$, the role of p_{T}^{δ} is precisely the same played by the transverse momentum cutoff mentioned in the previous section. This opens up three different possible scenarios:

1. The missing contribution coming from the terms below the cutoff, $\sigma_{<}$, is much larger than the part above, $\sigma_{>}$, for any reasonable value of p_{T}^{δ}. This is the most unfortunate scenario and it would mean that it is not possible to obtain a detailed description of the QED radiation pattern below p_{T}^{δ} and, as a consequence, to exploit the MiNLO′ method to its fullness.

2. The missing piece, $\sigma_{<}$, is much smaller than the contribution above the cutoff, $\sigma_{>}$. In other words, the increase of the differential cross section $d\sigma/dp_{\mathrm{T}}$ in the region at $p_{\mathrm{T}} < p_{\mathrm{T}}^{\delta}$ is somewhat negligible due to the width of the corresponding integration interval, namely the value of p_{T}^{δ}. Note that it always exists, in principle, some value of p_{T}^{δ} for which this is true: it is just a question of whether such value is accessible via the numerical integration. If so, this would be the ideal case, as it would mean that the method can be extended straightforwardly in QED.

3. The two contributions, $\sigma_>$ and $\sigma_<$, are comparable in size for all sensible values of p_{T}^{δ}. In this case it is important to estimate the contribution coming from $\sigma_<$ with the highest accuracy achievable, as the full result must be obtained by the sum of both terms. Note that the full computation is by definition independent of the choice of p_{T}^{δ}, which means that, if the eventual approximations used to compute $\sigma_<$ are reasonable, the dependence on the value of p_{T}^{δ} between the two contributions should cancel out, or at least be fairly suppressed.

A priori we do not know which one of these three scenarios will be realized in our computation, so we need a reliable way to estimate $\sigma_<$.

6.1 Approximation of the MiNLO′ master formula

In eq. (5.3.6) it was schematically shown that it is possible to approximate the singular part of the differential cross section at LO, in the small transverse momentum region, in such a way that the dependence on p_{T} is encoded in a total derivative. As a consequence, the integral over some transverse-momentum interval can be obtained by integrating out the total derivative, which amounts to evaluating the integrand at the boundaries. In this way it is possible to estimate the contribution of the $\sigma_<$ part without the need of a numerical integration which, as we saw in the previous chapter, is unfeasable. In order to avoid accuracy loss in the process, we need to be able to write the full NLO differential cross section as a total derivative in p_{T}, plus some terms that can be neglected as the transverse momentum approaches zero. To do so we exploit some of the ideas first introduced in Ref. [16] and then matured in the context of MiNNLO$_{\mathrm{PS}}$ [24, 25], which is an NNLO accurate extension of the MiNLO′ method.

We want to write the differential cross section in the following form

$$\frac{d\sigma}{d\Phi_B dp_{\mathrm{T}}} = \frac{d}{dp_{\mathrm{T}}}\Big[e^{-S(Q,p_{\mathrm{T}})}\mathcal{L}(p_{\mathrm{T}})\Big] + R_f(p_{\mathrm{T}}), \tag{6.1.1}$$

where R_f is the sum of all the terms that are non-singular in the vanishing transverse momentum limit. The luminosity factor $\mathcal{L}$ contains the parton luminosities, the hard-virtual coefficient for the underlying process, namely the full inclusive production of a Z boson, and the collinear coefficient functions. It is defined as

$$\mathcal{L}(p_{\mathrm{T}}) = \sum_c \frac{d|\mathcal{M}^{(0)}_{c\bar{c}\to Z}|^2}{d\Phi_B} \sum_{a_1 a_2} \Big\{\mathcal{H}^{ll}_{c\bar{c}}\Big(C_{ca_1}\otimes f_{a_1/h_1}\Big)\Big(C_{\bar{c}a_2}\otimes f_{a_2/h_2}\Big)\Big\}, \tag{6.1.2}$$

where $\mathcal{M}^{(0)}_{c\bar{c}\to Z}$ is the LO matrix element for the production of a Z boson, the hard-virtual coefficient $\mathcal{H}^{ll}_{c\bar{c}}$ is the one defined in eq. (5.2.6), that, if final-state massive charged leptons are present, must contain also the finite part of the subtraction operator, as in eq. (5.2.11).

Up to NLO we can write the non-singular contribution R_f as

$$R_f(p_{\mathrm{T}}) = \frac{d\sigma^{(\mathrm{NLO})}_{Z\gamma}}{d\Phi_B dp_{\mathrm{T}}} - \frac{\alpha(p_{\mathrm{T}})}{2\pi}\Sigma^{(1)}(p_{\mathrm{T}}) - \left(\frac{\alpha(p_{\mathrm{T}})}{2\pi}\right)^2 \Sigma^{(2)}(p_{\mathrm{T}}) + \mathcal{O}\left(\alpha^3(p_{\mathrm{T}})\right), \tag{6.1.3}$$

where $\Sigma^{(i)}$ is a shorthand notation for the perturbative coefficient of the i-th term of the singular component of the expnsion in $\alpha/2\pi$ of the cross section, i.e

$$\Sigma^{(1)}(p_{\mathrm{T}}) = \left[\frac{d\sigma^{(\mathrm{sing.})}_{Z\gamma}}{d\Phi_B dp_{\mathrm{T}}}\right]^{(1)}, \qquad \Sigma^{(2)}(p_{\mathrm{T}}) = \left[\frac{d\sigma^{(\mathrm{sing.})}_{Z\gamma}}{d\Phi_B dp_{\mathrm{T}}}\right]^{(2)}. \tag{6.1.4}$$

Additionally, we can write the expansion of the full NLO differential cross section that appears as the first term of eq. (6.1.3) as

$$\frac{d\sigma^{(\mathrm{NLO})}_{Z\gamma}}{d\Phi_B dp_{\mathrm{T}}} = \frac{\alpha(p_{\mathrm{T}})}{2\pi}\left[\frac{d\sigma_{Z\gamma}}{d\Phi_B dp_{\mathrm{T}}}\right]^{(1)} + \left(\frac{\alpha(p_{\mathrm{T}})}{2\pi}\right)^2 \left[\frac{d\sigma_{Z\gamma}}{d\Phi_B dp_{\mathrm{T}}}\right]^{(2)}. \tag{6.1.5}$$

We can perform the derivative in the first term on the right hand side of eq. (6.1.1) and factorize the Sudakov form factor so that we get

$$\frac{d\sigma}{d\Phi_B dp_{\mathrm{T}}} = e^{-S(Q,p_{\mathrm{T}})}\left[D(p_{\mathrm{T}}) + \frac{R_f(p_{\mathrm{T}})}{e^{-S(Q,p_{\mathrm{T}})}}\right], \tag{6.1.6}$$

where we defined

$$D(p_{\mathrm{T}}) \equiv \frac{d\mathcal{L}(p_{\mathrm{T}})}{dp_{\mathrm{T}}} - \mathcal{L}(p_{\mathrm{T}})\frac{dS(p_{\mathrm{T}})}{dp_{\mathrm{T}}}. \tag{6.1.7}$$

We want to perturbatively expand eq. (6.1.6) up to order $\alpha^2(p_{\mathrm{T}})$ so that the NLO accuracy is not spoiled. In order to do so, we introduce the following perturbative expansions

$$\mathcal{L}(p_{\mathrm{T}}) = \mathcal{L}^{(0)}(p_{\mathrm{T}}) + \frac{\alpha(p_{\mathrm{T}})}{2\pi}\mathcal{L}^{(1)}(p_{\mathrm{T}}) + \mathcal{O}\left(\alpha^2(p_{\mathrm{T}})\right), \tag{6.1.8}$$

$$\frac{d\mathcal{L}(p_{\mathrm{T}})}{dp_{\mathrm{T}}} = \frac{\alpha(p_{\mathrm{T}})}{2\pi}\left[\frac{d\mathcal{L}(p_{\mathrm{T}})}{dp_{\mathrm{T}}}\right]^{(1)} + \left(\frac{\alpha(p_{\mathrm{T}})}{2\pi}\right)^2\left[\frac{d\mathcal{L}(p_{\mathrm{T}})}{dp_{\mathrm{T}}}\right]^{(2)} + \mathcal{O}\left(\alpha^3(p_{\mathrm{T}})\right), \tag{6.1.9}$$

$$\frac{dS(p_{\mathrm{T}})}{dp_{\mathrm{T}}} = \frac{\alpha(p_{\mathrm{T}})}{2\pi}\left[\frac{dS(p_{\mathrm{T}})}{dp_{\mathrm{T}}}\right]^{(1)} + \left(\frac{\alpha(p_{\mathrm{T}})}{2\pi}\right)^2\left[\frac{dS(p_{\mathrm{T}})}{dp_{\mathrm{T}}}\right]^{(2)} + \mathcal{O}\left(\alpha^3(p_{\mathrm{T}})\right). \tag{6.1.10}$$

Thus we have

$$\begin{aligned}\frac{d\sigma}{d\Phi_B dp_{\mathrm{T}}} = e^{-S(Q,p_{\mathrm{T}})}\Bigg\{ & \frac{\alpha(p_{\mathrm{T}})}{2\pi}\left(\left[\frac{d\mathcal{L}}{dp_{\mathrm{T}}}\right]^{(1)} - \mathcal{L}^{(0)}\left[\frac{dS}{dp_{\mathrm{T}}}\right]^{(1)}\right) \\ & + \left(\frac{\alpha(p_{\mathrm{T}})}{2\pi}\right)^2\left(\left[\frac{d\mathcal{L}}{dp_{\mathrm{T}}}\right]^{(2)} - \mathcal{L}^{(0)}\left[\frac{dS}{dp_{\mathrm{T}}}\right]^{(2)} - \mathcal{L}^{(1)}\left[\frac{dS}{dp_{\mathrm{T}}}\right]^{(1)}\right) \\ & + R_f(p_{\mathrm{T}})\left(1 + \frac{\alpha(p_{\mathrm{T}})}{2\pi}S^{(1)}(Q,p_{\mathrm{T}})\right) + \mathcal{O}\left(\alpha^3(p_{\mathrm{T}})\right)\Bigg\}.\end{aligned} \tag{6.1.11}$$

Plugging in eqs. (6.1.3) and (6.1.5) and collecting the terms with the same power of the coupling constant, we have

$$\begin{aligned}\frac{d\sigma}{d\Phi_B dp_{\mathrm{T}}} = e^{-S(Q,p_{\mathrm{T}})}\Bigg\{ & \frac{\alpha(p_{\mathrm{T}})}{2\pi}\left(\left[\frac{d\mathcal{L}}{dp_{\mathrm{T}}}\right]^{(1)} - \mathcal{L}^{(0)}\left[\frac{dS}{dp_{\mathrm{T}}}\right]^{(1)} + \left[\frac{d\sigma_{Z\gamma}}{d\Phi_B dp_{\mathrm{T}}}\right]^{(1)} - \Sigma^{(1)}(p_{\mathrm{T}})\right) \\ & + \left(\frac{\alpha(p_{\mathrm{T}})}{2\pi}\right)^2\left(\left[\frac{d\mathcal{L}}{dp_{\mathrm{T}}}\right]^{(2)} - \mathcal{L}^{(0)}\left[\frac{dS}{dp_{\mathrm{T}}}\right]^{(2)} - \mathcal{L}^{(1)}\left[\frac{dS}{dp_{\mathrm{T}}}\right]^{(1)}\right. \\ & + \left[\frac{d\sigma_{Z\gamma}}{d\Phi_B dp_{\mathrm{T}}}\right]^{(2)} - \Sigma^{(2)}(p_{\mathrm{T}}) + \left[\frac{d\sigma_{Z\gamma}}{d\Phi_B dp_{\mathrm{T}}}\right]^{(1)} S^{(1)}(Q,p_{\mathrm{T}}) \\ & \left. - \Sigma^{(1)}(p_{\mathrm{T}})S^{(1)}(Q,p_{\mathrm{T}})\right) + \mathcal{O}\left(\alpha^3(p_{\mathrm{T}})\right)\Bigg\}.\end{aligned} \tag{6.1.12}$$

From eq. (5.2.10) we can extract, using the definition of $\mathcal{L}(p_{\mathrm{T}})$ in eq. (6.1.2), the expressions for the singular part of the differential cross section at LO and NLO, namely

$$\Sigma^{(1)}(p_{\mathrm{T}}) = D^{(1)}(p_{\mathrm{T}}) = \left[\frac{d\mathcal{L}(p_{\mathrm{T}})}{dp_{\mathrm{T}}}\right]^{(1)} - \mathcal{L}^{(0)}(p_{\mathrm{T}})\left[\frac{dS(p_{\mathrm{T}})}{dp_{\mathrm{T}}}\right]^{(1)} \tag{6.1.13}$$

$$\begin{aligned}\Sigma^{(2)}(p_{\mathrm{T}}) &= D^{(2)}(p_{\mathrm{T}}) - D^{(1)}(p_{\mathrm{T}})S^{(1)}(Q,p_{\mathrm{T}}) \\ &= \left[\frac{d\mathcal{L}(p_{\mathrm{T}})}{dp_{\mathrm{T}}}\right]^{(2)} - \mathcal{L}^{(1)}(p_{\mathrm{T}})\left[\frac{dS(p_{\mathrm{T}})}{dp_{\mathrm{T}}}\right]^{(1)} - \mathcal{L}^{(0)}(p_{\mathrm{T}})\left[\frac{dS(p_{\mathrm{T}})}{dp_{\mathrm{T}}}\right]^{(2)} \\ &\quad - \Sigma^{(1)}(p_{\mathrm{T}})S^{(1)}(Q,p_{\mathrm{T}}).\end{aligned} \tag{6.1.14}$$

Once we substitute the expressions for $\Sigma^{(1)}$ and $\Sigma^{(2)}$ back into eq. (6.1.12) we obtain

$$\begin{aligned}\frac{d\sigma}{d\Phi_B dp_{\mathrm{T}}} = e^{-S(Q,p_{\mathrm{T}})}\Bigg\{ & \frac{\alpha(p_{\mathrm{T}})}{2\pi}\left[\frac{d\sigma_{Z\gamma}}{d\Phi_B dp_{\mathrm{T}}}\right]^{(1)}\left(1 - \frac{\alpha(p_{\mathrm{T}})}{2\pi}S^{(1)}(Q,p_{\mathrm{T}})\right) \\ & + \left(\frac{\alpha(p_{\mathrm{T}})}{2\pi}\right)^2\left[\frac{d\sigma_{Z\gamma}}{d\Phi_B dp_{\mathrm{T}}}\right]^{(2)} + \mathcal{O}\left(\alpha^3(p_{\mathrm{T}})\right)\Bigg\}\end{aligned} \tag{6.1.15}$$

which is perfectly equivalent, up to NLO, to the abelianized MiNLO′ master formula.

Now if we assume that there is some value of p_{T}^{δ} that guarantees that the second term on the right hand side of eq. (6.1.1), namely the sum of the non-singular terms, can be safely ignored with respect to the first term, we can write

$$\frac{d\sigma_{<}(p_{\mathrm{T}}^{\delta})}{d\Phi_B} = \int_0^{p_{\mathrm{T}\,\delta}} \frac{d}{dp_{\mathrm{T}}}\left[e^{-S(Q,p_{\mathrm{T}})}\mathcal{L}(p_{\mathrm{T}})\right]dp_{\mathrm{T}}. \tag{6.1.16}$$

The integration is now trivial due to the presence of the total derivative. Moreover given the suppression provided by the Sudakov form factor,

$$\lim_{p_{\mathrm{T}}\to 0} e^{-S(Q,p_{\mathrm{T}})}\mathcal{L}(p_{\mathrm{T}}) = 0, \tag{6.1.17}$$

so we have that

$$\frac{d\sigma_{<}(p_{\mathrm{T}}^{\delta})}{d\Phi_B} = \left[e^{-S(Q,p_{\mathrm{T}})}\mathcal{L}(p_{\mathrm{T}})\right]_{p_{\mathrm{T}}=p_{\mathrm{T}}^{\delta}}. \tag{6.1.18}$$

This is an important result, as it allows us to reshape the challenging task represented by the integration within a region which is not numerically accessible to a much manageable job that consists in the evaluation of a function, as complex as it may be, in a single point.

The first two terms of the expansion of the luminosity factor, introduced in eq. (6.1.2), are given by

$$\mathcal{L}^{(0)}(p_{\mathrm{T}}) = \sum_c \frac{d|\mathcal{M}^{(0)}_{c\bar{c}\to Z}|^2}{d\Phi_B} f_{c/h_1} f_{\bar{c}/h_2}, \tag{6.1.19}$$

$$\begin{aligned}\mathcal{L}^{(1)}(p_{\mathrm{T}}) \;= &\sum_c \frac{d|\mathcal{M}^{(0)}_{c\bar{c}\to Z}|^2}{d\Phi_B} \left\{ \left(H^{ll\,(1)}_{c\bar{c}} + F_t^{(1)}\right) f_{c/h_1} f_{\bar{c}/h_2} \right. \\ &\left. + \sum_a \left[f_{c/h_1} \left(C^{(1)}_{\bar{c}a} \otimes f_{a/h_2}\right) + \left(C^{(1)}_{ca} \otimes f_{a/h_1}\right) f_{\bar{c}/h_2} \right] \right\}\end{aligned} \tag{6.1.20}$$

Note that the sum over the indices a_1 and a_2 in eq. (6.1.2) was removed because the underlying process, i.e. the inclusive production of a Z boson without any additional radiation, is described at leading order only by $q\bar{q}$-initiated processes.

It is important to study the origin of the transverse momentum dependence in the square brackets in eq. (6.1.16) in order to understand possible residual criticalities in this computation. More specifically, we want to expand on the transverse-momentum dependence of the luminosity factor $\mathcal{L}(p_{\mathrm{T}})$. The LO matrix element for the subprocess $c\bar{c} \to Z$ is determined by the inclusive underlying Born phase space Φ_B: therefore it is completely independent of the Z boson transverse momentum. Similarly both $H^{ll\,(1)}_{c\bar{c}}$ and $F_t^{(1)}$, despite being dependent on the kinematics in general, are uniquely determined by the phase-space configuration of the underlying Born and, as a consequence, cannot be p_{T}-dependent. The same can be said for the first-order collinear coefficient functions which can vary at most by some universal factor, depending on the choice of the resummation scheme. The dependence on the transverse momentum in the luminosity factor is carried by μ_{R} and μ_{F}, both of which must be evaluated at $\mu_{\mathrm{R}} = \mu_{\mathrm{F}} = p_{\mathrm{T}}$, according to the MiNLO′ prescription[1]. In particular, if we consider the factorization-scale dependence, this means that we have to evaluate the parton

[1]For a detailed discussion on the topic, see the original MiNLO [15] and MiNLO′ [16] papers.

distribution functions at $p_{\mathrm{T}} = p_{\mathrm{T}}^{\delta}$, which, as we already mentioned, is likely to be much smaller than the natural cutoff of QCD, of the order of a few hudreds MeV. As a consequence, many of the numerical packages that are used to handle the evolutions of the parton distribution functions might not be able to reach such values. Possible solutions are, if the code allows it, to turn off completely the QCD DGLAP evolution and perform the standard evolution only with QED towards $\mu_{\mathrm{F}} = p_{\mathrm{T}}^{\delta}$, or to introduce a freezing of the PDFs at the minimum possible value of the factorization scale. This aspect of the computation will be addressed again in Chapter 7, when we discuss the implementation of the formulae and the results.

6.2 Numerical validation

In order for the computation to work, we need to check if the assumption that was made in the previous section is solid. More specifically, in order to be able to use eq. (6.1.16) we need to determine, if it exists, a value of p_{T}^{δ} such that:

- It is within the numerically accessible region for the computation of $\sigma_{>}$, that is $p_{\mathrm{T}}^{\delta} > 10^{-3}$ GeV. Preferably closer to the GeV region, where we know from QCD that the standard integration can be performed without issues.
- The non singular terms can be neglected, which means that the differential cross section $d\sigma_{Z\gamma}/d\Phi_B dp_{\mathrm{T}}$ is approximated reasonably by its $p_{\mathrm{T}} \to 0$ limit.

We first rewrite eqs. (4.1.7) and (4.1.8) for the QED case in the following form

$$\frac{d\sigma_{h_1h_2\to Z\gamma}}{dp_{\mathrm{T}}^2\, dM^2\, dy\, d\Phi_B} = \sum_{a_1a_2} \int \frac{dz_1}{z_1} \int \frac{dz_2}{z_2}\, f_{a_1/h_1}\left(\frac{x_1}{z_1}, \mu_{\mathrm{F}}^2\right) f_{a_2/h_2}\left(\frac{x_2}{z_2}, \mu_{\mathrm{F}}^2\right) \times \int \frac{d^2\vec{b}}{4\pi}\, e^{i\vec{b}\cdot\vec{p}_{\mathrm{T}}}\, \mathcal{W}^{ll}_{a_1a_2}(b, z_1, z_2, \Phi_B; \alpha, \mu_{\mathrm{R}}^2, \mu_{\mathrm{F}}^2, Q^2), \quad (6.2.1)$$

where

$$\begin{aligned}\mathcal{W}^{ll}_{a_1a_2}(b, z_1, z_2, \Phi_B; \alpha, \mu_{\mathrm{R}}^2, \mu_{\mathrm{F}}^2, Q^2) = \sum_c \sigma^{(0)}_{c\bar{c},ll} \Bigg\{ & \delta_{ca_1}\, \delta_{\bar{c}a_2}\, \delta(1-z_1)\, \delta(1-z_2) \\ & + \sum_{n=1}^{\infty} \left(\frac{\alpha}{\pi}\right)^n \Bigg[\Sigma^{ll\,(n)}_{c\bar{c},a_1a_2}\left(z_1, z_2, L_b; \frac{M^2}{\mu_{\mathrm{R}}^2}, \frac{M^2}{\mu_{\mathrm{F}}^2}, \frac{M^2}{Q^2}\right) \\ & + \left[\, HCC \,\right]^{ll\,(n)}_{c\bar{c},a_1a_2}\left(z_1, z_2; \frac{M^2}{\mu_{\mathrm{R}}^2}, \frac{M^2}{\mu_{\mathrm{F}}^2}, \frac{M^2}{Q^2}\right) \Bigg] \Bigg\}. \end{aligned} \quad (6.2.2)$$

For ease of notation, we drop the superscript ll in the following. To perform the limit check we want to simplify the expressions as much as possible, so we will set the values of the renormalization and factorization scales to $\mu_{\mathrm{R}} = \mu_{\mathrm{F}} = M$. This is

perfectly reasonable as in this manuscript in general, and in particular for what we discuss here, we are not interested in the effect of the scale variation logarithms that would appear by changing the value of those two scales. In the same way we can take $Q = M$, where Q is the arbitrary auxiliary scale that was introduced to define the b-space logarithm used for the expansion in eq. (4.1.6). Furthermore we will consider for simplicity only the $u\bar{u}$-initiated processes and a charge-neutral massless final state, that is $Z \to \nu\bar{\nu}$. Finally, we set the electromagnetic constant to a non-physical value, i.e. $\alpha = \widetilde{\alpha}(0) = 0.04$. This is done in order to enhances the impact of the NLO corrections over the LO, allowing us to probe the limit at order $\mathcal{O}(\alpha^2)$.

We focus on the second line of eq. (6.2.2) which contains the logarithmically divergent terms expressed in powers of $L_b = \log(Q^2 b^2/b_0^2)$ up to the $2n$-th power, that is

$$\Sigma^{(n)}_{c\bar{c},a_1a_2}(z_1, z_2, L_b) = \sum_{k=1}^{2n} \Sigma^{(n,k)}_{c\bar{c},a_1a_2}(z_1, z_2)\, L_b^k. \tag{6.2.3}$$

More specifically, the first two orders are given by

$$\Sigma^{(1)}_{c\bar{c},a_1a_2}(z_1, z_2, L_b) = \Sigma^{(1,2)}_{c\bar{c},a_1a_2}(z_1, z_2)\, L_b^2 + \Sigma^{(1,1)}_{c\bar{c},a_1a_2}(z_1, z_2)\, L_b\,, \tag{6.2.4}$$

$$\begin{aligned}\Sigma^{(2)}_{c\bar{c},a_1a_2}(z_1, z_2, L_b) = {} & \Sigma^{(2,4)}_{c\bar{c},a_1a_2}(z_1, z_2)\, L_b^4 + \Sigma^{(2,3)}_{c\bar{c},a_1a_2}(z_1, z_2)\, L_b^3 \\ & + \Sigma^{(2,2)}_{c\bar{c},a_1a_2}(z_1, z_2)\, L_b^2 + \Sigma^{(2,1)}_{c\bar{c},a_1a_2}(z_1, z_2)\, L_b\,.\end{aligned} \tag{6.2.5}$$

These coefficients are usually expressed in literature in terms of their (N_1, N_2)-moments with respect to the variables z_1 and z_2. For this purpose, we define the double Mellin transform $f_{(N_1,N_2)}$ of the function $f(z_1, z_2)$ with respect to z_1 and z_2 as

$$f_{(N_1,N_2)} = \int_0^1 dz_1\; z_1^{N_1-1} \int_0^1 dz_2\; z_2^{N_2-1}\; f(z_1, z_2). \tag{6.2.6}$$

Note that the dependence on the impact parameter b rests entirely on the powers of L_b, while the coefficients of the expansion are left untouched by the Bessel integration. With some simplifications in the notation, we can rewrite the singular part of the differential cross section in eq. (6.2.1) as

$$\frac{d\sigma^{(\text{sing.})}}{dp_{\text{T}}^2} = \sum_{a_1a_2} \int [dz_1 z_2]\, f_{a_1/h_1} f_{a_2/h_2} \sum_c \sigma^{(0)}_{c\bar{c}} \left[\sum_{n=1}^{\infty} \left(\frac{\alpha}{\pi}\right)^n \tilde{\Sigma}^{(n)}_{c\bar{c},a_1a_2}(z_1, z_2, p_{\text{T}})\right] \tag{6.2.7}$$

with

$$\tilde{\Sigma}^{(n)}_{c\bar{c},a_1a_2}(z_1, z_2, p_{\text{T}}) = \sum_{k=1}^{2n} \Sigma^{(n,k)}_{c\bar{c},a_1a_2}(z_1, z_2)\, I_n(p_{\text{T}}, Q), \tag{6.2.8}$$

where the function $I_n(p_{\text{T}}, Q)$ is the Bessel transformation of the n-th power of L_b

$$I_n(p_{\text{T}}, Q) = \int \frac{d^2\vec{b}}{4\pi}\, e^{i\vec{b}\cdot\vec{p}_{\text{T}}} L_b^n. \tag{6.2.9}$$

It can be shown that [139, 140]

$$\int \frac{d^2\,\vec{b}}{(2\pi)^2}\, e^{i\,\vec{b}\cdot\vec{p}_{\rm T}}\, L_b^n = \sum_{k=0}^{n-1}(-1)^{k+1}\, n \binom{n-1}{k} R_2^{(n-k-1)}\, \mathfrak{L}_k(\vec{p}_{\rm T}, Q) \,+\, R_2^{(n)}\, \delta^{(2)}(\vec{p}_{\rm T}) \tag{6.2.10}$$

where the coefficient $R_2^{(n)}$ is given by

$$R_2^{(n)} = \frac{d^n}{da^n}\, e^{2\gamma_E a}\, \frac{\Gamma(1+a)}{\Gamma(1-a)}\bigg|_{a=0}. \tag{6.2.11}$$

The logarithm $\mathfrak{L}_k(\vec{p}_{\rm T}, Q)$ can be defined through a two dimensional plus distribution according to the convention used in Ref. [139] and, for $p_{\rm T}^2/Q^2 > 0$, it can be written as

$$\mathfrak{L}_k(\vec{p}_{\rm T}, Q) = \frac{1}{\pi p_{\rm T}^2}\left(\log\frac{p_{\rm T}^2}{Q^2}\right)^k = \frac{1}{\pi p_{\rm T}^2}\,(-2)^k\, L^k \tag{6.2.12}$$

where L is a shorthand notation for the $p_{\rm T}$-space logarithm

$$L = \log\frac{Q}{p_{\rm T}}. \tag{6.2.13}$$

In particular for $n \leq 4$ and $p_{\rm T} > 0$ we have[2]:

$$I_1(p_{\rm T}, Q) = -\pi\mathfrak{L}_0(\vec{p}_{\rm T}, Q) = -\frac{1}{p_{\rm T}^2}, \tag{6.2.14}$$

$$I_2(p_{\rm T}, Q) = 2\pi\mathfrak{L}_1(\vec{p}_{\rm T}, Q) = -\frac{4}{p_{\rm T}^2}L, \tag{6.2.15}$$

$$I_3(p_{\rm T}, Q) = -3\pi\mathfrak{L}_2(\vec{p}_{\rm T}, Q) = -\frac{12}{p_{\rm T}^2}L^2 \tag{6.2.16}$$

$$I_4(p_{\rm T}, Q) = 4\pi\mathfrak{L}_3(\vec{p}_{\rm T}, Q) + 16\pi\zeta_3\mathfrak{L}_0(\vec{p}_{\rm T}, Q) = -\frac{32}{p_{\rm T}^2}L^3 + \frac{16}{p_{\rm T}^2}\zeta_3 \tag{6.2.17}$$

In order to remove the $1/p_{\rm T}^2$ factors we can take

$$p_{\rm T}\frac{d\sigma}{dp_{\rm T}} = 2p_{\rm T}^2\frac{d\sigma}{dp_{\rm T}^2} \tag{6.2.18}$$

so that at LO we have

$$p_{\rm T}\frac{d\sigma_{\rm LO}^{(\rm sing.)}}{dp_{\rm T}} = \sum_{a_1a_2}\int [dz_1dz_2]\, f_{a_1/h_1} f_{a_2/h_2} \sum_c \sigma_{c\bar{c}}^{(0)}\left(\frac{\alpha}{2\pi}\right) \times 4\left[-4\,L\,\Sigma_{c\bar{c},a_1a_2}^{(1,2)}(z_1,z_2) - \Sigma_{c\bar{c},a_1a_2}^{(1,1)}(z_1,z_2)\right]. \tag{6.2.19}$$

[2] Analogous results can be found in Appendix B of Ref. [130].

The double Mellin moments of the $\Sigma^{(1,n)}_{c\bar{c},a_1a_2}$ coefficients for $Z \to \nu\bar{\nu}$ are given by

$$\Sigma^{(1,2)}_{c\bar{c},a_1a_2,(N_1,N_2)} = -\frac{1}{2} A^{(1)}_c \delta_{ca_1}\delta_{\bar{c}a_2}, \tag{6.2.20}$$

$$\Sigma^{(1,1)}_{c\bar{c},a_1a_2,(N_1,N_2)} = -[\delta_{ca_1}\delta_{\bar{c}a_2} B^{(1)}_c + \delta_{ca_1}\gamma^{(1)}_{\bar{c}a_2,N_2} + \gamma^{(1)}_{ca_1,N_1}\delta_{\bar{c}a_2}], \tag{6.2.21}$$

where the parton anomalous dimensions $\gamma^{(n)}_{ab,N}$ are defined as the coefficients of the expansions in α/π of the N-moments of the Altarelli-Parisi regularized splitting functions,

$$\gamma_{ab,N}(\alpha) = \int_0^1 dz\, z^{N-1}\, P_{ab}(\alpha, z) = \sum_{n=1}^{\infty} \left(\frac{\alpha}{\pi}\right)^n \gamma^{(n)}_{ab,N}. \tag{6.2.22}$$

Thus at LO we can easily write a complete expression for the $p_{\mathrm{T}} \to 0$ limit of the differential cross section as

$$p_{\mathrm{T}} \frac{d\sigma^{\mathrm{LO}}}{dp_{\mathrm{T}}} = \sum_c \int [dz_1 dz_2]\, f_{c/h_1} f_{\bar{c}/h_2}\, \sigma^{(0)}_{c\bar{c}} \left(\frac{\alpha}{2\pi}\right) \Bigg[\left(8\, L\, A^{(1)}_c + 4 B^{(1)}_c\right) + 2\, \frac{1}{f_{c/h_1} f_{\bar{c}/h_2}} \sum_a \left(f_{c/h_1} (P^{(0)}_{\bar{c}a} \otimes f_{a/h_2}) + (P^{(0)}_{ca} \otimes f_{a/h_1}) f_{\bar{c}/h_2} \right) \Bigg], \tag{6.2.23}$$

where, given the approximations discussed above, the sum over the index c contains only the up quark.

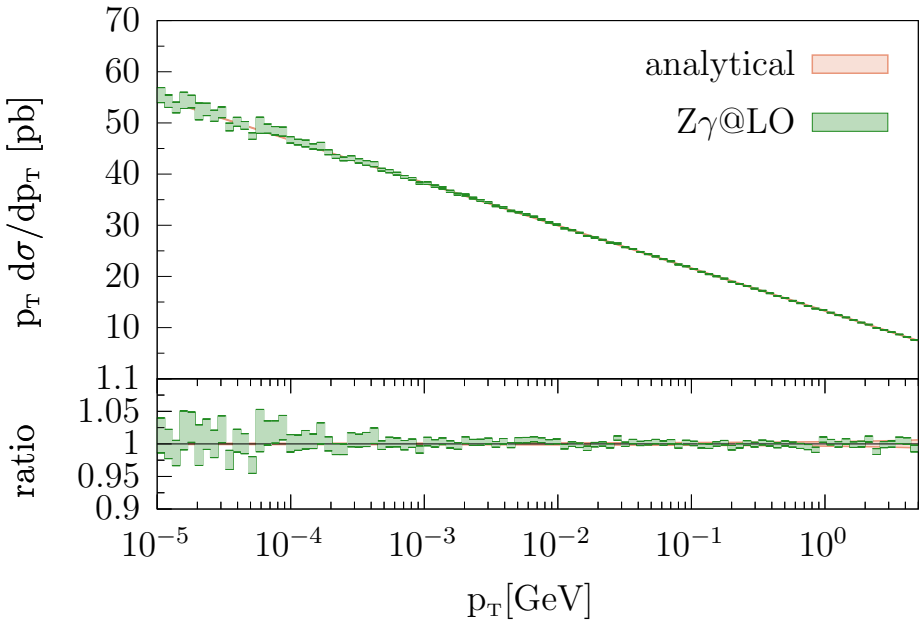

Figure 6.1: Comparison between the LO differential cross section and its analytical limit for small values of the transverse momentum of the Z boson.

In Fig. 6.1 we present the comparison between the full differential cross section at LO for the $u\bar{u}$-initiated subprocess and the result of the computation described in eq. (6.2.23). Despite its label, it is important to note that the computation is not fully analytical, in the sense that the term containing the convolutions between the splitting functions $P_{ab}^{(0)}$ and the PDFs was estimated through a numerical integration. We want to highlight that eq. (6.2.23) is written exactly in the way in which it is implemented in the code, where the result is automatically multiplied by the PDFs associated to the indices $c\bar{c}$ that specify the cross section $\sigma_{c\bar{c}}^{(0)}$. Hence why there is the compensating factor $1/f_{c/h_1} f_{\bar{c}/h_2}$. Moreover the LO cross section for the inclusive process, $\sigma_{c\bar{c}}^{(0)}$, was obtained with the same scale choices discussed earlier in this section. The plot shows a very good agreement between the LO differential cross section and its limit in a wide range of transverse momentum. Furthermore, the LO curve, in green, is very stable up to $p_{\text{T}} \sim 10^{-3}$ GeV with an increase of the uncertainty associated to the numerical integration for smaller values. The numerical estimation of the convolution term is shown in pink and the band corresponds to a variation around its central value obtained by adding and subtracting the uncertainty given by the numerical integration. The uncertainty associated with the value of $\sigma_{c\bar{c}}^{(0)}$ is completely negligible.

The study of the $p_{\text{T}} \to 0$ limit for the NLO corrections is more delicate, from a numerical point of view. Thus it is convenient to isolate the pure NLO contributions from the LO by defining

$$d\bar{\sigma}_{\text{NLO}} = -\left[d\sigma_{\text{NLO}} - d\sigma_{\text{LO}}\right], \tag{6.2.24}$$

so that we can write

$$\begin{aligned} p_{\text{T}} \frac{d\bar{\sigma}_{\text{NLO}}^{(\text{sing.})}}{dp_{\text{T}}} = \sum_{a_1 a_2} \int [dz_1 dz_2]\, f_{a_1/h_1} f_{a_2/h_2} \sum_c \sigma_{c\bar{c}}^{(0)} \left(\frac{\alpha}{2\pi}\right)^2 8 \Big[32\, L^3\, \Sigma_{c\bar{c},a_1a_2}^{(2,4)} \\ + 12\, L^2\, \Sigma_{c\bar{c},a_1a_2}^{(2,3)} + 4\, L\, \Sigma_{c\bar{c},a_1a_2}^{(2,2)} + \left(\Sigma_{c\bar{c},a_1a_2}^{(2,1)} - 16\, \zeta_3\, \Sigma_{c\bar{c},a_1a_2}^{(2,4)}\right) \Big]. \end{aligned} \tag{6.2.25}$$

The double Mellin moments of the $\Sigma_{c\bar{c},a_1a_2}^{(2,n)}$ coefficients are

$$\Sigma_{c\bar{c},a_1a_2,(N_1,N_2)}^{(2,4)} = \frac{1}{8} \left(A_c^{(1)}\right)^2 \delta_{ca_1} \delta_{\bar{c}a_2}, \tag{6.2.26}$$

$$\Sigma_{c\bar{c},a_1a_2,(N_1,N_2)}^{(2,3)} = -A_c^{(1)} \left[\left(\frac{1}{3}\bar{\beta}_0 - \frac{1}{2} B_c^{(1)} \right) \delta_{ca_1} \delta_{\bar{c}a_2} - \frac{1}{2} (\delta_{ca_1} \gamma_{\bar{c}a_2,N_2}^{(1)} + \gamma_{ca_1,N_1}^{(1)} \delta_{\bar{c}a_2}) \right], \tag{6.2.27}$$

$$
\begin{aligned}
\Sigma^{(2,2)}_{c\bar{c},a_1a_2,(N_1,N_2)} =& -\frac{1}{2}A_c^{(1)}H_{c\bar{c}}^{(1)}\delta_{ca_1}\delta_{\bar{c}a_2} - \frac{1}{4}A_c^{(2)}\delta_{ca_1}\delta_{\bar{c}a_2} \\
&- \frac{1}{2}A_c^{(1)}\left(\delta_{ca_1}\tilde{C}^{(1)}_{\bar{c}a_2,N_2} + \tilde{C}^{(1)}_{ca_1,N_1}\delta_{\bar{c}a_2}\right) \\
&+ \frac{1}{2}(B_c^{(1)} - \bar{\beta}_0)\left(B_c^{(1)}\delta_{ca_1}\delta_{\bar{c}a_2} + \delta_{ca_1}\gamma^{(1)}_{\bar{c}a_2,N_2} + \gamma^{(1)}_{ca_1,N_1}\delta_{\bar{c}a_2}\right) \\
&+ \frac{1}{2}\sum_{b_1b_2}\left(B_c^{(1)}\delta_{ca_1}\delta_{\bar{c}a_2} + \delta_{ca_1}\gamma^{(1)}_{\bar{c}a_2,N_2} + \gamma^{(1)}_{ca_1,N_1}\delta_{\bar{c}a_2}\right) \\
&\qquad\qquad \times\left(\delta_{b_1a_1}\gamma^{(1)}_{b_2a_2,N_2} + \gamma^{(1)}_{b_1a_1,N_1}\delta_{b_2a_2}\right) \\
=& \frac{1}{2}\left[-A_c^{(1)}H_{c\bar{c}}^{(1)} - \frac{1}{2}A_c^{(2)} + B_c^{(1)}(B_c^{(1)} - \bar{\beta}_0)\right]\delta_{ca_1}\delta_{\bar{c}a_2} \\
&- \frac{1}{2}A_c^{(1)}\left(\delta_{ca_1}\tilde{C}^{(1)}_{\bar{c}a_2,N_2} + \tilde{C}^{(1)}_{ca_1,N_1}\delta_{\bar{c}a_2}\right) \\
&+ \frac{1}{2}(B_c^{(1)} - \bar{\beta}_0)\left(\delta_{ca_1}\gamma^{(1)}_{\bar{c}a_2,N_2} + \gamma^{(1)}_{ca_1,N_1}\delta_{\bar{c}a_2}\right) \\
&+ \frac{1}{2}\sum_{b}\Bigg[B_c^{(1)}\left(\gamma^{(1)}_{ba_1,N_1} + \gamma^{(1)}_{ba_2,N_2}\right)\delta_{ca_1}\delta_{\bar{c}a_2} \\
&\qquad + \left(\delta_{ca_1}\gamma^{(1)}_{\bar{c}a_2,N_2} + \gamma^{(1)}_{ca_1,N_1}\delta_{\bar{c}a_2}\right)\left(\gamma^{(1)}_{ba_1,N_1} + \gamma^{(1)}_{ba_2,N_2}\right)\Bigg],
\end{aligned}
\tag{6.2.28}
$$

$$
\begin{aligned}
\Sigma^{(2,1)}_{c\bar{c},a_1a_2,(N_1,N_2)} =& -\sum_{b_1b_2}\left(H_{c\bar{c}}^{(1)}\delta_{cb_1}\delta_{\bar{c}b_2} + \delta_{cb_1}\tilde{C}^{(1)}_{\bar{c}b_2,N_2} + \tilde{C}^{(1)}_{cb_1,N_1}\delta_{\bar{c}b_2}\right) \\
&\quad\times\left(B_c^{(1)}\delta_{a_1b_1}\delta_{a_2b_2} + \delta_{b_1a_1}\gamma^{(1)}_{b_2a_2,N_2} + \gamma^{(1)}_{b_1a_1,N_1}\delta_{b_2a_2}\right) \\
&- B_c^{(2)}\delta_{ca_1}\delta_{\bar{c}a_2} + \bar{\beta}_0\left(\delta_{ca_1}\tilde{C}^{(1)}_{\bar{c}a_2,N_2} + \tilde{C}^{(1)}_{ca_1,N_1}\delta_{\bar{c}a_2}\right) \\
&- \left(\delta_{ca_1}\gamma^{(2)}_{\bar{c}a_2,N_2} + \gamma^{(2)}_{ca_1,N_1}\delta_{\bar{c}a_2}\right) \\
=& -\left(H_{c\bar{c}}^{(1)}B_c^{(1)} + B_c^{(2)}\right)\delta_{ca_1}\delta_{\bar{c}a_2} - \left(\tilde{C}^{(1)}_{ca_1,N_1}\gamma^{(1)}_{\bar{c}a_2,N_2} + \gamma^{(1)}_{ca_1,N_1}\tilde{C}^{(1)}_{\bar{c}a_2,N_2}\right) \\
&- \sum_{b}\left(\delta_{ca_1}\tilde{C}^{(1)}_{\bar{c}b,N_2}\gamma^{(1)}_{ba_2,N_2} + \tilde{C}^{(1)}_{cb,N_1}\gamma^{(1)}_{ba_1,N_1}\delta_{\bar{c}a_2}\right) \\
&- \left(B_c^{(1)} - \bar{\beta}_0\right)\left(\delta_{ca_1}\tilde{C}^{(1)}_{\bar{c}a_2,N_2} + \tilde{C}^{(1)}_{ca_1,N_1}\delta_{\bar{c}a_2}\right) \\
&- H_{c\bar{c}}^{(1)}\left(\delta_{ca_1}\gamma^{(1)}_{\bar{c}a_2,N_2} + \gamma^{(1)}_{ca_1,N_1}\delta_{\bar{c}a_2}\right) \\
&- \left(\delta_{ca_1}\gamma^{(2)}_{\bar{c}a_2,N_2} + \gamma^{(2)}_{ca_1,N_1}\delta_{\bar{c}a_2}\right),
\end{aligned}
\tag{6.2.29}
$$

where both $\gamma^{(i)}$ and $\tilde{C}^{(i)}$ are expanded in powers of α/π and we introduced the notation $\bar{\beta}_0 = \pi\beta_0$. We can now write the contributions to the differential cross section for the NLO corrections in the same form used for the LO and, for ease of

notation, we can separate them in the following way

$$p_{\mathrm{T}}\frac{d\bar{\sigma}^{\mathrm{NLO}}}{dp_{\mathrm{T}}} = \sum_{n=1}^{4} p_{\mathrm{T}}\left.\frac{d\bar{\sigma}^{\mathrm{NLO}}}{dp_{\mathrm{T}}}\right|_{(2,n)}, \tag{6.2.30}$$

where each contribution contains only terms proportional to $L^{(n-1)}$. The first two terms are very similar to the LO ones

$$p_{\mathrm{T}}\left.\frac{d\bar{\sigma}^{\mathrm{NLO}}}{dp_{\mathrm{T}}}\right|_{(2,4)} = \sum_c \int [dz_1 dz_2]\, f_{c/h_1} f_{\bar{c}/h_2}\, \sigma^{(0)}_{c\bar{c}} \left(\frac{\alpha}{2\pi}\right)^2 \left[32\, \left(A^{(1)}_c\right)^2\, L^3\right], \tag{6.2.31}$$

$$\begin{aligned} p_{\mathrm{T}}\left.\frac{d\bar{\sigma}^{\mathrm{NLO}}}{dp_{\mathrm{T}}}\right|_{(2,3)} = \sum_c \int [dz_1 dz_2]\, f_{c/h_1} f_{\bar{c}/h_2}\, \sigma^{(0)}_{c\bar{c}} \left(\frac{\alpha}{2\pi}\right)^2 \Bigg[&- 96\, A^{(1)}_c \left(\frac{1}{3}\bar{\beta}_0 - \frac{1}{2}B^{(1)}_c\right) L^2 \\ &+ 24\, A^{(1)}_c\, L^2 \frac{1}{f_{c/h_1} f_{\bar{c}/h_2}} \sum_a \Big(f_{c/h_1}(P^{(0)}_{\bar{c}a} \otimes f_{a/h_2}) + (P^{(0)}_{ca} \otimes f_{a/h_1}) f_{\bar{c}/h_2}\Big)\Bigg]. \end{aligned} \tag{6.2.32}$$

For the two subleading ones we have

$$\begin{aligned} p_{\mathrm{T}}\left.\frac{d\bar{\sigma}^{\mathrm{NLO}}}{dp_{\mathrm{T}}}\right|_{(2,2)} = &\sum_c \int [dz_1 dz_2]\, f_{c/h_1} f_{\bar{c}/h_2}\, \sigma^{(0)}_{c\bar{c}} \left(\frac{\alpha}{2\pi}\right)^2 16\, L \\ &\times \Bigg\{ \left(-A^{(1)}_c H^{(1)}_{c\bar{c}} - \frac{1}{2}A^{(2)}_c + B^{(1)}_c \left(B^{(1)}_c - \bar{\beta}_0\right)\right) \\ &+ \frac{1}{2}\frac{1}{f_{c/h_1} f_{\bar{c}/h_2}} \sum_a \Bigg[- A^{(1)}_c \Big(f_{c/h_1}(C^{(1)}_{\bar{c}a} \otimes f_{a/h_2}) + (C^{(1)}_{ca} \otimes f_{a/h_1}) f_{\bar{c}/h_2}\Big) \\ &\qquad + (2B^{(1)}_c - \bar{\beta}_0)\Big(f_{c/h_1}(P^{(0)}_{\bar{c}a} \otimes f_{a/h_2}) + (P^{(0)}_{ca} \otimes f_{a/h_1}) f_{\bar{c}/h_2}\Big)\Bigg] \\ &+ \frac{1}{4}\frac{1}{f_{c/h_1} f_{\bar{c}/h_2}} \sum_{ab} \Bigg[f_{c/h_1} \left(P^{(0)}_{\bar{c}b} \otimes P^{(0)}_{ba} \otimes f_{a/h_2}\right) \\ &\qquad + \left(P^{(0)}_{cb} \otimes P^{(0)}_{ba} \otimes f_{a/h_1}\right) f_{\bar{c}/h_2} \\ &\qquad + \left(P^{(0)}_{bc} \otimes f_{c/h_1}\right)\left(P^{(0)}_{\bar{c}a} \otimes f_{a/h_2}\right) \\ &\qquad + \left(P^{(0)}_{ca} \otimes f_{a/h_1}\right)\left(P^{(0)}_{b\bar{c}} \otimes f_{\bar{c}/h_2}\right)\Bigg]\Bigg\}, \end{aligned} \tag{6.2.33}$$

$$
\begin{aligned}
p_{\mathrm{T}}\,\frac{d\bar{\sigma}^{\mathrm{NLO}}}{dp_{\mathrm{T}}}\bigg|_{(2,1)} = & \sum_{c}\int [dz_1 dz_2]\, f_{c/h_1} f_{\bar{c}/h_2}\, \sigma^{(0)}_{c\bar{c}} \left(\frac{\alpha}{2\pi}\right)^2 \\
& \times 8 \Bigg\{ - H^{(1)}_{c\bar{c}} B^{(1)}_{c} - B^{(2)}_{c} - 2\zeta_3 \left(A^{(1)}_{c}\right)^2 \\
& - \frac{1}{2}\frac{1}{f_{c/h_1} f_{\bar{c}/h_2}} \sum_{a} \Bigg[H^{(1)}_{c\bar{c}} \left(f_{c/h_1} (P^{(0)}_{\bar{c}a} \otimes f_{a/h_2}) + (P^{(0)}_{ca} \otimes f_{a/h_1}) f_{\bar{c}/h_2} \right) \\
& \qquad + \left(B^{(1)}_{c} - \bar{\beta}_0\right) \left(f_{c/h_1} (C^{(1)}_{\bar{c}a} \otimes f_{a/h_2}) + (C^{(1)}_{ca} \otimes f_{a/h_1}) f_{\bar{c}/h_2} \right) \\
& \qquad + f_{c/h_1} \left(P^{(1)}_{\bar{c}a} \otimes f_{a/h_2} \right) + \left(P^{(1)}_{ca} \otimes f_{a/h_1} \right) f_{\bar{c}/h_2} \Bigg] \\
& - \frac{1}{4}\frac{1}{f_{c/h_1} f_{\bar{c}/h_2}} \sum_{ab} \Bigg[f_{c/h_1} \left(C^{(1)}_{\bar{c}b} \otimes P^{(0)}_{ba} \otimes f_{a/h_2} \right) \\
& \qquad + \left(C^{(1)}_{cb} \otimes P^{(0)}_{ba} \otimes f_{a/h_1} \right) f_{\bar{c}/h_2} \\
& \qquad + \left(C^{(1)}_{ca} \otimes f_{a/h_1} \right) \left(P^{(0)}_{\bar{c}b} \otimes f_{b/h_2} \right) \\
& \qquad + \left(P^{(0)}_{ca} \otimes f_{a/h_1} \right) \left(C^{(1)}_{\bar{c}b} \otimes f_{b/h_2} \right) \Bigg] \Bigg\},
\end{aligned}
\tag{6.2.34}
$$

These equations have been compared with the results presented in Ref. [141]. The result for the NLO correction, defined as in eq. (6.2.24), is shown in Fig. 6.2. We display the differential cross section from $p_{\mathrm{T}} = 10^{-2}$ GeV, since the differential cross section becomes completely unreliable below such value, mainly due to the instability of the numerical computation of the virtual corrections.

It is important to mention that, to simplify the computation, all the contributions associated with the photon distribution function f_{γ/h_i}, which is much smaller than its quark counterparts, have been neglected. Moreover the value of $\bar{\beta}_0$ was assumed to be constant, without taking into account any mass threshold of the fermions contributing to the photon self energy and excluding contributions from the top quark. Because of all of these small approximations and due to the intrinsic complexity of the computation, with respect to its LO counterpart, the agreement between the two curves is slightly worse than the one achieved at leading order, while still being satisfactory within a wide region of values of p_{T}.

The pink band is obtained as in Fig. 6.1 by taking the variation of the estimated value of the convolution terms equal to the corresponding numerical uncertainty. Note that, as mentioned before, the value of the factorization scale was taken equal to the high scale M, given by the Z boson mass, thus the evaluation of the convolution terms is not affected by the issues caused by the use of the freezing scale for the PDFs.

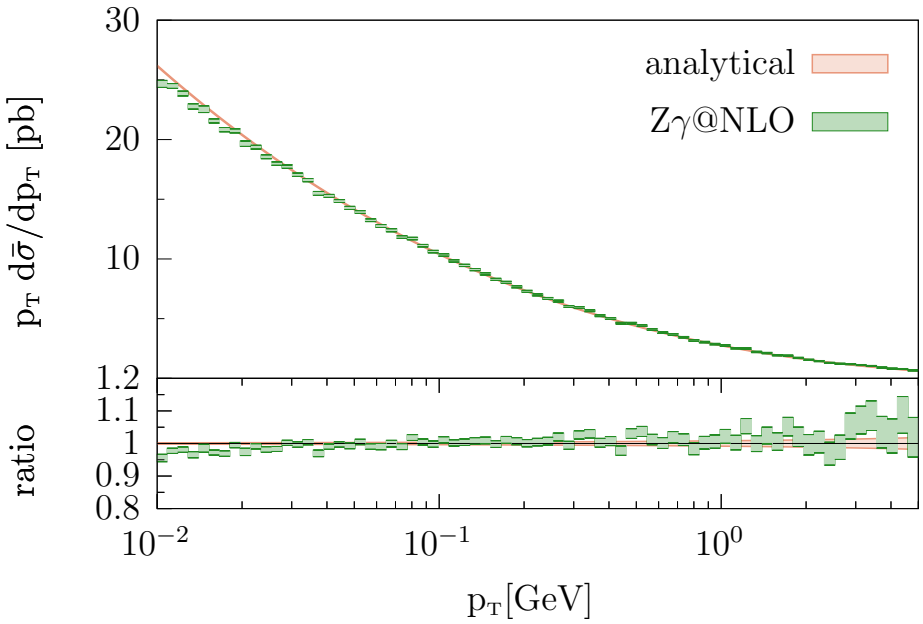

Figure 6.2: Comparison between the NLO correction to the differential cross section and its analytical limit for small values of the transverse momentum of the Z boson.

The plot in Fig. 6.2 shows a good agreement between the fixed order computation and its small transverse-momentum limit from $p_T \simeq 3 \times 10^{-2}$ GeV up to $p_T \simeq 1$ GeV. Considering this result, both for the LO case and the NLO corrections, we can take the value of p_T^δ to be roughly between 10^{-1} GeV and 1 GeV for the process with $\alpha = \widetilde{\alpha}(0)$. It is now important to determine whether the contributions coming from $\sigma_>(p_T^\delta)$ and $\sigma_<(p_T^\delta)$ are somewhat comparable in size for these values of p_T^δ and, if that is the case, study the dependence of the total result on this unphysical parameter.

Chapter 7

Implementation and results

In this chapter, we will discuss the implementation of the concepts presented in the previous chapters and subsequently their phenomenological implications. As already anticipated, most of the results discussed in this thesis are non-physical due to the use of a value of the QED coupling constant which is inflated with respect to the physical one. The reason behind this is that it will be possible to appreciate both the NLO accuracy resulting from the extension to QED of the MiNLO′ method and the dependence of the result on the arbitrary parameter p_{T}^{δ} that was introduced to overcome the numerical challenges discussed in Chapter 5. Hence why the results presented in this work are to be understood as a proof of concept for the abelianization of the MiNLO′ method and as a first step towards the subsequent extension to include mixed QED and QCD corrections rather than actual physical descriptions of the processes at the LHC. In the last part of this chapter we will also present a physical result.

Moreover we will focus on the simpler process where the final state is obtained from the decay of the Z boson into $\nu\bar{\nu}$, in other words without final-state massive charged particles. This greatly reduces the complexity of the computation. In addition, the main reason for this choice is the consistency of the calculation. Indeed it is well known that, when studying the neutral Drell-Yan process with charged leptons in the final state, one must take into account both the diagrams with a Z boson and a photon in s channel. This is perfectly well defined for LO processes and full NLO EW ones. However, if only NLO QED corrections are considered, the computation becomes inconsistent: this is because the so-called *photonic corrections*, i.e. the loop diagrams that can be obtained by just adding one photon line, are a gauge invariant subset of the EW corrections but diagrams involving fermion loops are not. This means that one cannot separate the photon self-energy from the mixed Z/γ loop diagrams and ultimately from pure weak corrections. As a consequence, it is not possible to perform the computation with all three of the following requests satisfied at once:

1. only NLO QED corrections;

2. the Z boson in the s channel;

3. final state charged leptons at LO.

Let us briefly discuss what renouncing to each of these features would entail.

1. For the first one there are two possibilities: either one considers the full EW corrections or only the photonic ones. The former is definitely the best option, as taking the full EW theory would mean that the computation is both complete and fully consistent, however it would increase the number of diagrams and in turn the complexity of the calculation. For this reason it would be best to include the full EW theory only after the feasibility of the method has been established. As for the latter, namely including only the photonic corrections, if would mean that fermion loops are not allowed anywhere in the computation and as a consequence the photon self-energy would receive no corrections at higher orders. This directly translates to the trivialization of the charge renormalization process and would imply that the running of the coupling constant is turned off. For this reason this is not an appealing option, as the behaviour of the coupling constant is one of the main differences between QED and QCD. Since one of the aims of this work is to test the abelianization of the MiNLO$'$ method in all its aspects, one of which is the running of the coupling constant, we have decided not to pursue this path.

2. As for the second one, giving up on the Z boson in the s channel would mean to effectively perform the computation in pure QED, without any term coming from the weak sector. This would allow to have charged leptons in the final state, keeping the full genuine QED corrections to the photon self energies. On the other hand, removing the Z boson contribution drastically changes the invariant mass distribution of the process which would be now only driven by the photon propagator which, due to its singularity, would require a cut exactly where the invariant mass is peaked. Moreover, removing the Z boson would also imply the lack of a hard scale: both the reference scale for the invariant mass of the process even at LO and the scale associated to the radiation would be in principle very small. It is important to note that the invariant mass cut needed to protect the computation from the photon singularity is not specific of this scenario. However the role of the cut itself is slightly different depending on the presence of a resonance, such as the Z boson peak. Indeed the issue with the absence of a resonance lies in the loss of an hard scale that drives the cross section away from the photon singularity. Without it, the value of the invariant mass cut would assume the role of a hard scale. This it is unpleasant due to the arbitrariness involved in the choice of the value for the cut, however it does

not represent a conceptual problem per se and is left as a future improvement of this work.

3. At last we have the simplest option, namely renouncing to final-state charged leptons. In this way one only has to take into account the radiation from initial-state particles, while some of the terms discussed in the previous chapters, which are related to large-angle soft-radiation from final-state particles, become zero. This is the most obvious choice as it has no actual drawbacks aside for the fact that the process becomes less interesting from a phenomenological point of view.

7.1 Implementation

We consider proton-proton collisions at the LHC with a hadronic center-of-mass energy of $\sqrt{s} = 13$ TeV. The process we are interested in is $pp \to Z(\to \nu\bar{\nu}) + \gamma$. The decay of the Z boson into a neutrino pair is understood in the following. We include NLO QED corrections and we do not require any photon or quark in the final state to be resolved. When upgraded according to the MiNLO′ procedure, such computation should reproduce the NLO QED corrections to the $pp \to Z$ process. At LO we include the processes

$$q\,\bar{q} \to Z + \gamma \qquad q\,\gamma \to Z + q \tag{7.1.1}$$

where $q = u, d$, i.e. we limit ourselves to have only u and d quarks in the initial state, both for the $pp \to Z$ NLO QED computation and the $pp \to Z + \gamma$ MiNLO′ one. The input parameters that we used are

$$\begin{aligned} &M_Z = 91.1876 \text{ GeV}, && \Gamma_Z = 2.4952 \text{ GeV}, \\ &m_e = 0.51099892 \times 10^{-3} \text{ GeV}, && m_\mu = 0.105 \text{ GeV}, \\ &m_\tau = 1.77699 \text{ GeV}, && \widetilde{\alpha}(m_e) = 0.04, \end{aligned} \tag{7.1.2}$$

and the 5 light quarks are taken to be massless. The evaluation of the matrix elements, both at tree level and one-loop, is performed using Recola [142, 143] with the Collier package [144–147][1]. The computation is carried out in the complex mass scheme. In order to only include QED corrections we use the `set_pure_QED_rcl` option in Recola to turn off all the one-loop corrections that are related to the weak sector. Moreover, since the LO and the real emission amplitudes are computed as tree level amplitudes and thus are not affected by such option, we need to turn off the coupling of the W boson with the fermions and remove the real emission diagrams in which a final state pair of quarks is produced via the decay of an additional Z boson.

[1] Other tools have been developed to handle the automated computation of processes involving NLO EW corrections, such as MadGraph [148, 149], GoSam [150, 151] and OpenLoops [152].

We use the `NNPDF31_nlo_as_0118_luxqed` PDF set [153] which is provided by LHAPDF 6 [154]. The evolution is handled using APFEL [155], an evolution package that with the `EnableNLOQEDCorrections` option allows performing the DGLAP evolution of the PDFs up to NLO in QED. Since in APFEL it is not possible to completely turn off the QCD evolution, we heavily suppress it by decreasing the input value of $\alpha_s(M_Z)$ by several orders of magnitude to make the QED evolution dominant. In principle we wanted to be able to evaluate the PDFs at a scale given by $\mu_{\text{F}} = p_{\text{T}}^{\delta}$, which can be as small as 10^{-2} GeV, however even with this suppression the evolution towards such small scales becomes unreliable so we introduced a freezing scale $\mu_{\text{F}}^{\text{min}}$. In this way the PDFs are evaluated with the NLO QED DGLAP evolution above $\mu_{\text{F}}^{\text{min}}$ while below such scale their value is frozen and the evolution is turned off[2]. The natural choice for the value of the freezing scale is the smallest scale specific of each PDF set which, in this case, corresponds to $\mu_{\text{F}}^{\text{min}} = 1.65$ GeV.

The running of the coupling constant is implemented via the use of mass thresholds, so that each fermion f contributes only for $\mu_{\text{R}} > m_f$. Moreover, due to the electron mass being used in the definition of the Thompson limit and the light quarks being considered massless, their contribution to the running is always taken into account, independently of the value of μ_{R}.

As mentioned before, the computation is divided in two parts, $\sigma_{>}$ and $\sigma_{<}$ respectively, so we shall discuss the two implementations separately.

7.1.1 Computation of $\sigma_{>}$

This is the standard MiNLO′ approach, described by the abelianization of eq. (2.3.1). We work in a mixed renormalization scheme, more specifically:

- The two powers of α of the underlying process, namely the two powers associated with the Z boson in the s channel, are evaluated in the $\alpha(M_Z)$ scheme at the hard scale $\mu_{\text{R}} = M_Z$.
- The subsequent powers of the coupling, namely the one associated with the radiation at LO and the one introduced with the NLO corrections, are evaluated at $\mu_{\text{R}} = p_{\text{T}}$ in the $\overline{\text{MS}}$ scheme, according to the MiNLO′ method.

In order to do so we first initialize Recola in the $\alpha(M_Z)$ scheme using as input a value of the coupling constant that is consistent with the one presented in eq. (7.1.2). Then for the terms that are computed as tree level amplitudes, namely the LO and the real emission contributions, it is sufficient to replace the coupling constant provided by Recola with the one evaluated at the transverse momentum. As mentioned before, this amounts to one power of the coupling constant for the LO amplitude and to two powers for the real emission terms. As for the one-loop virtual contributions,

[2] We performed some tests relative to the evaluation of the PDFs below $\mu_{\text{F}}^{\text{min}}$ with a LO QED evolution which yielded negligible effects.

instead, the replacement of two powers of α is not sufficient and one also needs to take care of the finite terms coming from the renormalization. Indeed in order to transition from the OS scheme used in RECOLA to $\overline{\text{MS}}$ we need to replace δZ_e^{OS} with $\delta Z_e^{\overline{\text{MS}}}$ as described by eq. (3.3.12). This corresponds the introduction of a shift in the one-loop virtual amplitude as

$$V^{\overline{\text{MS}}}(\mu_{\text{R}}^2) = V^{\text{OS}}(\mu_{\text{R}}^2) - B\, p\, \Delta\alpha^{\overline{\text{MS}}}(\mu_{\text{R}}^2), \tag{7.1.3}$$

where $p = 1$ is the number of powers of the coupling constant that were replaced in the LO amplitude. We first set the value of $\mu_{\text{R}}^2 = M_Z^2$ in eq. (7.1.3) and then run the result to $\mu_{\text{R}}^2 = p_{\text{T}}^2$ by requiring the result to be invariant up to order α^{N+1} under variations of μ_{R} where N is the number of powers of α in the LO. In practice this amounts to the following replacement

$$V^{\overline{\text{MS}}}(p_{\text{T}}^2) = V^{\overline{\text{MS}}}(M_Z^2) + B\left(\alpha(p_{\text{T}})\,\beta_0 \log\frac{p_{\text{T}}^2}{M_Z^2}\right), \tag{7.1.4}$$

as illustrated explicitely in eqs. (3.10) and (3.11) of the original MiNLO′ paper [16]. As a final remark we want to discuss the value of β_0 in the equation above. Typically, in the other implementations of the MiNLO′ method, the number of flavours contributing to the one-loop QCD β function is kept fixed throughout the computation, resulting in β_0 being constant. In this formulation of the MiNLO′ method, however, the values of the lepton mass thresholds in the fermionic contributions to the photon self-energy are close to the possible values of p_{T}^{δ}. For this reason we employ a non-constant value for the one-loop β function in eq. (7.1.4), namely $\beta_0 = \beta_0(p_{\text{T}})$, obtained by only including only the contributions of the fermions whose masses are smaller than p_{T}.

7.1.2 Computation of $\sigma_<$

The computation of this term is much simpler and it only requires the implementation of eq. (6.1.18). In order to do so we generate an independent phase space corresponding to the $q\,\bar{q} \to Z$ inclusive subprocess without the extra radiation. This process only requires the computation of the LO amplitude and the one-loop virtual term, which is encoded in the hard-virtual factor, denoted as $H_{c\bar{c}}^{(1)}$ in eq. (6.1.20), without the need to calculate the real emission amplitude. As far as the renormalization is concerned, in principle the same prescription illustrated in the previous section would apply. In practice, however, there is no additional power of the coupling constant at LO other than the two powers that are associated with the Z boson propagator, meaning that the shift described by eq. (7.1.3) would be performed with $p = 0$.

7.2 Phenomenological results

In the previous chapter we discussed the existence of three possible scenarios concerning the relative sizes of $\sigma_>$ and $\sigma_<$ with respect to the total cross section. More specifically we alluded to the fact that the abelianization of the MiNLO′ method can be achieved consistently only if $\sigma_>$ is at least somewhat comparable in size to its counterpart below p_{T}^{δ}. In particular, it would be desirable to be able to appreciate the compensation between $\sigma_>$ and $\sigma_<$ when varying the value of p_{T}^{δ}. Thus we can start by looking at the two contributions to the total cross section for different values of our arbitrary parameter p_{T}^{δ}.

In Tab 7.1 we collect the results of the total cross section contributions obtained in the two regions for two values of the transverse momentum separator, together with their sum, which corresponds to the MiNLO′ total cross section for $Z\gamma$. These results show that the two parts of the MiNLO′ computation, $\sigma_>$ and $\sigma_<$, contribute almost equally to the total cross section. This means that the abelianization process is numerically well posed but it cannot achieve the desired accuracy without taking into account the approximation of the missing terms represented by $\sigma_<$ as obtained in eq. (6.1.18). Moreover, the dependence of the final result on the arbitrary scale is roughly 5% of the total between $p_{\mathrm{T}}^{\delta} = 1$ GeV and $p_{\mathrm{T}}^{\delta} = 10^{-1}$ GeV. For comparison, the total cross section the fully inclusive process, computed at NLO in QED, with the same input parameters and PDF set discussed in Section 7.1, is

$$\sigma_Z^{\mathrm{NLO}} = 597.2(1)^{627.2}_{580.6}\ \mathrm{pb}. \tag{7.2.1}$$

In eq. (7.2.1) the central value corresponds to $\mu_{\mathrm{R}} = \mu_{\mathrm{F}} = M_Z$, while the other two values represent the three-point scale variation[3] and were obtained by multiplying both the renormalization scale and the factorization scale by a factor K_{R} and K_{F} respectively, with $(K_{\mathrm{R}}, K_{\mathrm{F}}) = \{(2,2), (\frac{1}{2}, \frac{1}{2})\}$. Furthermore the total cross section for Z@LO, i.e. the LO fully inclusive result, is $\sigma_Z^{\mathrm{LO}} = 574.1(1)$ pb which means that, with the value of the coupling constant that is being used, the NLO QED corrections to the process $p\,p \to Z$ amount to approximately 5%.

We observe that the MiNLO′ result for the total cross section seems fairly compatible with the inclusive computation with NLO accuracy, as predicted by the method, particularly so for values of $p_{\mathrm{T}}^{\delta} = 1$ GeV and 10^{-1} GeV. Note that at $p_{\mathrm{T}}^{\delta} = 10^{-2}$ GeV we approach the region where the comparison between the fixed-order computation is not in a good agreement with its limit (see Fig. 6.2). Indeed, although unpleasant, it is not surprising that the result for the total MiNLO′ cross section with $p_{\mathrm{T}}^{\delta} = 10^{-2}$ GeV, given by $\sigma_{\mathrm{TOT}} = 655.1(1)$, is further away from the one presented in eq. (7.2.1) with respect to the other results listed in Tab. 7.1.

[3] A fully consistent comparison would require the study of the scale variation also for the MiNLO′ result, both for $\sigma_>$ and $\sigma_<$, but this is left for a future work.

p_{T}^{δ} [GeV]	1	10^{-1}
$\sigma_{>}$ [pb]	115.2(1)	226.7(2)
$\sigma_{<}$ [pb]	484.1(1)	401.3(1)
σ_{TOT} [pb]	599.3(2)	628.1(3)

Table 7.1: Contributions to the total cross section of the MiNLO′ result for two different values of p_{T}^{δ} and their corresponding sum.

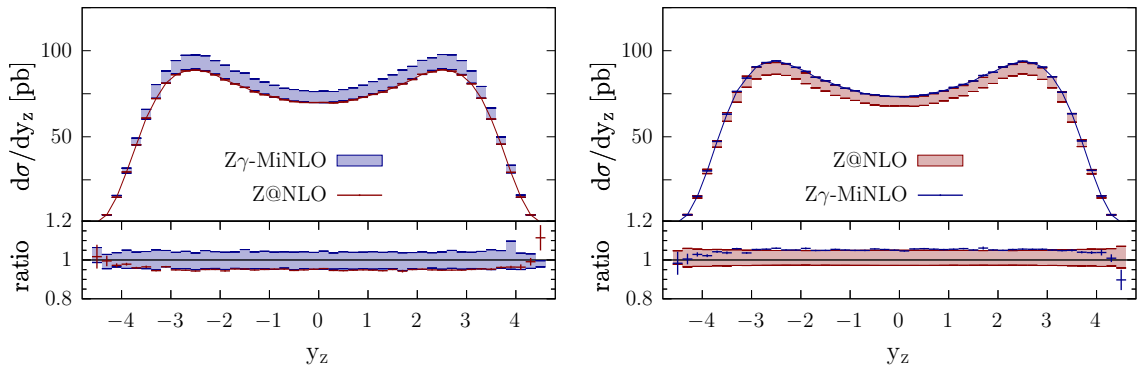

Figure 7.1: Comparison between the $Z\gamma$-MiNLO result and the Z@NLO result for the Z boson rapidity distribution. The blue band in the left plot is computed from the three values of p_{T}^{δ} of $Z\gamma$-MiNLO ($p_{\mathrm{T}}^{\delta} = 1$, 10^{-1} and 10^{-2} GeV), while the right plot shows the seven-point scale variation band of the Z@NLO result in red.

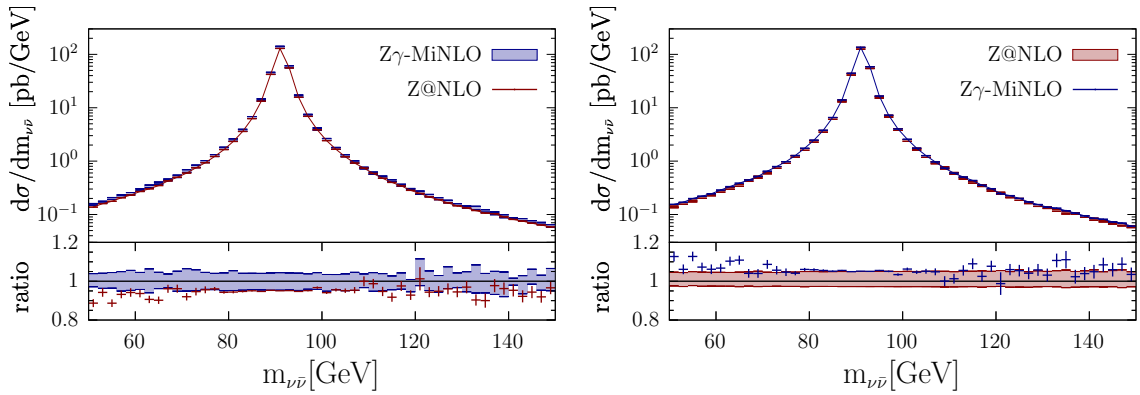

Figure 7.2: Comparison between the $Z\gamma$-MiNLO result and the Z@NLO result for the Z boson rapidity distribution. The bands are the same as in Fig. 7.1.

We present now the results for the differential distributions. We start from the observables that are inclusive over the QED radiation. By virtue of the MiNLO′ method, the rapidity of the Z boson, in Fig. 7.1, and its invariant-mass distribution, in Fig. 7.2, should reach NLO accuracy. So we can compare them with the results for the fully inclusive process Z@NLO. The agreement is expected up to higher-order

terms. The meaning of the blue band is intrinsically different from the meaning of the red band: the red band is the scale-variation band and was obtained by taking the upper and lower envelope of the results of a seven-point scale variation for the Z@NLO process. As mentioned before we do not have, at present time, the results for the scale variation of the abelianized MiNLO′ code. As a consequence, the blue band does not represent the scale variation and was instead obtained by taking the results corresponding to three values of p_{T}^{δ}, namely 10^{-2}, 10^{-1} and 1 GeV. As shown by the results in Tab. 7.1, the p_{T}^{δ}-band represents a variation of roughly 5% of the central value, given by $p_{\mathrm{T}}^{\delta} = 10^{-1}$ GeV. Moreover it is important to note that the lower bound of the blue band, which is the closest to the central value of the Z@NLO process, corresponds to $p_{\mathrm{T}}^{\delta} = 1$ GeV.

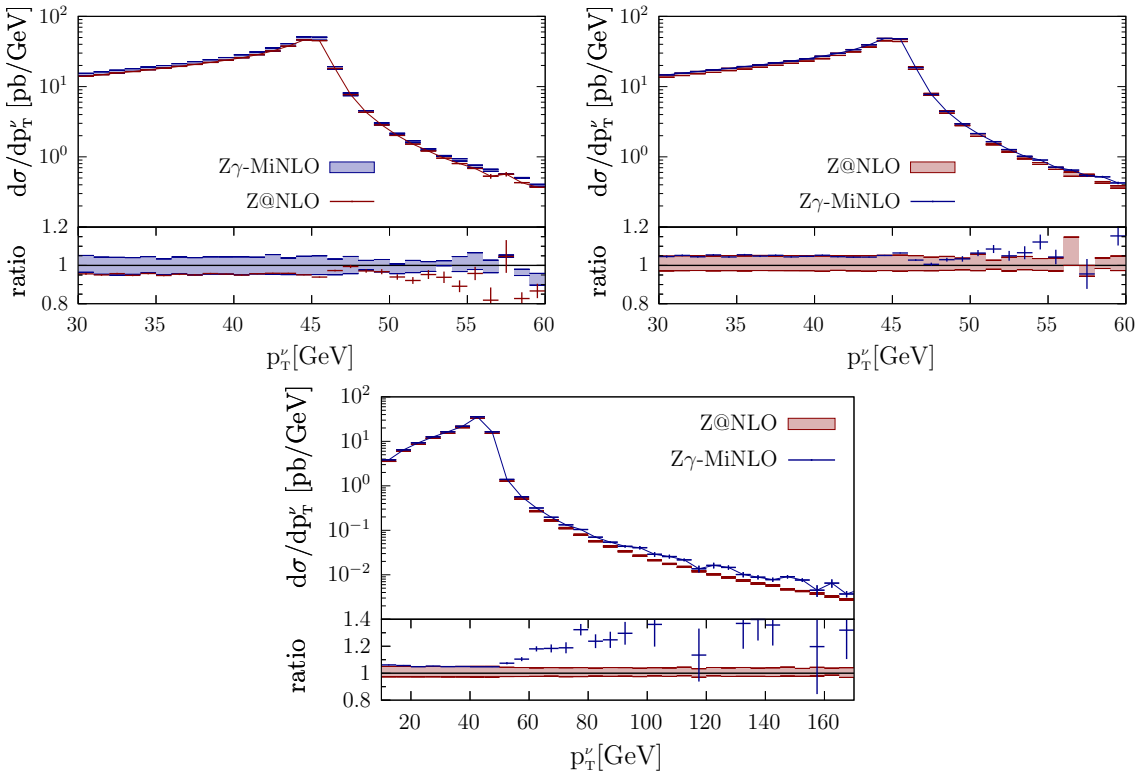

Figure 7.3: In the first row, comparison between $Z\gamma$-MiNLO and Z@NLO for the single-lepton transverse-momentum distribution in the region around the peak at $p_{\mathrm{T}}^{\nu} = M_Z/2$. In the second row, the same distribution for a wider p_{T}^{ν} range. The blue and red bands are the same as in Fig 7.1.

In Fig. 7.3 we show the transverse-momentum distribution the final-state neutrino produced in the decay of the Z boson. This quantity is interesting because it is clearly divided into two well defined regions by its peak, which is located at $p_{\mathrm{T}}^{\nu} = M_Z/2 \sim 45$ GeV. In Fig. 7.3 we can see that the $Z\gamma$-MiNLO results is compatible with the inclusive result with NLO accuracy only up to the peak and the two curves drift apart beyond such point. Indeed if we consider the inclusive process,

Z@NLO, we have that, above the $M_Z/2$ threshold, only the real emission diagrams fully contribute to the result while the Born-like terms, namely the LO and the one-loop virtual contributions, can only contribute when the Z boson is off-shell, which is suppressed given the relative small value of the Z-boson width. The blue and red bands in the plot are the same as before. Note that we only show the plot for the p_{T}^{δ} band in the region below the peak where the result is compatible with the inclusive process via MiNLO′ accuracy. In fact, beyond such value the band is not meaningful any longer due to the result being dominated by the contribution coming from $\sigma_{>}$. Moreover the region above the peak, in the third panel of Fig. 7.3, shows the fact that the p_{T} spectrum of the neutrino is harder for the MiNLO′ result with respect to the Z@NLO one. Indeed the MiNLO′ prediction is NLO accurate for both Z and $Z + \gamma$ production, while the Z@NLO result is, effectively, a LO prediction, given only by the tree-level contribution of $Z\gamma$@LO.

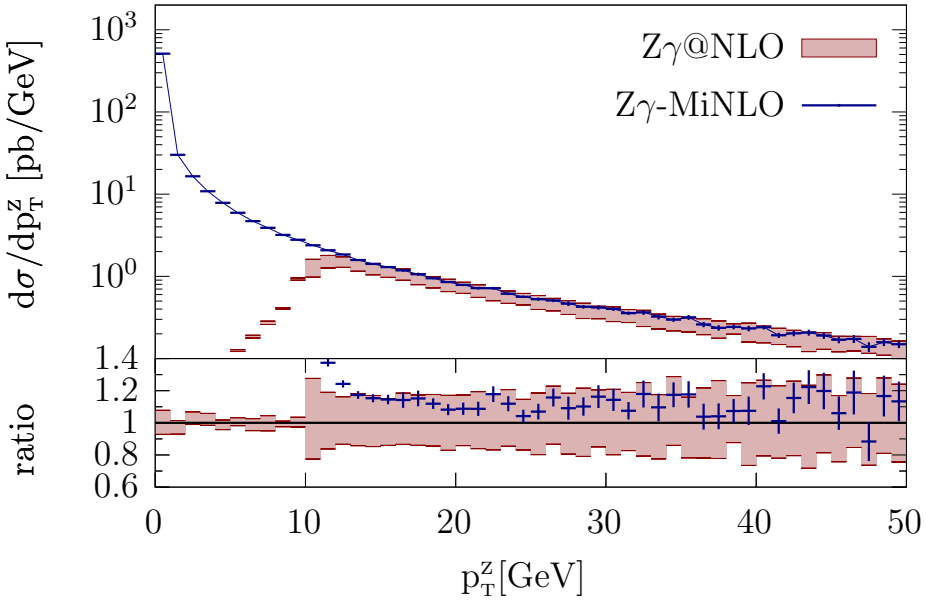

Figure 7.4: Comparison between the Z boson transverse-momentum distribution for the $Z\gamma$-MiNLO result and the $Z\gamma$@NLO result with $\mu_{\mathrm{R}} = M_Z$ and relative scale variation.

We want to briefly compare the Z boson transverse-momentum distribution of the $Z\gamma$-MiNLO result with the full NLO result for the $p\,p \to Z\,\gamma$ process without the use of the MiNLO method. Due to the absence of a Sudakov form factor, the latter requires the introduction of a generation cut that was set at $p_{\mathrm{T}}^{\mathrm{cut}} = 10$ GeV. Moreover the central value for the renormalization scale for the $Z\gamma$@NLO computation was taken as $\mu_{\mathrm{R}} = M_Z$. This comparison is to be understood as a sanity check since, according to the MiNLO′ method, the $Z\gamma$-MiNLO result should agree with the nominal $Z\gamma$@NLO prediction for large values of p_{T}, i.e. $p_{\mathrm{T}} \sim M_Z$. In Fig. 7.4 we show the comparison between the two results, where the red band represents the upper and lower envelope of the seven-point scale variation of the $Z\gamma$@NLO compu-

tation obtained in the same way as in Fig. 7.1 for the Z@NLO result. The difference between the values of p_{T}^{δ} is not shown, because, outside the small-p_{T} limit, this distribution is completely dominated by the contribution of $\sigma_{>}$, while the contribution coming from $\sigma_{<}$ would only be limited to the first bin.

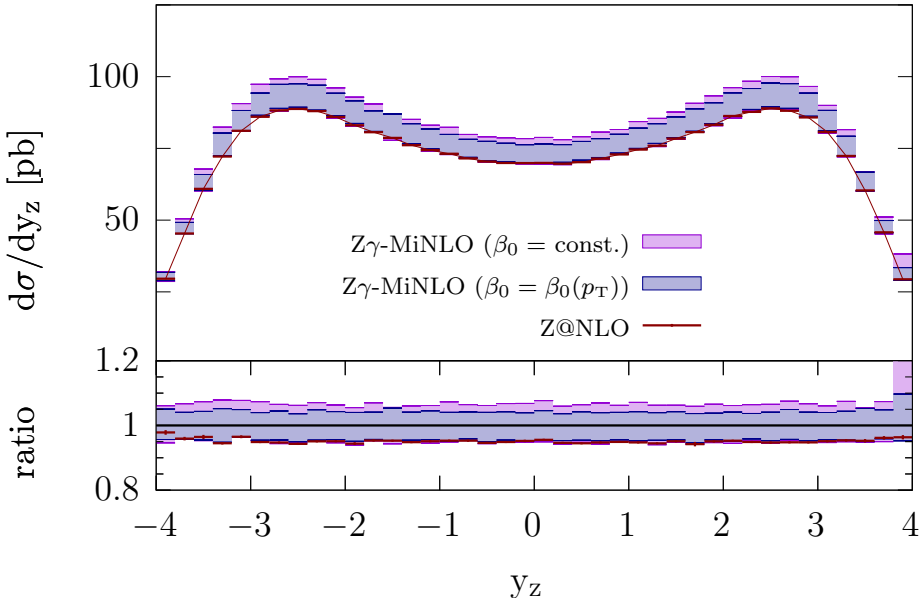

Figure 7.5: Difference in the $Z\gamma$-MiNLO result between the use of a constant value for β_0 (pink) and $\beta_0 = \beta_0(p_{\mathrm{T}})$ (blue) in eq. (7.1.4). As a reference, both are compared to the Z@NLO result (red).

Given the importance in keeping under control the dependence of the result on the choice of the value of p_{T}^{δ}, we want to show the role of one expedient that we discussed in the implementation of the formulae for the computation of $\sigma_{>}$. More specifically, we are referring to the use of a non-constant value for the one-loop QED β function in eq. (7.1.4), that is in the transition from the evaluation of the fixed-order virtual contribution from a high scale $\mu_{\mathrm{R}}^2 = M_Z^2$ to $\mu_{\mathrm{R}}^2 = p_{\mathrm{T}}^2$ according to the prescriptions of the MiNLO′ method. In Fig. 7.5 we show the difference between the typical implementation with a constant value of β_0 (pink) and the same result obtained using $\beta_0 = \beta_0(p_{\mathrm{T}})$ (blue) in eq. (7.1.4). The two curves, with their relative p_{T}^{δ}-bands, are compared to the usual result for the Z@NLO process. Despite both results being compatible with the inclusive process (red), it is possible to appreciate an improvement in the dependence on p_{T}^{δ} of the full $Z\gamma$-MiNLO result when using $\beta_0 = \beta_0(p_{\mathrm{T}})$.

Finally we want to show the results for the total cross section and the rapidity distribution in the physical case. We consider the same process discussed above, with $Z \to \nu\bar{\nu}$ and with $\alpha = \alpha(m_e)$, i.e. its physical value at the Thompson limit. The result for the total cross section for the process Z@NLO is

$$\sigma_Z^{\mathrm{NLO}} = 550.70(5)^{552.04}_{550.12}\ \mathrm{pb}, \tag{7.2.2}$$

Results for $\alpha = \alpha(m_e)$		
p_{T}^{δ} [GeV]	1	10^{-1}
$\sigma_{>}$ [pb]	10.822(3)	26.540(8)
$\sigma_{<}$ [pb]	539.63(12)	524.08(12)
σ_{TOT} [pb]	550.46(12)	550.62(12)

Table 7.2: Contributions to the total cross section for different values of p_{T}^{δ} (top) and result for the 3-point scale variation for the total cross section of the process Z@NLO (bottom).

where we used the same notation and the same values for μ_{R} and μ_{F} as in eq. (7.2.1), while the corresponding total cross section at LO is $\sigma_Z^{\mathrm{LO}} = 548.90(5)$ pb. In Tab. 7.2 we list the contributions to the total cross section given by $\sigma_{>}$ and $\sigma_{<}$ for two values of p_{T}^{δ} ($p_{\mathrm{T}}^{\delta} = \{1, 10^{-1}\}$ GeV) and their relative sum. First of all we can see an improvement in the dependence of the full result on the choice of the value of p_{T}^{δ} with respect to the $\widetilde{\alpha}$ case. Moreover, we can also see a better agreement between the total cross section of the $Z\gamma$-MiNLO process and the fully inclusive one with respect to the results discussed in Tab. 7.1. The same conclusions can be drawn also from the plots in Fig. 7.6, where we compare the rapidity distribution for the two processes and their relative bands, representing the p_{T}^{δ} dependence in the $Z\gamma$-MiNLO case and the envelope of the three-point scale variation in the Z@NLO case. From the plot we can see that the two results are compatible with each other within the percent level, which is consistent with the value of the coupling constant in use.

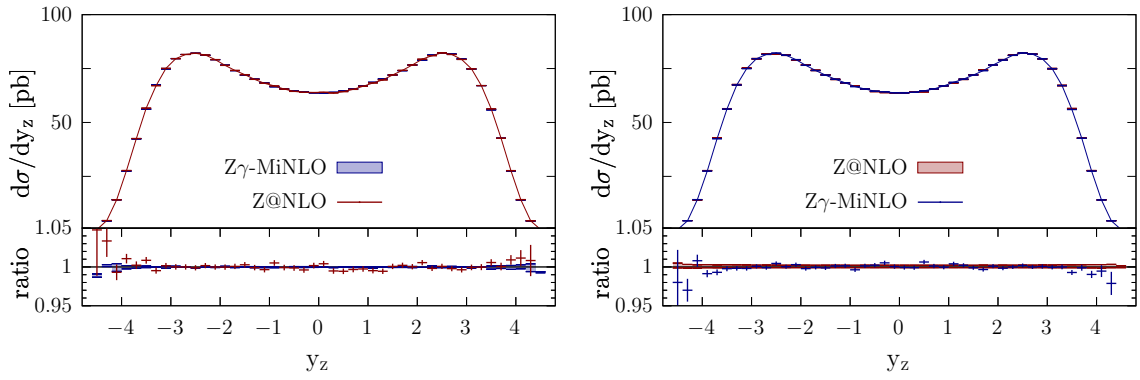

Figure 7.6: Comparison between the $Z\gamma$-MiNLO result and the Z@NLO result for the rapidity distribution of the Z boson obtained with the physical value of $\alpha = \alpha(m_e)$. The blue band represents a variation of the value of p_{T}^{δ} as in Tab. 7.2, while the red band is the envelope of the three-point scale variation.

Chapter 8

Conclusions

Given the level of accuracy achieved by modern collider experiments, it is crucial to provide theoretical prediction of very high accuracy, which, not only amounts to taking higher-order QCD corrections into account, but also to the inclusion of EW contributions and QCD×EW mixed effects. In this context, as a first step towards a fully consistent simultaneous inclusion of EW and QCD higher-order effects in (N)NLO computations matched to parton showers, we focused on QED corrections in Drell-Yan production.

In this thesis we have presented the abelianization of the MiNLO′ method and its implementation for the production of a Z boson decaying into a $\nu\bar{\nu}$ pair. In particular, after presenting the general formalism, valid also for final-state massive emitters, i.e. charged leptons, we discussed the numerical challenges that the abelianization process entails in the small transverse-momentum region of the QED Sudakov form factor with respect to its QCD counterpart. Indeed, we showed an estimate of the position of the peak of the abelianized MiNLO′ differential cross section, which is completely inaccessible. To overcome this issue we proposed a different solution for the computation of the contribution to the cross section in the small transverse-momentum region of the phase space, based on the analytical properties of the MiNLO′ master formula. As a result we introduced an arbitrary parameter, p_{T}^{δ}, acting as a separator between the two contributions, $\sigma_{>}$ and $\sigma_{<}$, and we discussed the dependence of the full result on the value of such parameter.

We mainly focused on the study of a non-physical case involving a value of the QED coupling constant which was made fictitiously large in order to allow for a deeper investigation of the effects of the abelianization. In this scenario, the dependence of the results on the arbitrary scale is not as negligible as one would have expected and it needs further study. Nonetheless we find results that are consistent with the fact that the MiNLO′ method should reproduce the fully inclusive prediction with NLO accuracy, particularly so when the physical value of the coupling constant is used.

This work represents a proof of concept for the abelianization of the MiNLO′ method and a first step towards its implementation within the POWHEG framework for the matching with the parton shower. Alongside a practical implementation of the massive final-state emitter case, for which the theoretical formalism has been discussed in this work, the next development on the line is the matching of this result with a QED parton shower via the POWHEG method. This must be done consistently both for $\sigma_>$ and $\sigma_<$. The former would be treated in a standard manner, i.e. by first generating the second emission according to the POWHEG prescription and then letting the successive QED cascade to be handled by a parton shower. For the latter, instead, as the contribution to the $\sigma_<$ cross section is defined through a tight constraint on the QED emissions, it seems natural to match it directly to a vetoed p_{T}-ordered QED parton shower, without using the POWHEG matching. On a longer timescale, the aim is to include also NLO QCD effects, and, eventually NNLO QCD and mixed QCD×EW corrections.

Appendix A

One-loop soft anomalous dimension

A.1 One-loop soft anomalous dimension matrix in QCD

We can start from the expression for the subtraction operator $\mathbf{I}$ given by eq. (9) of Ref. [156]:

$$\begin{aligned}\mathbf{I} =& \frac{(4\pi)^{\epsilon}}{\Gamma(1-\epsilon)} \left\{ q \frac{1}{2} \left(\frac{\beta_0}{\epsilon} - \bar{\beta}_0^{RS} \right) \right. \\ &+ \sum_{\substack{j,k=1 \\ k \neq j}}^{4} \mathbf{T}_j \cdot \mathbf{T}_k \left(\frac{\mu^2}{|s_{jk}|} \right)^{\epsilon} \left[V_{jk}(s_{jk}, m_j, m_k) + \frac{1}{v_{jk}} \left(\frac{1}{\epsilon} i\pi - \frac{\pi^2}{2} \right) \Theta(s_{jk}) \right] \\ &\left. - \sum_{j=1}^{4} \Gamma_j^{RS}(\mu, m_j) \right\}\end{aligned} \tag{A.1.1}$$

where we have defined $s_{jk} = 2p_j \cdot p_k$ and

$$v_{jk} = \sqrt{1 - \frac{m_j^2 m_k^2}{(p_j \cdot p_k)^2}} = \begin{cases} v & \text{if } j,k = 3,4 \text{ or } j,k = 4,3 \\ 1 & \text{otherwise} \end{cases} \tag{A.1.2}$$

The first term on the right-hand side of eq. (A.1.1) contains the ultraviolet divergences, to be removed via renormalization. The second term depends on the following functions

$$V_{jk}(s_{jk}, m_j, m_k) = \frac{1}{2\epsilon} \frac{1}{v_{jk}} \log \frac{1 - v_{jk}}{1 + v_{jk}} - \frac{1}{4} \left(\log^2 \frac{m_j^2}{|s_{jk}|} + \log^2 \frac{m_k^2}{|s_{jk}|} \right) - \frac{\pi^2}{6} \tag{A.1.3}$$

$$V_{jk}(s_{jk}, m, 0) = \frac{1}{2\epsilon^2} + \frac{1}{2\epsilon} \log \frac{m^2}{|s_{jk}|} - \frac{1}{4} \log^2 \frac{m^2}{|s_{jk}|} - \frac{\pi^2}{12} \tag{A.1.4}$$

$$V_{jk}(s_{jk}, 0, 0) = \frac{1}{\epsilon^2}. \tag{A.1.5}$$

Finally the last term is given by

$$\Gamma_q(\mu, m) = \mathbf{T}_j^2 \left(\frac{1}{\epsilon} - \log \frac{m^2}{\mu^2} - 2 \right) + \gamma_q \log \frac{m^2}{\mu^2} = C_{\text{F}} \left[\frac{1}{\epsilon} + \frac{1}{2} \log \frac{m^2}{\mu^2} - 2 \right] \tag{A.1.6}$$

$$\Gamma_q(\mu, 0) = \frac{1}{\epsilon} \gamma_q + \text{finite terms} \tag{A.1.7}$$

$$\Gamma_g(\mu) = \frac{1}{\epsilon} \gamma_g + \text{finite terms} \tag{A.1.8}$$

Let's start with the V_{jk} term in eq. (A.1.1):

$$F = \sum_{\substack{j.k=1 \\ k \neq j}}^{4} \mathbf{T}_j \cdot \mathbf{T}_k \left(\frac{\mu^2}{|s_{jk}|} \right)^{\epsilon} V_{jk}(s_{jk}, m_j, m_k) = \sum_{\substack{j,k=1 \\ k \neq j}}^{4} F_{jk} \tag{A.1.9}$$

We have three different contributions:

$$F_{II} = F_{12} + F_{21} = 2\, \mathbf{T}_1 \cdot \mathbf{T}_2 \left(\frac{\mu^2}{|s_{12}|} \right)^{\epsilon} V_{12}(s_{12}, 0, 0) \tag{A.1.10}$$

$$F_{FF} = F_{34} + F_{43} = 2\, \mathbf{T}_3 \cdot \mathbf{T}_4 \left(\frac{\mu^2}{|s_{34}|} \right)^{\epsilon} V_{34}(s_{34}, m, m) \tag{A.1.11}$$

$$F_{IF} = \sum_{\substack{j=1,2 \\ k=3,4}} 2F_{jk} = \sum_{\substack{j=1,2 \\ k=3,4}} 2\mathbf{T}_j \cdot \mathbf{T}_k \left(\frac{\mu^2}{|s_{jk}|} \right)^{\epsilon} V_{jk}(s_{jk}, m, 0) \tag{A.1.12}$$

By substituting V_{jk} and factorizing $(\mu^2/M^2)^{\epsilon}$ with $s_{12} = M^2$ we get

$$F_{II} = \left(\frac{\mu^2}{M^2} \right)^{\epsilon} 2\, \mathbf{T}_1 \cdot \mathbf{T}_2 \frac{1}{\epsilon^2} \tag{A.1.13}$$

$$\begin{aligned} F_{FF} &= \left(\frac{\mu^2}{M^2} \right)^{\epsilon} 2\, \mathbf{T}_3 \cdot \mathbf{T}_4 \left(1 + \mathcal{O}(\epsilon)\right) \left(\frac{1}{\epsilon} \frac{1}{2v} \log \frac{1-v}{1+v} - \frac{1}{2} \log^2 \frac{m^2}{|s_{34}|} - \frac{\pi^2}{6} \right) \\ &= \left(\frac{\mu^2}{M^2} \right)^{\epsilon} 2\, \mathbf{T}_3 \cdot \mathbf{T}_4 \left(\frac{1}{\epsilon} \frac{1}{2v} \log \frac{1-v}{1+v} + \text{ finite terms} \right) \end{aligned} \tag{A.1.14}$$

$$\begin{aligned} F_{IF} &= \left(\frac{\mu^2}{M^2} \right)^{\epsilon} \sum_{\substack{j=1,2 \\ k=3,4}} 2\mathbf{T}_j \cdot \mathbf{T}_k \left(1 - \epsilon \log \frac{M^2}{s_{jk}} + \mathcal{O}(\epsilon^2) \right) \\ &\qquad \times \left(\frac{1}{2\epsilon^2} + \frac{1}{2\epsilon} \log \frac{m^2}{|s_{jk}|} - \frac{1}{4} \log^2 \frac{m^2}{|s_{jk}|} - \frac{\pi^2}{12} \right) \\ &= \left(\frac{\mu^2}{M^2} \right)^{\epsilon} \sum_{\substack{j=1,2 \\ k=3,4}} 2\mathbf{T}_j \cdot \mathbf{T}_k \left(\frac{1}{2\epsilon^2} + \frac{1}{2\epsilon} \log \frac{m^2}{|s_{jk}|} + \frac{1}{2\epsilon} \log \frac{M^2}{|s_{jk}|} + \text{ finite terms} \right) \\ &= \left(\frac{\mu^2}{M^2} \right)^{\epsilon} \sum_{\substack{j=1,2 \\ k=3,4}} \mathbf{T}_j \cdot \mathbf{T}_k \left(\frac{1}{\epsilon^2} + \frac{1}{\epsilon} \log \frac{m^2 M^2}{s_{jk}^2} + \text{ finite terms} \right). \end{aligned} \tag{A.1.15}$$

Putting all terms together we obtain

$$F = \left(\frac{\mu^2}{M^2}\right)^{\epsilon} \left[\frac{1}{\epsilon^2} \left(2\,\mathbf{T}_1 \cdot \mathbf{T}_2 + \sum_{\substack{j=1,2 \\ k=3,4}} \mathbf{T}_j \cdot \mathbf{T}_k \right) + \frac{1}{\epsilon} \left(2\,\mathbf{T}_3 \cdot \mathbf{T}_4 \frac{1}{2v} \log \frac{1-v}{1+v} + \sum_{\substack{j=1,2 \\ k=3,4}} \mathbf{T}_j \cdot \mathbf{T}_k \log \frac{m^2 M^2}{s_{jk}^2} \right) \right] \tag{A.1.16}$$

where we can use colour conservation to rewrite the coefficient of the $1/\epsilon^2$ pole as

$$2\,\mathbf{T}_1 \cdot \mathbf{T}_2 + \sum_{\substack{j=1,2 \\ k=3,4}} \mathbf{T}_j \cdot \mathbf{T}_k = \mathbf{T}_1 \cdot (\mathbf{T}_2 + \mathbf{T}_3 + \mathbf{T}_4) + \mathbf{T}_2 \cdot (\mathbf{T}_1 + \mathbf{T}_3 + \mathbf{T}_4) = -(\mathbf{T}_1^2 + \mathbf{T}_2^2). \tag{A.1.17}$$

We can now focus on the last term of eq. (A.1.1) which is quite simple

$$\begin{aligned} -\sum_{j=1}^{4} \Gamma_j^{RS}(\mu, m_j) &= \left(\frac{\mu^2}{M^2}\right)^{\epsilon} \left[-2C_{\mathrm{F}} \frac{1}{\epsilon} - \frac{2}{\epsilon}\gamma_c \right] \\ &= \left(\frac{\mu^2}{M^2}\right)^{\epsilon} \left[-(\mathbf{T}_3^2 + \mathbf{T}_4^2) \frac{1}{\epsilon} - \frac{2}{\epsilon}\gamma_c \right] \end{aligned} \tag{A.1.18}$$

where $c = g, q$ refers to initial state partons.

The last thing we need to address are the imaginary terms in the second line of eq. (A.1.1). If we factorize the usual $(\mu^2/M^2)^{\epsilon}$ and we consider only the $1/\epsilon$ pole, we have

$$F_{\text{imaginary}} = \left(\frac{\mu^2}{M^2}\right)^{\epsilon} \frac{1}{\epsilon} \sum_{\substack{j,k=1 \\ k \neq j}}^{4} \mathbf{T}_j \cdot \mathbf{T}_k \frac{i\pi \Theta(s_{jk})}{v_{jk}}. \tag{A.1.19}$$

Using eq. (A.1.2) and knowing that $s_{jk} > 0$ only if j, k are both initial state or final state partons (since all the momenta are outgoing) we have

$$F_{\text{imaginary}} = \left(\frac{\mu^2}{M^2}\right)^{\epsilon} \frac{1}{\epsilon} i\pi \left[2\,\mathbf{T}_1 \cdot \mathbf{T}_2 + \frac{1}{v} 2\,\mathbf{T}_3 \cdot \mathbf{T}_4 \right]. \tag{A.1.20}$$

We can now use colour conservation $\sum_i^4 \mathbf{T}_i = 0$ to rewrite

$$2\,\mathbf{T}_1 \cdot \mathbf{T}_2 = 2\,\mathbf{T}_3 \cdot \mathbf{T}_4 + (\mathbf{T}_3^2 + \mathbf{T}_4^2) - (\mathbf{T}_1^2 + \mathbf{T}_2^2) \tag{A.1.21}$$

so we end up with

$$F_{\text{imaginary}} = \left(\frac{\mu^2}{M^2}\right)^{\epsilon} \frac{1}{\epsilon} i\pi \left[-(\mathbf{T}_1^2 + \mathbf{T}_2^2) + (\mathbf{T}_3^2 + \mathbf{T}_4^2) + 2\,\mathbf{T}_3 \cdot \mathbf{T}_4 \left(\frac{1}{v} + 1 \right) \right]. \tag{A.1.22}$$

The final result is then given by

$$\mathbf{I} = -\frac{(4\pi)^\epsilon}{\Gamma(1-\epsilon)}\left(\frac{\mu^2}{M^2}\right)^\epsilon \left\{(\mathbf{T}_1^2+\mathbf{T}_2^2)\left(\frac{1}{\epsilon^2}+\frac{i\pi}{\epsilon}\right)+\frac{2}{\epsilon}\gamma_c-\frac{4}{\epsilon}\mathbf{\Gamma}_t^{(1)}+\text{ finite terms}\right\} \tag{A.1.23}$$

where

$$\mathbf{\Gamma}_t^{(1)} = -\frac{1}{4}\left\{(\mathbf{T}_3^2+\mathbf{T}_4^2)(1-i\pi)+\sum_{\substack{j=1,2\\k=3,4}}\mathbf{T}_j\cdot\mathbf{T}_k\log\frac{(2\,p_j\cdot p_k)^2}{m^2M^2}\right.$$
$$\left.+\,2\,\mathbf{T}_3\cdot\mathbf{T}_4\left[\frac{1}{2v}\log\frac{1+v}{1-v}-i\pi\left(\frac{1}{v}+1\right)\right]\right\}. \tag{A.1.24}$$

A.1.1 Comments

1. Note that all real terms in eq. (A.1.24) come from either initial-final or final-final contributions. On the other hand, for what concerns imaginary parts only the $1/v$ term comes from final-final interactions while the other terms come from initial-initial contributions using eq. (A.1.21).

2. Eq. (A.1.1) is written using the formalism employed by Catani, Dittmaier and Trocsanyi [156], in which the amplitude is expanded in powers of $\alpha_s/4\pi$. This means that in order to adapt these results to the choice of the expansion parameter $\alpha_s/2\pi$ used in this work we need to multiply eq. (A.1.23) by a factor $1/2$.

A.2 Abelianization

We can now apply the abelianization techniques described in Section 5.1 to eq. (A.1.24):

$$\Gamma_t^{\text{QED},(1)} = -\frac{1}{4}\left\{(Q_3^2+Q_4^2)(1-i\pi)+\sum_{\substack{j=1,2\\k=3,4}}(-Q_jQ_k)\log\frac{(2\,p_j\cdot p_k)^2}{m^2M^2}\right.$$
$$\left.+\,2\,Q_3Q_4\left[\frac{1}{2v}\log\frac{1+v}{1-v}-i\pi\left(\frac{1}{v}+1\right)\right]\right\}. \tag{A.2.1}$$

We also have

$$\begin{aligned} Q_1 &= -Q_2, \qquad & |Q_1| &= |Q_2| = Q_{\text{ini}},\\ Q_3 &= -Q_4, \qquad & |Q_3| &= |Q_4| = Q_{\text{fin}}, \end{aligned} \tag{A.2.2}$$

which leads to

$$\begin{aligned}\Gamma_t^{\mathrm{QED},(1)} &= -\frac{1}{4}\left\{2Q_{\mathrm{fin}}^2\left[1-\frac{1}{2v}\log\frac{1+v}{1-v}+\frac{i\pi}{v}\right]+\sum_{\substack{j=1,2\\k=3,4}}(-Q_jQ_k)\log\frac{(2\,p_j\cdot p_k)^2}{m^2M^2}\right\}\\ &= -\frac{1}{4}\left\{2Q_{\mathrm{fin}}^2\left[1-\frac{1}{2v}\log\frac{1+v}{1-v}+\frac{i\pi}{v}\right]-2\,Q_1Q_3\log\frac{(p_1\cdot p_3)(p_2\cdot p_4)}{(p_1\cdot p_4)(p_2\cdot p_3)}\right\}.\end{aligned} \tag{A.2.3}$$

Thus for a heavy lepton pair in the final state we have

$$\Gamma_{t,q}^{\mathrm{QED},(1)} = -\frac{1}{2}\left\{1-\frac{1}{2v}\log\frac{1+v}{1-v}+\frac{i\pi}{v}-Q_q\log\frac{(p_1\cdot p_3)(p_2\cdot p_4)}{(p_1\cdot p_4)(p_2\cdot p_3)}\right\} \tag{A.2.4}$$

where Q_q is the charge of the parton with momentum p_1.

Appendix B

Two-loop soft anomalous dimension

B.1 Two-loop soft anomalous dimension matrix in QCD

From Ref. [127] we can extract the expression for the second order anomalous dimension matrix, namely

$$\begin{aligned}\mathbf{\Gamma}_t^{(2)} = -\frac{1}{4}\Bigg\{ &\left[(\mathbf{T}_3+\mathbf{T}_4)^2(-i\pi) + \sum_{\substack{i=1,2\\ j=3,4}} \mathbf{T}_i\cdot\mathbf{T}_j \log\frac{(2p_i\cdot p_j)^2}{M^2m^2}\right]\gamma_{\text{cusp}}^{(2)} \\ &- 4\gamma_Q^{(2)} + 2\,\mathbf{T}_3\cdot\mathbf{T}_4\,\gamma_{\text{cusp}}^{(2)}(v) + \sum_{j=1,2} if^{abc}\,T_3^a\,T_4^b\,T_j^c\,g(v)\log\frac{p_4\cdot p_j}{p_3\cdot p_j} \\ &+ \left[\mathbf{\Gamma}_t^{(1)},\mathbf{F}_t^{(1)}\right] + \pi\beta_0\mathbf{F}_t^{(1)}\Bigg\},\end{aligned} \tag{B.1.1}$$

where the coefficients $\gamma_{\text{cusp}}^{(2)}$, $\gamma_Q^{(2)}$ and $\gamma_{\text{cusp}}^{(2)}(v)$ are the second order coefficients of the perturbative expansions of their respective anomalous dimension functions

$$\gamma_{\text{cusp}}(\alpha_s) = \sum_{n=1}^{\infty}\left(\frac{\alpha_s}{\pi}\right)\gamma_{\text{cusp}}^{(n)} \tag{B.1.2}$$

$$\gamma_Q(\alpha_s) = \sum_{n=1}^{\infty}\left(\frac{\alpha_s}{\pi}\right)\gamma_Q^{(n)} \tag{B.1.3}$$

$$\gamma_{\text{cusp}}(v,\alpha_s) = \sum_{n=1}^{\infty}\left(\frac{\alpha_s}{\pi}\right)\gamma_{\text{cusp}}^{(n)}(v). \tag{B.1.4}$$

For massless quarks and gluons, the two-loop cusp anomalous dimension was computed in Ref. [157] and it reads

$$\gamma_{\text{cusp}}^{(2)} = \left(\frac{67}{36}-\frac{\pi^2}{12}\right)C_{\text{A}} - \frac{5}{9}T_{\text{R}}n_f. \tag{B.1.5}$$

The second-order anomalous dimension for massive partons [158] is given by

$$\gamma_Q^{(2)} = \frac{1}{16}\left[\left(\frac{2}{3}\pi^2 - \frac{98}{9} - 4\zeta_3\right) C_{\rm F}C_{\rm A} + \frac{40}{9}C_{\rm F}T_{\rm R}n_f\right] \tag{B.1.6}$$

and the two-loop cusp anomalous dimension for massive quarks [158] can be written as

$$\begin{aligned}\gamma_{\rm cusp}^{(2)}(v) = \gamma_{\rm cusp}^{(2)}\frac{1}{v}\left(\frac{1}{2}L_v - i\pi\right)&\\ + \frac{C_{\rm A}}{2}\Bigg\{\frac{1}{4}L_v^2 - \frac{5}{6}\pi^2 + \zeta_3 - i\pi L_v + \frac{1}{v^2}\Bigg[\mathrm{Li}_{3v} + \frac{1}{2}L_v\,\mathrm{Li}_{2v}&\\ + \frac{1}{24}L_v^3 - \frac{5}{12}\pi^2 L_v - \zeta_3 + i\pi\left(-\mathrm{Li}_{2v} - \frac{1}{4}L_v^2 + \frac{\pi^2}{6}\right)\Bigg]&\\ + \frac{1}{v}\Bigg[-\frac{1}{24}L_v^3 + \mathrm{Li}_{2v} - \frac{1}{4}L_v^2 - L_v\log\left(\frac{2v}{1-v}\right) + \frac{5}{12}\pi^2 L_v&\\ + \frac{5}{6}\pi^2 + i\pi\left(\frac{1}{4}L_v^2 + L_v + 2\log\left(\frac{2v}{1-v}\right) - \frac{\pi^2}{6}\right)\Bigg]\Bigg\}&\end{aligned} \tag{B.1.7}$$

where v is the relative velocity given by eq. (4.1.27) and we introduced the shorthand notations

$$L_v = \log\left(\frac{1+v}{1-v}\right), \quad \mathrm{Li}_{2v} = \mathrm{Li}_2\left(\frac{1-v}{1+v}\right), \quad \mathrm{Li}_{3v} = \mathrm{Li}_3\left(\frac{1-v}{1+v}\right) \tag{B.1.8}$$

with the usual polylogarithm functions

$$\mathrm{Li}_2(z) = -\int_0^z \frac{dt}{t}\log(1-t), \quad \mathrm{Li}_3(z) = -\int_0^z \frac{dt}{t}\log(t)\log(1-zt). \tag{B.1.9}$$

Finally the function $g(v)$ is [159]

$$\begin{aligned}g(v) = -\frac{1}{4}L_v^2 + \frac{5}{6}\pi^2 + i\pi L_v + \frac{1}{v}\Bigg[-\mathrm{Li}_{2v} + \frac{1}{4}L_v^2 + L_v\log\left(\frac{2v}{1-v}\right)&\\ - \frac{5}{6}\pi^2 - i\pi\left(2\log\left(\frac{2v}{1-v}\right) + L_v\right)\Bigg].&\end{aligned} \tag{B.1.10}$$

B.2 Abelianization

By applying the abelianization rules to eq. (B.1.1) we get

$$\begin{aligned}\Gamma_t^{\rm QED,(2)} = -\frac{1}{4}\Bigg\{\sum_{\substack{i=1,2\\ j=3,4}}(-Q_iQ_j)\log\frac{(2p_i\cdot p_j)^2}{M^2m^2}\gamma_{\rm cusp}^{\rm QED,(2)}&\\ - 4\gamma_f^{\rm QED,(2)} - 2Q_l^2\,\gamma_{\rm cusp}^{\rm QED,(2)}(v) + \pi\beta_0 F_t^{\rm QED,(1)}\Bigg\},&\end{aligned} \tag{B.2.1}$$

with

$$\gamma_{\rm cusp}^{\rm QED,(2)} = -\frac{5}{18}\, N^{(2)}, \tag{B.2.2}$$

$$\gamma_{f}^{\rm QED,(2)} = \frac{5}{36}\, Q_f^2\, N^{(2)}, \tag{B.2.3}$$

$$\gamma_{\rm cusp}^{\rm QED,(2)}(v) = -\frac{5}{18}\, N^{(2)}\, \frac{1}{v} \left[\frac{1}{2} \log\left(\frac{1+v}{1-v}\right) - i\pi\right]. \tag{B.2.4}$$

Note that all the contributions left after the abelianization procedure in $\gamma_{\rm cusp}^{\rm QED,(2)}$, $\gamma_{f}^{\rm QED,(2)}$ and $\gamma_{\rm cusp}^{\rm QED,(2)}(v)$ are proportional to $N^{(2)}$. This is due to the fact that their origin is tied to the splitting of a photon into a fermion-antifermion pair in the final state.

We stress that the results discussed in this appendix stem from the formulas presented in Ref. [127], where the perturbative expansion is performed in powers of α_s/π. Since throughout this work we employ an expansion in $\alpha_s/2\pi$ (or equivalently $\alpha/2\pi$ in QED), we need to adjust these results accordingly.

Appendix C

Increasing the value of α

Some of the computation in this work required us to change the reference value of the QED coupling constant to increase the effect of the QED corrections and at the same time alleviate the numerical complexity. One possible choice would be to use a new value of α at the Thompson limit that is somewhat similar to the value of the QCD coupling constant at the scale of the Z boson mass. In this way we would be able to make a direct comparison between the QED results and the well known QCD ones. However this is not possible, due to the shift in the position of the QED Landau pole. Indeed, by changing the value of the coupling constant, the position of the pole associated with its running also change and not by a small amount.

We want to determine what is the maximum value that we can use to define the Thompson limit of $\widetilde{\alpha}(q^2)$ such that the position of the Landau pole does not fall within the reach of the LHC. In order to do so we can just use the formula for the LO evolution of the coupling constant, given by

$$\widetilde{\alpha}(q^2) = \frac{\widetilde{\alpha}(m_e^2)}{1 + \beta_0\, \widetilde{\alpha}(m_e^2) \log(q^2/m_e^2)}, \tag{C.0.1}$$

where we keep the first-order coefficient of the β function fixed, namely $\beta_0 = -20/9\pi$ which corresponds to all fermions but the top quark contributing to the photon self energy loop. We need to find $\widetilde{\alpha}(m_e^2)$ such that

$$1 + \widetilde{\alpha}(m_e^2)\, \beta_0 \log\left(\frac{Q^2}{m_e^2}\right) = 0 \quad \text{for} \quad Q = 13 \text{ TeV} \tag{C.0.2}$$

that gives us approximately $\widetilde{\alpha}(m_e^2) = 0.04$.

Appendix D

Explicit computation of the double convolutions

We want to explicitly compute a couple of the terms that contain double convolutions appearing in eqs. (6.2) and (6.2). In particular, we focus on the two most complicated ones, namely

$$\left(P_{qq}^{(0)} \otimes (P_{qq}^{(0)} \otimes f)\right) \quad \text{and} \quad \left(C_{qq}^{(1)} \otimes (P_{qq}^{(0)} \otimes f)\right) \tag{D.0.1}$$

which involve the following splitting function and coefficient function

$$P_{qq}^{(0)}(z) = Q_f^2 \left[\frac{1+z^2}{(1-z)_+} + \frac{3}{2}\delta(1-z)\right], \tag{D.0.2}$$

$$C_{qq}^{(1)}(z) = Q_q^2 \left[(1-z) - \delta(1-z)\frac{\pi^2}{12}\right]. \tag{D.0.3}$$

We can start by recalling the plus distribution, denoted as

$$\frac{g(z)}{(1-z)_+}, \tag{D.0.4}$$

whose integral with a smooth test function $f(z)$ is defined as

$$\int_0^1 dz \frac{g(z)}{(1-z)_+} f(z) = \int_0^1 \frac{dz}{1-z} \left[g(z) - g(1)\right] f(z). \tag{D.0.5}$$

The standard convolution between the splitting function $P_{qq}^{(0)}$ and a generic function f representing the parton distribution function is then given by

$$\begin{aligned}(P_{qq}^{(0)} \otimes f)(x) &= \int_x^1 \frac{dz}{z} f\left(\frac{x}{z}\right) Q_q^2 \left[\frac{1+z^2}{(1-z)_+} + \frac{3}{2}\delta(1-z)\right] \\ &= Q_q^2 \int_x^1 \frac{dz}{1-z}\left[\frac{1+z^2}{z} f\left(\frac{x}{z}\right) - 2f(x)\right] + \frac{3}{2}Q_q^2 f(x).\end{aligned} \tag{D.0.6}$$

So that the double convolutions in eq. (D.0.1) can be written as

$$\begin{aligned}\Big(P_{qq}^{(0)}\otimes(P_{qq}^{(0)}\otimes f)\Big)(y) &= Q_q^4\int_y^1\frac{dx}{x}\left[\frac{1+x^2}{(1-x)_+}+\frac{3}{2}\delta(1-x)\right]\\ &\quad\times\left\{\int_{\frac{y}{x}}^1\frac{dz}{1-z}\left[\frac{1+z^2}{z}f\left(\frac{y}{xz}\right)-2f\left(\frac{y}{x}\right)\right]+\frac{3}{2}f\left(\frac{y}{x}\right)\right\}\\ &= Q_q^4\int_y^1\frac{dx}{1-x}\Bigg\{-2\left(\int_y^1\frac{dz}{1-z}\left[\frac{1+z^2}{z}f\left(\frac{y}{z}\right)-2f(y)\right]+\frac{3}{2}f(y)\right)\\ &\quad+\frac{1+x^2}{x}\left[\int_{\frac{y}{x}}^1\frac{dz}{1-z}\left[\frac{1+z^2}{z}f\left(\frac{y}{xz}\right)-2f\left(\frac{y}{x}\right)\right]+\frac{3}{2}f\left(\frac{y}{x}\right)\right]\Bigg\}\\ &\quad+\frac{3}{2}Q_q^4\left\{\int_y^1\frac{dz}{1-z}\left[\frac{1+z^2}{z}f\left(\frac{y}{z}\right)-2f(y)\right]+\frac{3}{2}f(y)\right\}\end{aligned}\tag{D.0.7}$$

$$\begin{aligned}\Big(C_{qq}^{(1)}\otimes(P_{qq}^{(0)}\otimes f)\Big)(y) &= Q_q^4\int_y^1\frac{dx}{x}\left[(1-x)-\frac{\pi^2}{12}\delta(1-x)\right]\\ &\quad\times\left\{\int_{\frac{y}{x}}^1\frac{dz}{1-z}\left[\frac{1+z^2}{z}f\left(\frac{y}{xz}\right)-2f\left(\frac{y}{x}\right)\right]+\frac{3}{2}f\left(\frac{y}{x}\right)\right\}\\ &= Q_q^4\int_y^1 dx\,\frac{1-x}{x}\Bigg\{\int_{\frac{y}{x}}^1\frac{dz}{1-z}\\ &\quad\times\left[\frac{1+z^2}{z}f\left(\frac{y}{xz}\right)-2f\left(\frac{y}{x}\right)\right]+\frac{3}{2}f\left(\frac{y}{x}\right)\Bigg\}\\ &\quad-Q_q^4\frac{\pi^2}{12}\left\{\int_y^1\frac{dz}{1-z}\left[\frac{1+z^2}{z}f\left(\frac{y}{z}\right)-2f(y)\right]+\frac{3}{2}f(y)\right\}\end{aligned}\tag{D.0.8}$$

Bibliography

[1] ATLAS collaboration, G. Aad et al., *Observation of a new particle in the search for the Standard Model Higgs boson with the ATLAS detector at the LHC*, *Phys. Lett. B* **716** (2012) 1 [1207.7214].

[2] CMS collaboration, S. Chatrchyan et al., *Observation of a New Boson at a Mass of 125 GeV with the CMS Experiment at the LHC*, *Phys. Lett. B* **716** (2012) 30 [1207.7235].

[3] A. Huss, J. Huston, S. Jones and M. Pellen, *Les Houches 2021—physics at TeV colliders: report on the standard model precision wishlist*, *J. Phys. G* **50** (2023) 043001 [2207.02122].

[4] T. Sjostrand and P. Z. Skands, *Transverse-momentum-ordered showers and interleaved multiple interactions*, *Eur. Phys. J. C* **39** (2005) 129 [hep-ph/0408302].

[5] C. Bierlich et al., *A comprehensive guide to the physics and usage of PYTHIA 8.3*, *SciPost Phys. Codeb.* **2022** (2022) 8 [2203.11601].

[6] J. Bellm et al., *Herwig 7.2 release note*, *Eur. Phys. J. C* **80** (2020) 452 [1912.06509].

[7] S. Schumann and F. Krauss, *A Parton shower algorithm based on Catani-Seymour dipole factorisation*, *JHEP* **03** (2008) 038 [0709.1027].

[8] T. Gleisberg, S. Hoeche, F. Krauss, M. Schonherr, S. Schumann, F. Siegert et al., *Event generation with SHERPA 1.1*, *JHEP* **02** (2009) 007 [0811.4622].

[9] Sherpa collaboration, E. Bothmann et al., *Event Generation with Sherpa 2.2*, *SciPost Phys.* **7** (2019) 034 [1905.09127].

[10] P. Nason, *A New method for combining NLO QCD with shower Monte Carlo algorithms*, *JHEP* **11** (2004) 040 [hep-ph/0409146].

[11] S. Frixione, P. Nason and C. Oleari, *Matching NLO QCD computations with Parton Shower simulations: the POWHEG method*, *JHEP* **11** (2007) 070 [0709.2092].

[12] S. Alioli, P. Nason, C. Oleari and E. Re, *A general framework for implementing NLO calculations in shower Monte Carlo programs: the POWHEG BOX*, *JHEP* **06** (2010) 043 [1002.2581].

[13] S. Frixione and B. R. Webber, *Matching NLO QCD computations and parton shower simulations*, *JHEP* **06** (2002) 029 [hep-ph/0204244].

[14] S. Frixione, P. Nason and B. R. Webber, *Matching NLO QCD and parton showers in heavy flavor production*, *JHEP* **08** (2003) 007 [hep-ph/0305252].

[15] K. Hamilton, P. Nason and G. Zanderighi, *MINLO: Multi-Scale Improved NLO*, *JHEP* **10** (2012) 155 [1206.3572].

[16] K. Hamilton, P. Nason, C. Oleari and G. Zanderighi, *Merging H/W/Z + 0 and 1 jet at NLO with no merging scale: a path to parton shower + NNLO matching*, *JHEP* **05** (2013) 082 [1212.4504].

[17] S. Hoeche, F. Krauss, M. Schonherr and F. Siegert, *QCD matrix elements + parton showers: The NLO case*, *JHEP* **04** (2013) 027 [1207.5030].

[18] L. Lönnblad and S. Prestel, *Merging Multi-leg NLO Matrix Elements with Parton Showers*, *JHEP* **03** (2013) 166 [1211.7278].

[19] S. Plätzer, *Controlling inclusive cross sections in parton shower + matrix element merging*, *JHEP* **08** (2013) 114 [1211.5467].

[20] R. Frederix and S. Frixione, *Merging meets matching in MC@NLO*, *JHEP* **12** (2012) 061 [1209.6215].

[21] C. W. Bauer, F. J. Tackmann and J. Thaler, *GenEvA. I. A New framework for event generation*, *JHEP* **12** (2008) 010 [0801.4026].

[22] C. W. Bauer, F. J. Tackmann and J. Thaler, *GenEvA. II. A Phase space generator from a reweighted parton shower*, *JHEP* **12** (2008) 011 [0801.4028].

[23] S. Alioli, C. W. Bauer, C. Berggren, F. J. Tackmann, J. R. Walsh and S. Zuberi, *Matching Fully Differential NNLO Calculations and Parton Showers*, *JHEP* **06** (2014) 089 [1311.0286].

[24] P. F. Monni, P. Nason, E. Re, M. Wiesemann and G. Zanderighi, *MiNNLO$_{PS}$: a new method to match NNLO QCD to parton showers*, *JHEP* **05** (2020) 143 [1908.06987].

[25] P. F. Monni, E. Re and M. Wiesemann, *MiNNLO$_{PS}$: optimizing $2 \to 1$ hadronic processes*, *Eur. Phys. J. C* **80** (2020) 1075 [2006.04133].

[26] S. Höche, Y. Li and S. Prestel, *Drell-Yan lepton pair production at NNLO QCD with parton showers*, *Phys. Rev. D* **91** (2015) 074015 [1405.3607].

[27] S. Höche, Y. Li and S. Prestel, *Higgs-boson production through gluon fusion at NNLO QCD with parton showers*, *Phys. Rev. D* **90** (2014) 054011 [1407.3773].

[28] S. Höche, S. Kuttimalai and Y. Li, *Hadronic Final States in DIS at NNLO QCD with Parton Showers*, *Phys. Rev. D* **98** (2018) 114013 [1809.04192].

[29] J. M. Campbell, S. Höche, H. T. Li, C. T. Preuss and P. Skands, *Towards NNLO+PS matching with sector showers*, *Phys. Lett. B* **836** (2023) 137614 [2108.07133].

[30] S. Prestel, *Matching N3LO QCD calculations to parton showers*, *JHEP* **11** (2021) 041 [2106.03206].

[31] V. Bertone and S. Prestel, *Combining N3LO QCD calculations and parton showers for hadronic collision events*, 2202.01082.

[32] S. D. Drell and T.-M. Yan, *Massive Lepton Pair Production in Hadron-Hadron Collisions at High-Energies*, *Phys. Rev. Lett.* **25** (1970) 316.

[33] CMS collaboration, *Measurement of the W boson mass in proton-proton collisions at $\sqrt{s}$ = 13 TeV*, tech. rep., CERN, Geneva, 2024.

[34] CMS collaboration, A. Hayrapetyan et al., *Measurement of the Drell–Yan forward-backward asymmetry and of the effective leptonic weak mixing angle in proton-proton collisions at $\sqrt{s}$ = 13 TeV*, 2408.07622.

[35] ATLAS collaboration, M. Aaboud et al., *Measurement of the W-boson mass in pp collisions at $\sqrt{s} = 7$ TeV with the ATLAS detector*, *Eur. Phys. J. C* **78** (2018) 110 [1701.07240].

[36] LHCb collaboration, R. Aaij et al., *Measurement of the W boson mass*, *JHEP* **01** (2022) 036 [2109.01113].

[37] NNPDF collaboration, R. D. Ball, S. Carrazza, L. Del Debbio, S. Forte, Z. Kassabov, J. Rojo et al., *Precision determination of the strong coupling constant within a global PDF analysis*, *Eur. Phys. J. C* **78** (2018) 408 [1802.03398].

[38] R. Boughezal, A. Guffanti, F. Petriello and M. Ubiali, *The impact of the LHC Z-boson transverse momentum data on PDF determinations*, *JHEP* **07** (2017) 130 [1705.00343].

[39] CMS collaboration, A. M. Sirunyan et al., *Search for resonant and nonresonant new phenomena in high-mass dilepton final states at $\sqrt{s}$ = 13 TeV*, *JHEP* **07** (2021) 208 [2103.02708].

[40] ATLAS collaboration, G. Aad et al., *Search for New Phenomena in Final States with Two Leptons and One or No b-Tagged Jets at $\sqrt{s} = 13$ TeV Using the ATLAS Detector*, *Phys. Rev. Lett.* **127** (2021) 141801 [2105.13847].

[41] J. C. Collins, D. E. Soper and G. F. Sterman, *Factorization of Hard Processes in QCD*, *Adv. Ser. Direct. High Energy Phys.* **5** (1989) 1 [hep-ph/0409313].

[42] T. Kinoshita, *Mass singularities of Feynman amplitudes*, *J. Math. Phys.* **3** (1962) 650.

[43] T. D. Lee and M. Nauenberg, *Degenerate Systems and Mass Singularities*, *Phys. Rev.* **133** (1964) B1549.

[44] R. K. Ellis, D. A. Ross and A. E. Terrano, *The Perturbative Calculation of Jet Structure in e+ e- Annihilation*, *Nucl. Phys. B* **178** (1981) 421.

[45] S. Catani and M. H. Seymour, *A General algorithm for calculating jet cross-sections in NLO QCD*, *Nucl. Phys. B* **485** (1997) 291 [hep-ph/9605323].

[46] S. Frixione, Z. Kunszt and A. Signer, *Three jet cross-sections to next-to-leading order*, *Nucl. Phys. B* **467** (1996) 399 [hep-ph/9512328].

[47] S. Frixione, *A General approach to jet cross-sections in QCD*, *Nucl. Phys. B* **507** (1997) 295 [hep-ph/9706545].

[48] P. Nason and B. Webber, *Next-to-Leading-Order Event Generators*, *Ann. Rev. Nucl. Part. Sci.* **62** (2012) 187 [1202.1251].

[49] M. Dasgupta, F. A. Dreyer, K. Hamilton, P. F. Monni, G. P. Salam and G. Soyez, *Parton showers beyond leading logarithmic accuracy*, *Phys. Rev. Lett.* **125** (2020) 052002 [2002.11114].

[50] F. Herren, S. Höche, F. Krauss, D. Reichelt and M. Schoenherr, *A new approach to color-coherent parton evolution*, *JHEP* **10** (2023) 091 [2208.06057].

[51] J. R. Forshaw, J. Holguin and S. Plätzer, *Building a consistent parton shower*, *JHEP* **09** (2020) 014 [2003.06400].

[52] R. Frederix and K. Hamilton, *Extending the MINLO method*, *JHEP* **05** (2016) 042 [1512.02663].

[53] N. Lavesson and L. Lonnblad, *Extending CKKW-merging to One-Loop Matrix Elements*, *JHEP* **12** (2008) 070 [0811.2912].

[54] S. Alioli, K. Hamilton and E. Re, *Practical improvements and merging of POWHEG simulations for vector boson production*, *JHEP* **09** (2011) 104 [1108.0909].

[55] T. Gehrmann, S. Hoche, F. Krauss, M. Schonherr and F. Siegert, *NLO QCD matrix elements + parton showers in e^+e^- → hadrons*, *JHEP* **01** (2013) 144 [1207.5031].

[56] S. Alioli, C. W. Bauer, C. Berggren, A. Hornig, F. J. Tackmann, C. K. Vermilion et al., *Combining Higher-Order Resummation with Multiple NLO Calculations and Parton Showers in the GENEVA Monte Carlo Framework*, 1305.5246.

[57] S. Catani, F. Krauss, R. Kuhn and B. R. Webber, *QCD matrix elements + parton showers*, *JHEP* **11** (2001) 063 [hep-ph/0109231].

[58] D. de Florian and M. Grazzini, *The Structure of large logarithmic corrections at small transverse momentum in hadronic collisions*, *Nucl. Phys. B* **616** (2001) 247 [hep-ph/0108273].

[59] S. Catani, E. D'Emilio and L. Trentadue, *The Gluon Form-factor to Higher Orders: Gluon Gluon Annihilation at Small Q^- transverse*, *Phys. Lett. B* **211** (1988) 335.

[60] J. Kodaira and L. Trentadue, *Single Logarithm Effects in electron-Positron Annihilation*, *Phys. Lett. B* **123** (1983) 335.

[61] C. T. H. Davies and W. J. Stirling, *Nonleading Corrections to the Drell-Yan Cross-Section at Small Transverse Momentum*, *Nucl. Phys. B* **244** (1984) 337.

[62] G. Parisi and R. Petronzio, *Small Transverse Momentum Distributions in Hard Processes*, *Nucl. Phys. B* **154** (1979) 427.

[63] R. K. Ellis and S. Veseli, *W and Z transverse momentum distributions: Resummation in q_T space*, *Nucl. Phys. B* **511** (1998) 649 [hep-ph/9706526].

[64] G. Altarelli, R. Ellis and G. Martinelli, *Large perturbative corrections to the Drell-Yan process in QCD*, *Nuclear Physics B* **157** (1979) 461.

[65] R. Hamberg, W. van Neerven and T. Matsuura, *A complete calculation of the order α_s^2 correction to the Drell-Yan K-factor*, *Nuclear Physics B* **359** (1991) 343.

[66] C. Anastasiou, L. J. Dixon, K. Melnikov and F. Petriello, *High precision QCD at hadron colliders: Electroweak gauge boson rapidity distributions at NNLO*, *Phys. Rev. D* **69** (2004) 094008 [hep-ph/0312266].

[67] K. Melnikov and F. Petriello, *Electroweak gauge boson production at hadron colliders through $\mathcal{O}(\alpha_s^2)$*, *Phys. Rev. D* **74** (2006) 114017 [hep-ph/0609070].

[68] S. Catani, L. Cieri, G. Ferrera, D. de Florian and M. Grazzini, *Vector boson production at hadron colliders: a fully exclusive QCD calculation at NNLO*, *Phys. Rev. Lett.* **103** (2009) 082001 [0903.2120].

[69] R. Gavin, Y. Li, F. Petriello and S. Quackenbush, *FEWZ 2.0: A code for hadronic Z production at next-to-next-to-leading order*, *Comput. Phys. Commun.* **182** (2011) 2388 [1011.3540].

[70] U. Baur, S. Keller and W. K. Sakumoto, *QED radiative corrections to Z boson production and the forward backward asymmetry at hadron colliders*, *Phys. Rev. D* **57** (1998) 199 [hep-ph/9707301].

[71] U. Baur, O. Brein, W. Hollik, C. Schappacher and D. Wackeroth, *Electroweak radiative corrections to neutral current Drell-Yan processes at hadron colliders*, *Phys. Rev. D* **65** (2002) 033007 [hep-ph/0108274].

[72] V. A. Zykunov, *Weak radiative corrections to Drell-Yan process for large invariant mass of di-lepton pair*, *Phys. Rev. D* **75** (2007) 073019 [hep-ph/0509315].

[73] C. M. Carloni Calame, G. Montagna, O. Nicrosini and A. Vicini, *Precision electroweak calculation of the production of a high transverse-momentum lepton pair at hadron colliders*, *JHEP* **10** (2007) 109 [0710.1722].

[74] A. Arbuzov, D. Bardin, S. Bondarenko, P. Christova, L. Kalinovskaya, G. Nanava et al., *One-loop corrections to the Drell–Yan process in SANC. (II). The Neutral current case*, *Eur. Phys. J. C* **54** (2008) 451 [0711.0625].

[75] S. Dittmaier and M. Huber, *Radiative corrections to the neutral-current Drell-Yan process in the Standard Model and its minimal supersymmetric extension*, *JHEP* **01** (2010) 060 [0911.2329].

[76] R. Boughezal, Y. Li and F. Petriello, *Disentangling radiative corrections using the high-mass Drell-Yan process at the LHC*, *Phys. Rev. D* **89** (2014) 034030 [1312.3972].

[77] T. Ahmed, M. Mahakhud, N. Rana and V. Ravindran, *Drell-Yan Production at Threshold to Third Order in QCD*, *Phys. Rev. Lett.* **113** (2014) 112002 [1404.0366].

[78] S. Catani, L. Cieri, D. de Florian, G. Ferrera and M. Grazzini, *Threshold*

resummation at N^3LL accuracy and soft-virtual cross sections at N^3LO, Nucl. Phys. B **888** (2014) 75 [1405.4827].

[79] C. Duhr, F. Dulat and B. Mistlberger, *Drell-Yan Cross Section to Third Order in the Strong Coupling Constant*, Phys. Rev. Lett. **125** (2020) 172001 [2001.07717].

[80] C. Duhr and B. Mistlberger, *Lepton-pair production at hadron colliders at N^3LO in QCD*, JHEP **03** (2022) 116 [2111.10379].

[81] J. Baglio, C. Duhr, B. Mistlberger and R. Szafron, *Inclusive production cross sections at N^3LO*, JHEP **12** (2022) 066 [2209.06138].

[82] X. Chen, T. Gehrmann, N. Glover, A. Huss, T.-Z. Yang and H. X. Zhu, *Dilepton Rapidity Distribution in Drell-Yan Production to Third Order in QCD*, Phys. Rev. Lett. **128** (2022) 052001 [2107.09085].

[83] T. Neumann and J. Campbell, *Fiducial Drell-Yan production at the LHC improved by transverse-momentum resummation at $N^4LL_p+N^3LO$*, Phys. Rev. D **107** (2023) L011506 [2207.07056].

[84] M. Guzzi, P. M. Nadolsky and B. Wang, *Nonperturbative contributions to a resummed leptonic angular distribution in inclusive neutral vector boson production*, Phys. Rev. D **90** (2014) 014030 [1309.1393].

[85] A. Kulesza and W. J. Stirling, *Soft gluon resummation in transverse momentum space for electroweak boson production at hadron colliders*, Eur. Phys. J. C **20** (2001) 349 [hep-ph/0103089].

[86] S. Catani, D. de Florian, G. Ferrera and M. Grazzini, *Vector boson production at hadron colliders: transverse-momentum resummation and leptonic decay*, JHEP **12** (2015) 047 [1507.06937].

[87] C. Balazs and C. P. Yuan, *Soft gluon effects on lepton pairs at hadron colliders*, Phys. Rev. D **56** (1997) 5558 [hep-ph/9704258].

[88] F. Landry, R. Brock, P. M. Nadolsky and C. P. Yuan, *Tevatron Run-1 Z boson data and Collins-Soper-Sterman resummation formalism*, Phys. Rev. D **67** (2003) 073016 [hep-ph/0212159].

[89] G. Bozzi, S. Catani, G. Ferrera, D. de Florian and M. Grazzini, *Production of Drell-Yan lepton pairs in hadron collisions: Transverse-momentum resummation at next-to-next-to-leading logarithmic accuracy*, Phys. Lett. B **696** (2011) 207 [1007.2351].

[90] S. Mantry and F. Petriello, *Transverse Momentum Distributions from Effective Field Theory with Numerical Results*, Phys. Rev. D **83** (2011) 053007 [1007.3773].

[91] W. Bizoń, X. Chen, A. Gehrmann-De Ridder, T. Gehrmann, N. Glover, A. Huss et al., *Fiducial distributions in Higgs and Drell-Yan production at $N^3LL+NNLO$*, JHEP **12** (2018) 132 [1805.05916].

[92] E. Re, L. Rottoli and P. Torrielli, *Fiducial Higgs and Drell-Yan distributions at*

N^3LL'+NNLO with RadISH, *Journal of High Energy Physics* **2021** (2021) [2104.07509].

[93] S. Camarda, L. Cieri and G. Ferrera, *Drell-Yan lepton-pair production: q_T resummation at N3LL accuracy and fiducial cross sections at N3LO*, *Phys. Rev. D* **104** (2021) L111503 [2103.04974].

[94] S. Camarda, L. Cieri and G. Ferrera, *Drell-Yan lepton-pair production: q_T resummation at approximate N^4LL+N^4LO accuracy*, *Phys. Lett. B* **845** (2023) 138125 [2303.12781].

[95] L. Cieri, G. Ferrera and G. F. R. Sborlini, *Combining QED and QCD transverse-momentum resummation for Z boson production at hadron colliders*, *JHEP* **08** (2018) 165 [1805.11948].

[96] A. Autieri, L. Cieri, G. Ferrera and G. F. R. Sborlini, *Combining QED and QCD transverse-momentum resummation for W and Z boson production at hadron colliders*, *JHEP* **07** (2023) 104 [2302.05403].

[97] S. Dittmaier, A. Huss and C. Schwinn, *Mixed QCD-electroweak $\mathcal{O}(\alpha_s\alpha)$ corrections to Drell-Yan processes in the resonance region: pole approximation and non-factorizable corrections*, *Nucl. Phys. B* **885** (2014) 318 [1403.3216].

[98] S. Dittmaier, A. Huss and C. Schwinn, *Dominant mixed QCD-electroweak $O(\alpha_s\alpha)$ corrections to Drell–Yan processes in the resonance region*, *Nucl. Phys. B* **904** (2016) 216 [1511.08016].

[99] S. Dittmaier, A. Huss and J. Schwarz, *Mixed NNLO QCD $\times$ electroweak corrections to single-Z production in pole approximation: differential distributions and forward-backward asymmetry*, *JHEP* **05** (2024) 170 [2401.15682].

[100] D. de Florian, M. Der and I. Fabre, *QCD$\oplus$QED NNLO corrections to Drell Yan production*, *Phys. Rev. D* **98** (2018) 094008 [1805.12214].

[101] R. Bonciani, F. Buccioni, N. Rana, I. Triscari and A. Vicini, *NNLO QCD$\times$EW corrections to Z production in the $q\bar{q}$ channel*, *Phys. Rev. D* **101** (2020) 031301 [1911.06200].

[102] R. Bonciani, F. Buccioni, N. Rana and A. Vicini, *Next-to-Next-to-Leading Order Mixed QCD-Electroweak Corrections to on-Shell Z Production*, *Phys. Rev. Lett.* **125** (2020) 232004 [2007.06518].

[103] R. Bonciani, F. Buccioni, N. Rana and A. Vicini, *On-shell Z boson production at hadron colliders through $\mathcal{O}(\alpha\alpha_s)$*, *JHEP* **02** (2022) 095 [2111.12694].

[104] M. Delto, M. Jaquier, K. Melnikov and R. Röntsch, *Mixed QCD$\otimes$QED corrections to on-shell Z boson production at the LHC*, *JHEP* **01** (2020) 043 [1909.08428].

[105] F. Buccioni, F. Caola, M. Delto, M. Jaquier, K. Melnikov and R. Röntsch, *Mixed QCD-electroweak corrections to on-shell Z production at the LHC*, *Phys. Lett. B* **811** (2020) 135969 [2005.10221].

[106] L. Cieri, D. de Florian, M. Der and J. Mazzitelli, *Mixed QCD⊗QED corrections to exclusive Drell Yan production using the q_T -subtraction method*, *JHEP* **09** (2020) 155 [2005.01315].

[107] R. Bonciani, L. Buonocore, M. Grazzini, S. Kallweit, N. Rana, F. Tramontano et al., *Mixed Strong-Electroweak Corrections to the Drell-Yan Process*, *Phys. Rev. Lett.* **128** (2022) 012002 [2106.11953].

[108] T. Armadillo, R. Bonciani, S. Devoto, N. Rana and A. Vicini, *Two-loop mixed QCD-EW corrections to neutral current Drell-Yan*, *JHEP* **05** (2022) 072 [2201.01754].

[109] T. Armadillo, R. Bonciani, S. Devoto, N. Rana and A. Vicini, *Evaluation of Feynman integrals with arbitrary complex masses via series expansions*, *Comput. Phys. Commun.* **282** (2023) 108545 [2205.03345].

[110] F. Buccioni, F. Caola, H. A. Chawdhry, F. Devoto, M. Heller, A. von Manteuffel et al., *Mixed QCD-electroweak corrections to dilepton production at the LHC in the high invariant mass region*, *JHEP* **06** (2022) 022 [2203.11237].

[111] C. Bernaciak and D. Wackeroth, *Combining NLO QCD and Electroweak Radiative Corrections to W boson Production at Hadron Colliders in the POWHEG Framework*, *Phys. Rev. D* **85** (2012) 093003 [1201.4804].

[112] L. Barze, G. Montagna, P. Nason, O. Nicrosini and F. Piccinini, *Implementation of electroweak corrections in the POWHEG BOX: single W production*, *JHEP* **04** (2012) 037 [1202.0465].

[113] L. Barze, G. Montagna, P. Nason, O. Nicrosini, F. Piccinini and A. Vicini, *Neutral current Drell-Yan with combined QCD and electroweak corrections in the POWHEG BOX*, *Eur. Phys. J. C* **73** (2013) 2474 [1302.4606].

[114] A. Mück and L. Oymanns, *Resonace-improved parton-shower matching for the Drell-Yan process including electroweak corrections*, *JHEP* **05** (2017) 090 [1612.04292].

[115] M. Chiesa, C. L. Del Pio and F. Piccinini, *On electroweak corrections to neutral current Drell–Yan with the POWHEG BOX*, *Eur. Phys. J. C* **84** (2024) 539 [2402.14659].

[116] L. Buonocore, L. Rottoli and P. Torrielli, *Resummation of combined QCD-electroweak effects in Drell Yan lepton-pair production*, *JHEP* **07** (2024) 193 [2404.15112].

[117] A. Denner and S. Dittmaier, *Electroweak Radiative Corrections for Collider Physics*, *Phys. Rept.* **864** (2020) 1 [1912.06823].

[118] A. Aeppli, F. Cuypers and G. J. van Oldenborgh, *$O(\Lambda)$ corrections to W pair production in e^+e^- and $\gamma\gamma$ collisions*, *Phys. Lett. B* **314** (1993) 413 [hep-ph/9303236].

[119] R. G. Stuart, *General renormalization of the gauge-invariant perturbation expansion near the Z^0 resonance*, *Physics Letters B* **272** (1991) 353.

[120] A. Denner, S. Dittmaier, M. Roth and D. Wackeroth, *Predictions for all processes $e^+e^- \to 4$ fermions + γ*, *Nucl. Phys. B* **560** (1999) 33 [hep-ph/9904472].

[121] A. Denner, S. Dittmaier, M. Roth and L. H. Wieders, *Electroweak corrections to charged-current $e^+e^- \to 4$ fermion processes: Technical details and further results*, *Nucl. Phys. B* **724** (2005) 247 [hep-ph/0505042].

[122] A. Denner and S. Dittmaier, *The Complex-mass scheme for perturbative calculations with unstable particles*, *Nucl. Phys. B Proc. Suppl.* **160** (2006) 22 [hep-ph/0605312].

[123] S. Eidelman and F. Jegerlehner, *Hadronic contributions to (g-2) of the leptons and to the effective fine structure constant $\alpha(M_Z^2)$*, *Z. Phys. C* **67** (1995) 585 [hep-ph/9502298].

[124] J. Erler, *Calculation of the QED coupling $\alpha(M_Z)$ in the modified minimal subtraction scheme*, *Phys. Rev. D* **59** (1999) 054008 [hep-ph/9803453].

[125] A. Denner, *Techniques for calculation of electroweak radiative corrections at the one loop level and results for W physics at LEP-200*, *Fortsch. Phys.* **41** (1993) 307 [0709.1075].

[126] J. Erler and M. J. Ramsey-Musolf, *The Weak mixing angle at low energies*, *Phys. Rev. D* **72** (2005) 073003 [hep-ph/0409169].

[127] S. Catani, M. Grazzini and A. Torre, *Transverse-momentum resummation for heavy-quark hadroproduction*, *Nucl. Phys. B* **890** (2014) 518 [1408.4564].

[128] H. Sargsyan, *Heavy-Quark Pair Production at Hadron Collider: Transverse-Momentum Resummation, NNLO Corrections and Azimuthal Asymmetries*, Ph.D. thesis, Zurich U., 2017. 10.5167/uzh-142437.

[129] A. Banfi, G. P. Salam and G. Zanderighi, *Resummed event shapes at hadron - hadron colliders*, *JHEP* **08** (2004) 062 [hep-ph/0407287].

[130] G. Bozzi, S. Catani, D. de Florian and M. Grazzini, *Transverse-momentum resummation and the spectrum of the Higgs boson at the LHC*, *Nucl. Phys. B* **737** (2006) 73 [hep-ph/0508068].

[131] J. Mazzitelli, P. F. Monni, P. Nason, E. Re, M. Wiesemann and G. Zanderighi, *Top-pair production at the LHC with MINNLO$_{PS}$*, *JHEP* **04** (2022) 079 [2112.12135].

[132] S. Catani, D. de Florian and M. Grazzini, *Universality of nonleading logarithmic contributions in transverse momentum distributions*, *Nucl. Phys. B* **596** (2001) 299 [hep-ph/0008184].

[133] A. Manohar, P. Nason, G. P. Salam and G. Zanderighi, *How bright is the proton? A precise determination of the photon parton distribution function*, *Phys. Rev. Lett.* **117** (2016) 242002 [1607.04266].

[134] A. V. Manohar, P. Nason, G. P. Salam and G. Zanderighi, *The Photon Content of the Proton*, *JHEP* **12** (2017) 046 [1708.01256].

[135] D. de Florian, G. F. R. Sborlini and G. Rodrigo, *Two-loop QED corrections to the Altarelli-Parisi splitting functions*, *JHEP* **10** (2016) 056 [1606.02887].

[136] M. Roth and S. Weinzierl, *QED corrections to the evolution of parton distributions*, *Phys. Lett. B* **590** (2004) 190 [hep-ph/0403200].

[137] L. Buonocore, M. Grazzini and F. Tramontano, *The q_T subtraction method: electroweak corrections and power suppressed contributions*, *Eur. Phys. J. C* **80** (2020) 254 [1911.10166].

[138] L. Buonocore, *Ultimate Precision for the Drell-Yan Process: Mixed QCDxQED(EW) Corrections, Final State Radiation and Power Suppressed Contributions*, Ph.D. thesis, Zurich U., Naples U., 2020.

[139] M. A. Ebert and F. J. Tackmann, *Resummation of Transverse Momentum Distributions in Distribution Space*, *JHEP* **02** (2017) 110 [1611.08610].

[140] G. Billis, M. A. Ebert, J. K. L. Michel and F. J. Tackmann, *A toolbox for q_T and 0-jettiness subtractions at N^3LO*, *Eur. Phys. J. Plus* **136** (2021) 214 [1909.00811].

[141] P. B. Arnold and R. P. Kauffman, *W and Z production at next-to-leading order: From large q(t) to small*, *Nucl. Phys. B* **349** (1991) 381.

[142] S. Actis, A. Denner, L. Hofer, A. Scharf and S. Uccirati, *Recursive generation of one-loop amplitudes in the Standard Model*, *JHEP* **04** (2013) 037 [1211.6316].

[143] S. Actis, A. Denner, L. Hofer, J.-N. Lang, A. Scharf and S. Uccirati, *RECOLA: REcursive Computation of One-Loop Amplitudes*, *Comput. Phys. Commun.* **214** (2017) 140 [1605.01090].

[144] A. Denner and S. Dittmaier, *Scalar one-loop 4-point integrals*, *Nucl. Phys. B* **844** (2011) 199 [1005.2076].

[145] A. Denner and S. Dittmaier, *Reduction of one loop tensor five point integrals*, *Nucl. Phys. B* **658** (2003) 175 [hep-ph/0212259].

[146] A. Denner and S. Dittmaier, *Reduction schemes for one-loop tensor integrals*, *Nucl. Phys. B* **734** (2006) 62 [hep-ph/0509141].

[147] A. Denner, S. Dittmaier and L. Hofer, *Collier: a fortran-based Complex One-Loop LIbrary in Extended Regularizations*, *Comput. Phys. Commun.* **212** (2017) 220 [1604.06792].

[148] J. Alwall, R. Frederix, S. Frixione, V. Hirschi, F. Maltoni, O. Mattelaer et al., *The automated computation of tree-level and next-to-leading order differential cross sections, and their matching to parton shower simulations*, *JHEP* **07** (2014) 079 [1405.0301].

[149] R. Frederix, S. Frixione, V. Hirschi, D. Pagani, H. S. Shao and M. Zaro, *The*

automation of next-to-leading order electroweak calculations, *JHEP* **07** (2018) 185 [1804.10017].

[150] GoSam collaboration, G. Cullen et al., *GOSAM-2.0: a tool for automated one-loop calculations within the Standard Model and beyond*, *Eur. Phys. J. C* **74** (2014) 3001 [1404.7096].

[151] GoSam collaboration, G. Cullen, N. Greiner, G. Heinrich, G. Luisoni, P. Mastrolia, G. Ossola et al., *Automated One-Loop Calculations with GoSam*, *Eur. Phys. J. C* **72** (2012) 1889 [1111.2034].

[152] F. Buccioni, J.-N. Lang, J. M. Lindert, P. Maierhöfer, S. Pozzorini, H. Zhang et al., *OpenLoops 2*, *Eur. Phys. J. C* **79** (2019) 866 [1907.13071].

[153] NNPDF collaboration, V. Bertone, S. Carrazza, N. P. Hartland and J. Rojo, *Illuminating the photon content of the proton within a global PDF analysis*, *SciPost Phys.* **5** (2018) 008 [1712.07053].

[154] A. Buckley, J. Ferrando, S. Lloyd, K. Nordström, B. Page, M. Rüfenacht et al., *LHAPDF6: parton density access in the LHC precision era*, *Eur. Phys. J. C* **75** (2015) 132 [1412.7420].

[155] V. Bertone, S. Carrazza and J. Rojo, *APFEL: A PDF Evolution Library with QED corrections*, *Comput. Phys. Commun.* **185** (2014) 1647 [1310.1394].

[156] S. Catani, S. Dittmaier and Z. Trocsanyi, *One loop singular behavior of QCD and SUSY QCD amplitudes with massive partons*, *Phys. Lett. B* **500** (2001) 149 [hep-ph/0011222].

[157] G. Korchemsky and A. Radyushkin, *Renormalization of the Wilson loops beyond the leading order*, *Nuclear Physics B* **283** (1987) 342.

[158] T. Becher and M. Neubert, *Infrared singularities of QCD amplitudes with massive partons*, *Phys. Rev. D* **79** (2009) 125004 [0904.1021].

[159] A. Ferroglia, M. Neubert, B. D. Pecjak and L. L. Yang, *Two-loop divergences of massive scattering amplitudes in non-abelian gauge theories*, *JHEP* **11** (2009) 062 [0908.3676].